Republic of Iraq
Ministry of Higher Education and Scientific Research
University of Babylon
College of Science For Women
Department of Laser Physics

Spectroscopic Study of Surface Plasmon Resonance in Laser Active Media

A Thesis
Submitted to the Council of the College of Science for Women, University of Babylon
In Partial Fulfillment of the Requirements for the Degree of Doctor of Philosophy in Science / Laser Physics and its Applications

By:

Lubna Abbas Muhammed Al-Bassam

B.Sc. , Laser Physics 2013

M.Sc. , Laser Physics 2017

Supervised by:

Asst.Prof. Dr. Lazem Hassan Aboud

2021 A.D. 1443 A.H.

جمهورية العراق

وزارة التعليم العالي والبحث العلمي

جامعة بابل

كلية العلوم للبنات ـ قسم فيزياء الليزر

دراسة طيفية لرنين البلازمون السطحي في اوساط فعالة ليزرية

اطروحة مقدمة الى

قسم فيزياء الليزر في كلية العلوم للبنات – جامعة بابل

كجزء من متطلبات نيل درجة دكتوراه فلسفة في العلوم ـ فيزياء الليزر وتطبيقاته

من قبل

لبنى عباس محمد البصام

بكالوريوس علوم فيزياء الليزر 2013

ماجستير علوم فيزياء الليزر 2017

بإشراف

أ.م.د. لازم حسن عبود

2021 م

1442 ه

Dedication

*To the soul that I love and miss, that remains with me and protects me forever, to the memory of my kind , warm and wonderful " **Mother** "*

*To my amazing " **Father** " for his continuous love, help, support, and encouragement.*

To the beautiful hearts that I love

*my sweet sisters " **Fatin, Lina** "*

*my great brother " **Mustafa** "*

*and my nice sister-in-law " **Zahraa** "*

*To my best friend "**Raneem**" who helps me all the time, and I'm so lucky to have such a lovely and beautiful friend.*

Acknowledgements

I am grateful to " ***Almighty Allah*** *" Who has given me his blessings, strength and patience to finish my research .*

I would like to express my thanks and appreciation to my supervisor " ***Dr. Lazem Hassan*** *" for his support and help.*

The words are not enough to express my great thanks and respect to " ***Dr. Saddam Flayeh*** *" for his continuous help and engorgement. The laser Physics Department is so lucky to have such a glorious teacher.*

Big appreciation should also go to " ***Dr. Nizar Salem*** *" for his valuable help.*

Great thanks go to the presidency and the staff of laser Physics Department for their valuable support.

بِسْـــــــــمِ اللهِ الرَحْمَنِ الرَحِيمْ

اقْرَأْ بِاسمِ رَبِكَ الَذي خَلَق ۝ خَلَقَ الإنسَانَ مِنْ عَلَق ۝ اقْرَأْ وَرَبُكَ الأكرم

۝ الَذي عَلَمَ بِالقَلَم ۝ عَلَمَ الإنسَانَ مَا لَمْ يَعلَم۝

صَدَقَ اللهُ العَليُ العَظيم

العلق (5)

Abstract

In this research , it was used (RhB dye) with different concentrations, and then studied the absorption spectrum of these samples by using UV-VIS spectrometer, the emission spectrum by using fluorescence spectrometer, and then the plasmonic spectrum by using the emission spectrophotometer (LIF). It was used a better concentration of RhB dye ($1*10^{-5}$ M) to mix with different concentrations of Ag NPs that have been prepared by the ablation method .To get different concentrations of Ag NPs, it was changed the pulse number (500, 600, 700, 800, 900) p and keep the energy constant at (600 mJ), it will play a major role in changing the absorption and the emission spectra properties. It was found a strong dependence of the emission characteristics (the emission intensity, threshold for lasing) on the concentration of Ag NPs. However, to get different sizes of Ag NPs, it was changed the energy (500, 600, 700, 800, 900) mJ and keep the pulse number constant at (400 p). Also studied different concentrations of Ag NWs, and then studied the absorption, emission, and the plasmonic spectra to all the previous mixture (RhB dye with Ag NPs) , (RhB dye with Ag NWs). The same (better concentration of RhB dye $1*10^{-5}$ M) was mixed with Au NPs that have been prepared by the same previous ablation steps, and also studied the absorption, emission, and the plasmonic spectra.

All previous samples Ag NPs, Ag NWs, and Au NPs (with different pulses and different energies) was checked up by FE-SEM to find out the size of the nanomaterials.

Nevertheless, thin film was studied that have been fabricated of multilayer structure and introduced as the main gain media including polydimethylsiloxane (PDMS) substrate/ Gold Nano rods covered by the Rhodamine B (RhB) as the first gain media and it was covered by PVP

polymer (Fabrication of RhB into 2D Nano grating), deposited (RhB $1*10^{-5}$ M) on this thin film, also, (RhB $1*10^{-5}$ M + Ag NPs 800 p), (RhB $1*10^{-5}$ M + Ag NPs 600 mJ), (RhB $1*10^{-5}$ M + Ag NWs 2 gm/mol), (RhB $1*10^{-5}$ M + Au NPs 700 p) and (RhB $1*10^{-5}$ M + Au NPs 700 mJ), were deposited on the thin film, and then studied the plasmonic spectrum by using the emission spectrophotometer (LIF) to study the effect of plasmon phenomena on the emission spectrum.

Also, all these 2D thin film samples was checked up by SEM.

الخلاصة :

في هذا البحث ، تم استخدام صبغة (الرودامين B) بتراكيز مختلفة وتم دراسة طيف الامتصاص لهذه العينات باستخدام مطياف (UV-VIS)، طيف الانبعاث بإستخدام مطياف الفلورة، وطيف البلازمون بإستخدام الفلورة بالحث بالليزر (LIF). وتم استخدام افضل تركيز من صبغة (الرودامين B) ($1*10^{-5}$ M) لتمزج مع تراكيز مختلفة من الجسيمات النانوية للفضة (Ag NPs) التي تم تحضيرها بطريقة الاستئصال. للحصول على تراكيز مختلفة من (Ag NPs) تم تغيير عدد النبضات p (500, 600, 700, 800, 900) وتثبيت الطاقة عند 600 mJ) والذي سيلعب دور اساسي في تغيير خصائص اطياف الامتصاص و الانبعاث ، حيث وجد اعتمادا قويا لخصائص الانبعاث (شدة الانبعاث، عتبة الفعل الليزري) على تركيز الجسيمات النانوية للفضة، تم تغيير الطاقة mJ (500, 600, 700, 800, 900) وتثبيت عدد النبضات عند (400 p). وايضا تم دراسة تراكيز مختلفة من الاسلاك النانوية للفضة (Ag NWs) وايضا دراسة اطياف الامتصاص، الانبعاث ، وطيف البلازمون لكل الخليط السابق (RhB mixed with Ag NPs) و (RhB mixed with Ag NWs). تم مزج نفس افضل تركيز لصبغة (الرودامين B) ($1*10^{-5}$ M) مع الجسيمات النانوية للذهب (Au NPs) والذي تم تحضيرها بنفس خطوات طريقة الاستئصال السابقة وايضا تم دراسة اطياف الامتصاص، الانبعاث ، وطيف البلازمون. كل العينات السابقة (Ag NPs, Ag NWs, Au NPs) (بنبضات و طاقات مختلفة) تم فحصها بواسطة جهاز (FE-SEM) لمعرفة حجم المواد النانوية.

ومن ثم تم دراسة الغشاء الرقيق الذي تم تصنيعه من تركيب طبقات متعددة واستخدمت كأوساط فعالة رئيسية تتضمن ارضية (PDMS)، (Gold nanorods) ومغطاه ب (RhB) كأول وسط فعال، ومن ثم تمت تغطيته بواسطة بوليمر (PVP) (تصنيع RhB الى محزز نانوي ثنائي الابعاد)، تم ترسيب (RhB $1*10^{-5}$ M) على الغشاء الرقيق، وايضا

(RhB $1*10^{-5}$ M + Ag NPs 800 p), (RhB $1*10^{-5}$ M + Ag NPs 600 mJ) ,(RhB $1*10^{-5}$ M + Ag NWs 2 gm/mol), (RhB $1*10^{-5}$ M + Au NPs 700 p) و(RhB $1*10^{-5}$ M + Au NPs 700 mJ) تم ترسيبها على الغشاء الرقيق، وتم دراسة طيف البلازمون بإستخدام مطياف الانبعاث (الفلورة بالحث بالليزر LIF) لدراسة تأثير ظاهرة البلازمون على طيف الانبعاث. وايضا، كل عينات الغشاء الرقيق (2D) تم فحصها بواسطة جهاز (SEM).

List of Contents

Contents

Chapter One

Chapter Two

Chapter Three

Chapter Four

Chapter Five

List of Symbols

Symbol	Description
E	Electric field
ρ_e	Total charge density
B	Magnetic flux density
$\epsilon_\circ$	Free space permittivity
$\mu_\circ$	Free space permeability
J	Total current density
m_e	Electron mass
γ	Electron damping ratio
q_e	Electron charge
ω	Angular frequency
Pa	Polarizability
D	Electric displacement
ω_p	Plasma frequency
ϵ	Material permittivity
ϵ_d	Permittivity of surrounding medium
σ_{scs}	Scattering cross section
σ_{acs}	Absorption cross section
k	Wave vector
ε_2	Propagation in a dielectric medium
Ω_R	Rabi splitting energy
V	Coupling parameter
Υ_p	The line width of the bare plasmon
Υ_e	The line width of the bare exciton
Φ_F	Fluorescence quantum yield

Φ_T	The transfer efficiency
R_O	The critical Förster radius
τ_F	Fluorescence lifetime
Γ	The decay rate

List of Abbreviations

Abbreviations	Description
Ag	Silver
Au	Gold
ATR	Attenuated total reflection
CCD	Charge coupled detector
EM	Electromagnetic
FE-SEM	Field emission scanning electron microscopes
LAL	Laser ablation in liquid
LSP	Localized surface plasmon
NPs	Nanoparticles
NWs	Nanowires
PDMS	Polydimethylsiloxan
PVP	Polyvinylpyrrolidone
QED	Quantum electrodynamics
RET	Resonance energy transfer
RhB	Rhodamine B
SEM	Scanning electron microscopes
SP	Surface plamon
SPP	Surface plasmon polariton
SPR	Surface plasmon resonance

List of Tables

List of Figures

1.1 Introduction :

Spectroscopy is the analysis of the interaction between matter and any portion of the electromagnetic spectrum. Traditionally, spectroscopy involved the visible spectrum of light, but X-ray, gamma, and UV spectroscopy also are valuable analytical techniques **[1]**. Spectroscopy can involve any interaction between light and matter, including absorption, emission, scattering, etc. Data obtained from spectroscopy is usually presented as a spectrum that is a plot of the factor being measured as a function of either frequency or wavelength. Emission spectra and absorption spectra are common examples **[2]**.

Nevertheless, When a beam of electromagnetic radiation passes through a sample, the photons interact with the sample. They may be absorbed, reflected, refracted, etc. Absorbed radiation affects the electrons and chemical bonds in a sample. In some cases, the absorbed radiation leads to the emission of lower-energy photons. Spectroscopy looks at how the incident radiation affects the sample. Emitted and absorbed spectra can be used to gain information about the material. Because the interaction depends on the wavelength of radiation **[3]**.

The visible radiation that emit from the most organic dyes helps their usability as an active medium in dye lasers, this led them to be considered as a first tunable laser **[4]**. In the visible spectrum regions, because it has a broad fluorescence spectrum, this allowed the laser output tuned at whatever value chosen within this wide range, and because of availability of a huge number of fluorescent dyes, it became possible to choose the compound that can produce laser emission, in any part of ultraviolet, visible, and near-infrared regions. Whereas, dye lasers produce laser

output can be tuned in the range of wavelengths that located between (340-1200 nm) , and according to the type of the used dye **[2]**.

The interaction between light and disordered amplifying media results in a noticeably narrow light emission **[3]**. Metallic nanoparticles (NPs) suspended in colloidal solutions or embedded in polymer films were shown to produce efficient enhancement in the laser emission **[4]**. In gain media containing metal NPs, SPR enhances the laser emission; this happens when the wavelength of the SPR coincides with the emission of the dye **[5]**. It is worth noting that by varying NPs shape, dimension, state of aggregation and external conditions, the SPR wavelength is tunable throughout the visible and near-IR region **[6]**.

It is important to consider how the laser emission occurs in a system consisting of dye molecules in the presence of metallic NPs. On the other hand, when metallic particles are used, if a dye molecule is located a few nanometers from a metal NP, a large enhancement of the fluorescence emitted by the molecule may be observed due to influence of localized surface plasmons (LSPs) excited in the NPs **[7]**. The LSP is the quanta of conduction-electron oscillations in a metallic NP. Its resonance frequency depends on the metallic material, shape, and size of the NPs as well as host material **[8]**. Metal NPs enhance the lasing efficiency via two different mechanisms **[9]**: (i) enhancement of localized electromagnetic (EM) field in the vicinity of metal NP due to localized surface-plasmon resonance (LSPR) **[10]**, and (ii) enhancement of the scattering strength, resulted from large scattering cross section of metal NP **[11]**.

1.2 Literature Review:

[O. Popov et al. , 2007] measured over a large range of particle sizes, indicate that the lasing properties (threshold for lasing, emission intensity) strongly depend on the size of the nanoparticles and agree well with the predictions of the Mie theory. The lasing properties are all enhanced by the presence of NP in the polymer films. The minimum in the threshold versus the particle size and the maximum in the experiment versus the particle size are in agreement and provide the optimal particle size for optimal lasing performance. Using diffusion equations, we could simulate the spectral narrowing **[12]**.

[X. Meng et al. ,2009] observed the emission spectra from rarely reported amplifying the active media using metal nanoparticles as scattering centers. They found that the pump threshold was lowered and the emission intensity was enhanced by replacing TiO_2 nanoparticles with the same sized Ag nanoparticles as scattering centers in PMMA-R6G films. Ag nanoparticles are preferable scattering centers in the design of active media with high intensity and low threshold **[13]**.

[M. Shunsuke et al. ,2010] studied the scattering characteristics of noble NPs, one of the memorable lineaments related to localized surface Plasmon resonance, and depict the NPs application as components of a cavity, and confirm the advantages of scatters in metallic NPs compared to dielectric NPs, emphasizing an excellent scattering efficiency compared to dielectric NPs. The silver (Ag) and gold (Au) have (LSPR) in the visible range, for this reason, attention to only noble metals. The author also summed up the highlight on a recently explained surface plasmon-based nanolaser, in which a single NPs acts as a cavity **[14]**.

[Christian T. et al. , 2011] demonstrated the lasing action in PMMA films doped with Ag NPs and Rh6G dye. The enhancement of lasing

emission in the samples containing Ag NPs is attributed to the increase of the local field in the vicinity of the silver NPs. The contribution of multiple scattering of light is small because the average diameter of the Ag NPs is ≈ (12 nm) **[15]**.

[Wang C. et al. ,2012] reported a surface plasmon resonance-enhanced emission spectra properties from disordered ZnO NWs with Pt NPs. The underlying mechanism of the enhanced lasing efficiency can be attributed to the energy transfer from Pt NPs to ZnO NWs due to the strong local field induced by the surface plasmon resonance of Pt NPs. Furthermore, the Pt NPs can serve as an excellent scattering medium, which enormously increases the multiple scattering probability experienced by the cavity modes **[16]**.

[B. Kumar et al. , 2013] synthesized the nanostructures (NPs, NRs, and NTs) of titanium oxide and used them as scatterers in dye solution to investigate the PL emission under optical excitation. The PL of Rh B dye solution was investigated under various conditions. NPs of two different sizes and shapes, NRs, and NTs were used as scatterers in dye solution **[17]**.

[G. Ramiro et al. ,2014] studied threshold in silica gel containing Rh6G doped silica NPs under one and two-photon excitation. They observed by two-photon pumping the lasing threshold is (50) times higher than that after one-photon excitation. The experimental results (spectral and temporal pulse widths) are in agreement with the theoretical calculations (time pulse widths) by using a light diffusive propagation model **[18]**.

[SH. Ning et al. ,2015] investigated the lasing based on a series of Ag NPs with the diameter ranging from (8 nm to 250 nm). The effects of different sizes of Ag NPs on the lasing characteristics were investigated. The lowest threshold is achieved by introducing Ag NPs with the diameter of (150 nm). By studying the enhanced localized EM field and

the scattering effect of Ag NPs in experiment and Mie theory, they found that the effects of localized EM field enhancement and scattering all contribute to the reduced lasing threshold **[19]**.

[Wan Zakiah et al. , 2015] observed improved performance with a lower lasing threshold, higher emission peak intensity and narrower emission line width for both Rh6G and Rh640 with relatively low concentrations of gold nanoparticle scatterers in comparison with dielectric scattering particles. These observations are attributed to the enhanced scattering and absorption of gold nanoparticles and increased spectral overlap between the dye fluorescence spectrum and the gold extinction spectrum, which induces localized surface plasmons and resonance energy transfer **[20]**.

[J. Yin et al. , 2016] studied the effect of the shape of Au scattering particles on the Rh6G dye-doped PMMA polymer. In particular, the effect on the centre wavelength and the threshold were considered. Rh6G dye-doped PMMA polymer disordered media containing Au nanospheres and nanorods were fabricated, using the same volume fraction of each **[21]**.

[Y. Wang et al. ,2016] demonstrated an ultrathin plasmonic active medium fabricated by a simple lift off technique, which consists of a polymer membrane embedded with Ag NPs. A low threshold can be observed when the (200 nm) thick laser device is optically pumped, which is about (2 $\mu J/cm^2$). It attributes to the strong plasmonic scattering by the Ag NPs and the high quality confinement by the polymer membrane. Furthermore, the laser device can be attached to a fiber end face to achieve the lasing **[22]**.

[T. Zhai et al. ,2017] studied multilayer structure to achieve the RGB plasmonic emission. Three polymer waveguides embedded with Ag NPs enable strong amplification of the scattered light. The surface plasmon

resonance of Ag NPs provides enhanced pumping for the RGB emission spectrum. Dynamic tuning of the mixed colors of the laser device is presented on the CIE chromaticity diagram. The multilayer structure provides an alternative for the fabrication of RGB plamonic emission, which may be used to design integrated laser sources **[23]**.

[E. J. Villar et al. , 2017] studied that the Core−shell TiO_2 and Silica NPs at [140×10^{10} NPs mL^{-1}] in an ethanol solution of R6G [1×10^{-4} M] allowed us to study the lasing action at the localization transition. An absorption emission saturation phenomenon was observed in the active medium. This phenomenon was associated with the absorption emission saturation of the localized modes called the peaks mode **[24]**.

[N. Asgari, S.M. Hamidi, 2018] studied two dimensional plasmonic crystals as a periodic metallic structure to use its plasmonic band gap for tuning the coupling strength of the plasmon to different dye exciton. The plasmonic structure, prepared by nanoimprint lithography, is covered by Rhodamine-B and 6G as organic dyes in Polyvinylpyrrolidone as host medium. The results indicated the coupling between exciton and plasmon by the dispersion relation and polar diagram for different coupling regime **[25]**.

[N. Asgari, S.M. Hamidi, 2018] indicated that there are fantastic new modes in the plasmonic band gap of dispersion relation due to the weak exciton-plasmon coupling in PVP (RB)/Gold nano-grating. The selected samples demonstrated an increase in the coupling due to an increase in the concentration and thickness of dye layer, leading to the creation of new sharp modes. Finally, polarization dependency was confirmed in plasmonic excitation of nano-grating on the coupling modes. The results can open the new insight in engineering and tuning the coupling between exciton and plasmons in one-dimensional nanostructures **[26]**.

[S. F. Haddawi et al. ,2019] We have demonstrated a new green–blue plasmonic random laser by 1D and 2D plasmonic structure as gain media deposited with Au nanostructures and different concentrations and thickness of RhB dye. We want to increase the light confinement by more enhances of light scattering in the medium. We observe with 2D plasmonic structure at low energy pumping (0.13 mJ) the output intensity and blue–green range enhances dramatically as the dye concentration increased. Also more sharp spikes with width less than 0.5 nm appeared and higher random lasing emission intensity can be achieved when increasing pump energy to 1.95 mJ due to the interaction between the emitted photons of RhB and localized surface plasmon of the Au nanorods is increased **[27]**.

[S. F. Haddawi et al. ,2020] demonstrated the plasmonic random lasing in two types of dyes (Rh6G and RhB) with 1.5×10^{-5} concentrations mixed with Au, Ag, Au@Ag, Ag@Au and Au, Ag mixed NPs prepared by LAL with different concentrations. It was observed that at high NP concentration, the scattering mean free path and the lasing threshold reduced. In addition, the random lasing intensity in Au NPs was higher than that of Ag NPs under the same condition and the spike width was smaller than Ag NPs. The gain length was enhanced via two ways; first by increasing the pumping energy and second by increasing the dye concentration. The dye concentration should be increased in an appropriate manner because on the contrary, the emission intensity will decrease **[28]**.

[S. A. Suheil et al. ,2021] studied the absorption spectrum of polymer solutions with the dye, it was clear that the absorbance had increased by the increasing of concentrations. Then studied the emission spectrum of the prepared samples, the phenomenon of surface plasmon resonance (SPR) occurs when the pulse energy (80 mJ) is applied at concentrations

(0.1mg / ml) of the silver nanoparticles (Ag NPs) and SPR effecting on threshold pumping and increase the efficiency of wave guide **[29]**.

[N. Roostaei et al. ,2021] proposed and fabricated a broadband plasmonic metasurface absorber based on etalon nanostructure through a soft nanolithography method. The designed structure consists of poly-dimethyl-siloxane flexible membrane and gold 2D grating structure on both sides of the structure, which acts as a Fabry–Pérot interferometer (FPI) or etalon. The etalon-based absorber achieved light absorption from (500 to 700) nm compared to one face gold grating which works in the wavelength range (500 to 600) nm with half of the absorbed power. Thus, the proposed structure acts as a good broadband absorber with a high efficiency **[30]**.

[S. F. Haddawi et al. ,2021] studied multi-wavelength random lasing in two dimensional flexible plexcitonic nanostructures through surface lattice plasmon amplification by using Au NPs in order to increase the energy coupling. Based on the results, the energy coupling between plasmonic Au NPs and excitons in two-dimensional nanostructure increased by enhancing the concentration of Au NPs, which smoothed the stimulated emission of multi-wavelength lasing. In addition, the efficiency of this multi-wavelength random lasing can be controlled by increasing these energy couplings **[31]**.

1.3 Aim of Research :

Improvement of the laser output of the laser active media (dye lasers) through the study of the emission spectrum of plasmonic resulting from using a laser beam with a different energies, in addition to study the spectrum that resulting from the interaction of the exciton with the plasmon and its effect on the laser output.

Also, studying different samples (RhB dye mixed with Ag NPs, Ag NWs, and Au NPs) and [(thin film) 2D nano grating deposited with RhB dye mixed with Ag NPs, Ag NWs, and Au NPs] that achieved phenomena related to surface plasmon resonance (localized surface plasmon, surface plasmon polariton) to reach a new sample that has a highest improvement to the laser induce emission spectrum to the laser dyes that used as an active medium.

2.1 Introduction:

This chapter presents the physical properties of the dye that used, and its energy level. Also, show a different types and shapes of the nanoparticles. Demonstrate the basic concepts of the plasmonic phenomenon and the types of surface plasmon ; Surface Plasmon Polariton (SPP) and localized surface plasmon (LSP) and the coupling between the plasmon and exciton.

2.2 Laser dyes :

The laser dyes can be used in many practical systems as a gain medium. The dye consists of fluorescence molecules in organic or water solvent **[32]**. A dye can be pumped efficiently and can exhibit high gain, due to the high fluorescence quantum efficiency and broad emission and absorption cross-sections. For this reason, the dye used as a gain medium. The large bandwidth of the gain in the dyes gives a broad tuning range for the laser emission **[33]**.

2.3 Photophysical properties of dye molecules :

To study the photophysical properties (absorption and emission) for dyes, and the explanation and description of the radiative and non radiative laser process, first, it have to know and understand the energy level diagram for the laser dyes.

2.4 Dyes energy levels :

Laser dyes are complex organic molecules containing long chains of conjugated double bonds (i.e., alternating single and double carbon bonds, =C–C=C–). The large molecular size and the relatively free moving π-electrons in the conjugated double bonds give rise to the large dipole moments of dye molecules (or equivalently, oscillator strengths).

The complex molecular structure also leads to many vibrational and rotational levels within a single electronic state **[34]**. Therefore, laser dyes often have strong and wide absorption bands in the UV and visible region. Figure (2-1) shows the typical energy levels of a dye molecule. S_0 and S_1 are the ground and the first excited singlet electronic states. T_1 and T_2 are the first and second excited triplet states. In a singlet state, the spin of the excited electron is anti-parallel to the spin of the remaining molecule and the total spin quantum number is S = 0, whereas in a triplet state the two spins are parallel and (S = 1). Therefore, singlet–singlet and triplet–triplet transitions are allowed, while singlet–triplet transitions are forbidden because of the selection rule ($\Delta S = 0$) **[34]**. As mentioned earlier, each electronic state is further split into many vibrational and rotational sublevels due to the complex dye molecular structure. In addition, the effective homogenous line broadening mechanism due to the collisions with solvent molecules smears these sublevels into unresolved overlapping bands. The homogenous broadened spectra of dye molecules enable very efficient channeling of the pump energy into narrow band laser emissions **[35]**. It is important to realize that the dye laser is a classical four-level system (if neglect the triplet states) where the four energy levels are marked (0–3) in figure (2-1). Under optical excitation, dye molecules are pumped from the bottom of the ground state S_0 (ground level 0) to some vibrational– rotational sublevels in the first singlet state S_1 (intermediate pump level 3). The dye molecules in level (3) quickly relax to the bottom of S_1 (upper laser level 2). This non radiative decay process happens on the time scale of a few picoseconds or less. The energy lost in this process contributes to the heating of the solvent. From the upper laser level (2), dye molecules can undergo either spontaneous emission or stimulated emission to some vibrational–rotational sublevels in S_0 (lower laser level 1) **[36]**.

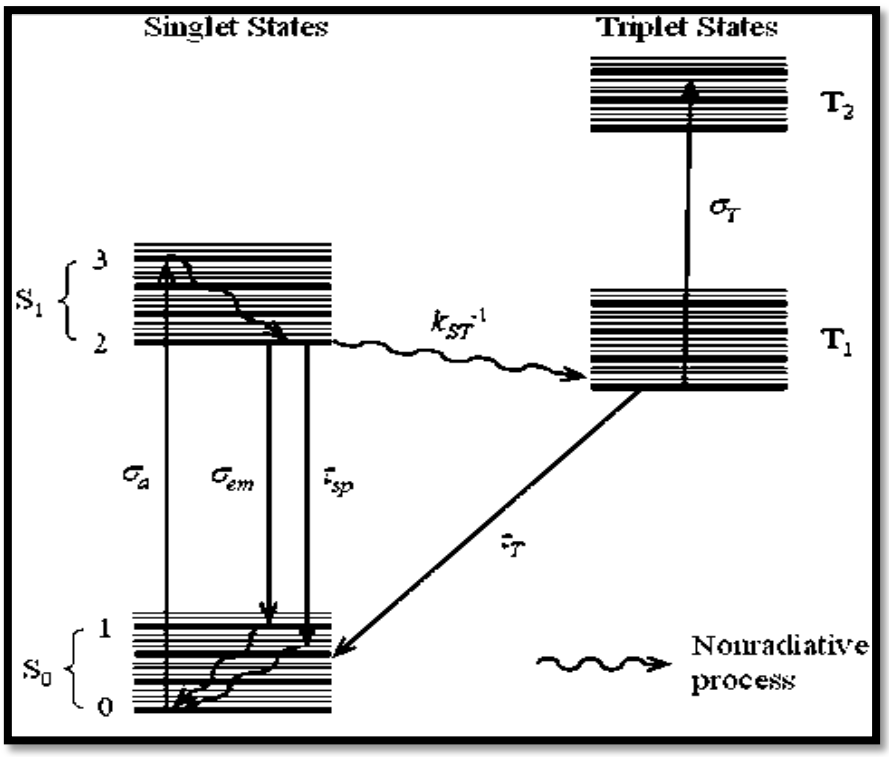

Figure (2-1): Typical energy levels of a dye molecule [36].

The non radiative decay time from the lower laser level (1) to the bottom of the ground state S_0 (ground level 0) is also a few picoseconds. Due to the extremely fast non radiative decay processes, the populations of the lower laser level n_1 and the intermediate pump level n_3 are negligibly small. Therefore, dye lasers can reach threshold at very small population inversions, with typical (n_2/n) of only 0.01 or less **[35]**. However, due to the short upper state lifetimes (a few nanoseconds), dye lasers still need high pump intensities to reach threshold. The real situations are further complicated by the triplet state effects. The excited molecules at the upper laser level (2) undergo not only radiative transitions to S_0 but also non radiative intersystem crossing to the dark triplet state T_1. As mentioned before, this process requires a spin flip of the excited electron and thus is spin-forbidden **[36]**. This is the reason that intersystem cross has a relative slow transition rate ($1/k_{ST}$ ~100 ns) and the triplet state lifetime is long (τ_T~ 100 ns). The metastable triplet state has two

detrimental effects on laser oscillation. First, the long-lived triplet state T_1 traps the dye molecules and decreases the available population inversion. Second, the absorption. from the first triplet state T_1 to the second triplet state T_2 tends to overlap with the laser emission and produces extra losses at the laser wavelength. Therefore, short pump pulses, fast circulation of dye solutions and triplet state quenchers are often utilized to minimize the triplet state influences in different types of dye lasers. For example, in conventional CW dye lasers, the dye solutions flow by the excitation region at velocities as high as (10 m/s) to circumvent the triplet state trapping and thermal distortion problems **[34]**.

2.5 Molecular spectra :

When continues electromagnetic radiation pass through a transparent materials, a portion of the radiation may be absorbed and residual radiation, when passed through a prism, may yield a spectrum with gaps in it. Such a spectrum is called an absorption spectrum. During the absorption process the atoms or molecules of the material pass from a state of low energy to one of higher energy **[37]**. When atoms or molecules in an excited state revert to a state of lower energy, losing energy, they may emit radiation and give rise to an emission spectrum.

In both absorption and emission processes, the relation between the energy change in the atom or molecule and the frequency of the radiation absorbed or emitted is given by the well-known Bohr condition **[38]**:

$$|\Delta E| = \left|E_f - E_i\right| = h\nu \qquad (2.1)$$

Where (ν) is the frequency of the radiation, (E_i and E_f) are the energies of atom or molecule in the initial and final state, respectively.

The absolute value of the energy difference (ΔE) is called the transition energy. For absorption the value of (ΔE) is positive; for emission is negative. The frequency (ν) is related to the wavelength (λ) by ($\nu = c/\lambda$), in which (c) is the velocity of light (2.9988×10^{10} cm/sec in vacuum).Therefor, the smaller the transition energy, the longer is the wavelength of the radiation absorbed or emitted. The molecular absorption spectra are classified into three types: rotation, vibration, and electronic, as shown in figure (2-2) **[39]**.

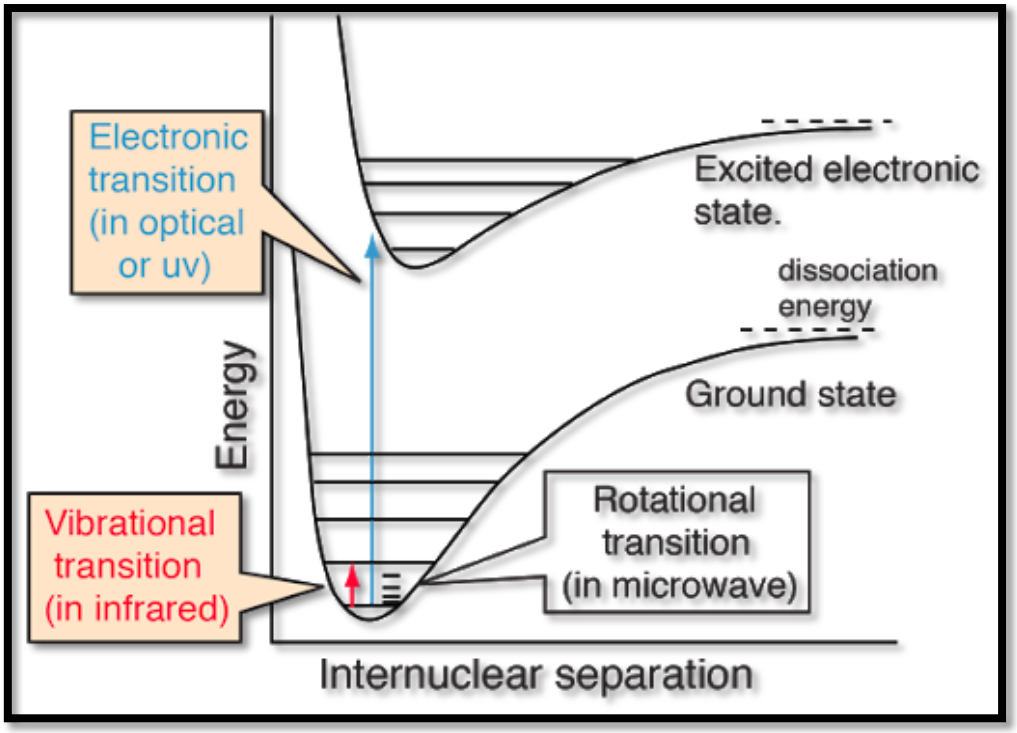

Figure (2-2): Transitions between energy levels of a molecule [39].

The rotation spectrum of molecule is associated with changes which occur in the rotational state of the molecule (selection rule: $\Delta J=\pm 1$) without simultaneous changes in the vibrational and electronic state. Since the energy levels for the rotation of the molecule are relatively close to one another, the frequency of the absorbed radiation is low, and the wavelength long **[40]**. Actually, the rotation spectra of the molecules occur in the far infrared region, at wavelengths beyond (20 μm) and those

of heavy molecules are situated in the microradio wave region, at wavelengths of the order of (0.1-10 cm).

The vibration (or vibration rotation) spectrum of a molecule is associated with changes which occur in the vibrational state of the molecule (selection rule: $\Delta v = \pm 1$) without simultaneous changes in the electronic state. The changes in the vibrational states are generally accompanied with changes in rotational states, so the vibration spectrum has generally rotational fine structure **[38]**. The most important vibration spectra occur in the near and the middle infrared region from about (1 to 3 μm). Absorptions associated with transitions between energy level of vibrational modes with relatively small force constant, such as torsional vibrations about single bonds, occur at longer wavelengths, e.g about (60 μm) (for infrared region) **[40]**.

Finally, electronic spectra arise from transitions between electronic states. The electronic spectra occur in the ultraviolet (at wavelengths below 400 μm) and visible (wavelengths 400-800 μm) regions, and sometimes extend into the near infrared region. Electronic transitions are accompanied with simultaneous changes in the vibrational and rotational states **[41]**. Therefore, a transitions between two electronic states does not result in only a single spectral line, but results in a large number of lines not widely spaced from one another. In fact, electronic spectra of gaseous molecules may assume a very complicated structure arising from the superposition of vibrational and rotational changes on the electronic transitions. In electronic spectra of liquids, solutions, and solids, the rotational structure is unreasonable, and even the vibrational structure is not always reasonable. The electronic spectra thus consist of relatively broad bands **[42]**.

2.6 Rhodamine B laser dye :

Rhodamine B laser dye has red to violet color. It has the molecular formula of $C_{28}H_{31}CIN_2O_3$ and (479.02 g/mol) molecular weight. The laser emission by Rhodamine B is tunable about (610 nm), while it has a quantum yield of about (0.49- 1.0) dependent on the temperature **[43]**. When it is excited by second harmonic generation Q-switched Nd: YAG laser, the quantum yield of absolute fluorescence had been appeared. The chemical structure of a Rhodamine B dye had been drawn in Figure (2-3) **[44]**.

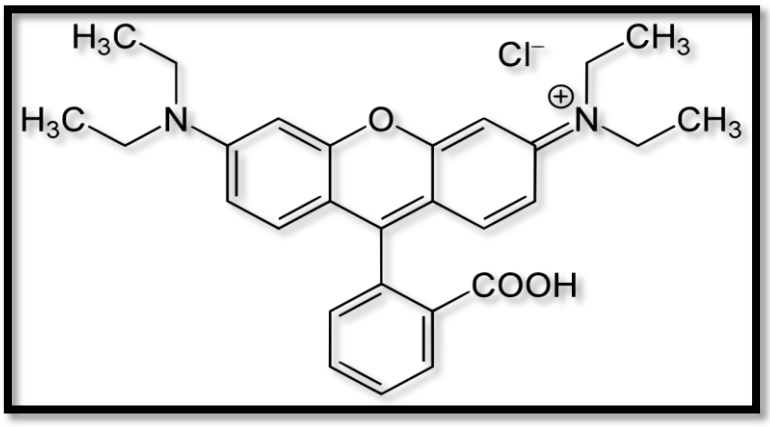

Figure (2-3): The chemical structure of rhodamine B dye [44].

2.7 Nanostructure :

Rapidly growth of nanotechnology is related to infinite applications of devices, systems and structures, by controlling size, shape and structure at nanometer scale **[45]**. Materials at this scale provide many advantages, depending upon the size, shape, structure and method of preparation **[46]**.

Particles of different types and materials at the range between (1) to (100) nm can be classified according to agglomeration of atoms and molecules as shown in figure (2-4) into:

1) Zero dimensional nanoparticles: these nanoparticles have all the three direction length in the nanometer scale. Zero dimensional

nanoparticles are isolated from each other such as nanocluster materials, metal particles (Ag, Au NP's) or semiconductor (quantum dots) particles.

2) One dimensional nanoparticle: these nanoparticles have only one direction length out of the nanometer range including nanorods, nanowires, and nanotubes.

3) Two dimensional nanoparticles: these nanoparticles have two direction out of the nanometer range, including nanofilms, coating surface, and nanosheets **[47]**.

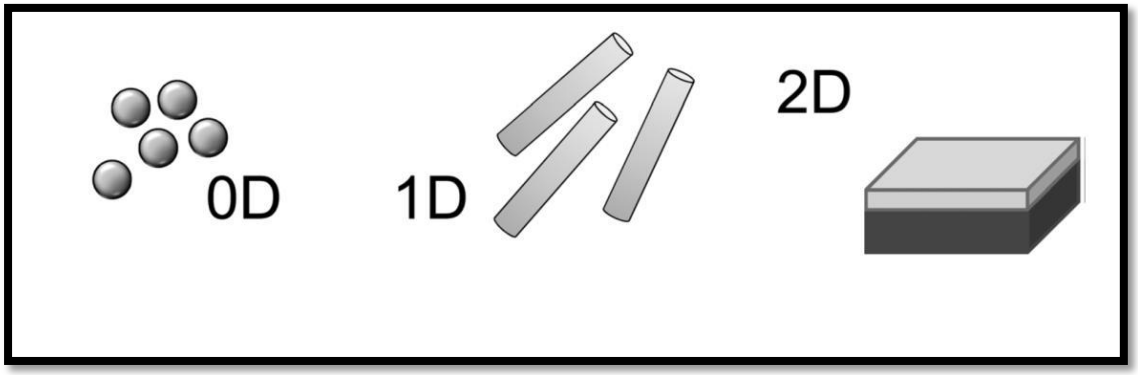

Figure (2-4): Nanoparticles classified according to their directions [48].

Agglomerate state of nanoparticles occurs over short distances due to van der Waals force; this agglomeration affects the chemical and the electromagnetic properties of nanoparticles **[49]**. The agglomeration process depends on the type of nanoparticles, conditions of synthesis method and concentration of nanoparticles in solvent. Agglomeration process can be avoided by several processes such as coating the nanoparticle surface by another organic or inorganic substance or chemically stabilization by polishing slurries in aqueous suspension **[50]**. The high development in nanoparticles synthesis techniques enables to synthesis different types of NP's such as spherical NP's **[51]**, wire NP's **[52]**.

Nanoparticles have larger enhancement of physical and chemical properties compared to bulk material due to their extremely large surface area to volume ratio **[53]**.

Nanoparticles characteristics (physical and chemical properties) are based on the size, shape, structure, physical stability, and distribution of the nanoparticles, which can be investigated using different microscopic technique such as scanning electron microscopy, transmission electron microscopy and scanning electron microscopy **[54]**.

2.7.1 Silver (Ag) Nanoparticles :

The Ag nanoparticles have more conduction electrons, the strong interaction between the particles and the light photons had been occurred, which leads to a collective resonance oscillation **[55]**. This behavior can be attributed to the higher cross-sections for both scattering and absorption. Depending on the size of the particle and the refractive index of the metal surface, the peak resonance wavelength may be varied at the range of (400-530) nm. While the shift of the peak resonance wavelengths to longer wavelengths, had been resulted in the increase of particle size diameter and using a rod or plate silver nanoparticles **[56]**.

2.7.2 Gold (Au) Nanoparticles :

Gold nanoparticles have unique optical properties because they support surface plasmons. At specific wavelengths of light, the surface plasmons are driven into resonance and strongly absorb or scatter incident light **[57]**. This effect is so strong that it allows for individual gold nanoparticles as small as (50) nm **[58]**. So the Absorption and scattering of light by gold nanoparticles of sufficiently small size that are comparable to or less than the mean free path of electrons in a spatially

extended material should be mentioned especially **[59]**. In this case, it becomes necessary to account for the scattering of free electrons at the boundary of the gold nanoparticle. This is usually interpreted as a limitation of the mean free path of electrons, which leads to an additional pathway of free electron energy dissipation **[60]**.

2.8 Plasmonic :

Plasmonic is the field of study the optical phenomena that results from interaction of conduction free electrons of noble metal nanoparticles with electromagnetic waves (especially at visible optical frequencies) and collective oscillation called as surface plasmon **[61]**, where the plasmons are collective charge density oscillations and longitudinal waves propagating in a bulk metal, and they cannot couple directly with light. However, at the interface between a metal and dielectric the oscillation mode of the electron wave to couple with light exists under certain matching conditions. **[62]** This mode is called surface plasmons (SPs) or surface plasmon polaritons (SPPs) that are localized at a metal surface and propagate along the interface between a metal and dielectric. SPs are represented schematically in Figure (2-5). When SPs are excited, an electric field in the z-direction is enhanced, providing a remarkably high sensitivity for interfacial characterizations. For this reason, new optics utilizing this resonance character has attracted attention in various fields**[63]**. If light is directly incident on a flat metal film, SPs are not excited since the dispersion relation is different of SPs from light propagating in free space. Hence, the optical system to match the condition is needed to excite SPs. Otto **[64]** and Kretschmann **[65]** designed optical systems using total reflection to excite SPs. Fast electrons or gratings can also excite SPs, however, the technique exciting SPs would be restricted to the total-reflective optical systems **[62]**.

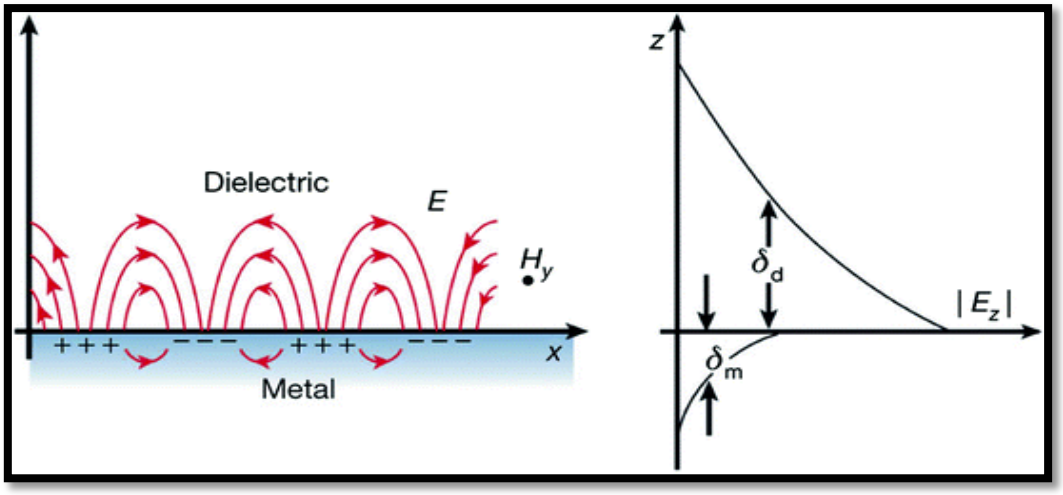

Figure (2-5): Schematics of the electromagnetic field of surface plasmons or SPP propagating along the interface between a metal and dielectric. (δ_d) is a decay length into the dielectric and (δ_m) is a decay length (skin depth) into the metal [62].

Plasmonic is a major part of the nanophotonics which can confine electromagnetic waves smaller than the diffraction limit. The development of nanofabrication techniques helps to increase applications of plasmonic nanostructures **[66]**.

When electromagnetic waves are incident on a metal surface, it will accelerate electrons and lead to induce polarization that creates restoring force which causes an oscillation of the free electron of the metal as shown in Figure (2-6). This oscillation is quantized and free electrons oscillation is quantization of plasma oscillations and it's called a plasmon **[67]**.

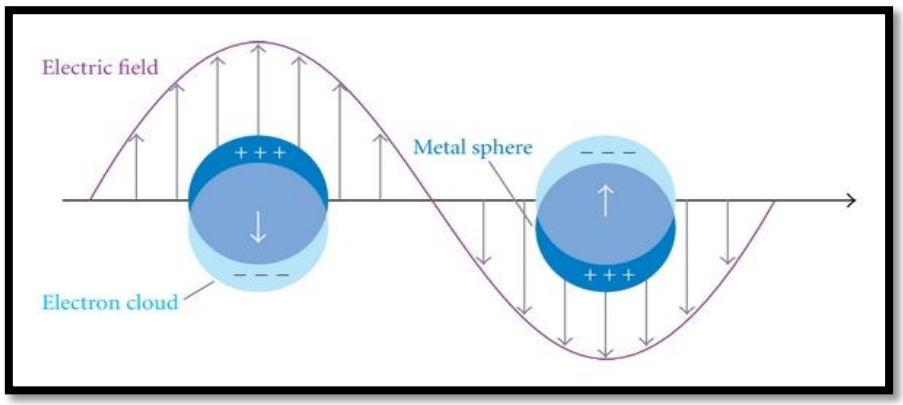

Figure (2-6): Localized Surface Plasmon resonance of metallic nanoparticle [68].

There are two types of surface plasmon according to their interface: Surface Plasmon Polariton (SPP) and localized surface plasmon (LSP).

1) **Surface Plasmon Polariton (SPP):** are longitudinal waves, which propagate at the interface between a dielectric and metal. These waves travel parallel to the direction of propagation; so they cannot be excited by a transverse waves. The most effective way to excite a plasmon is to use electrons i.e. when light excites the electrons, electrons will pass through a thin metal layer and lose some energy, this loss in energy use to excite SPP **[69]**.
2) **Localized Surface Plasmon (LSP):** are non-propagating waves. In case of a spherical nanoparticle, the curved surface of the nanoparticle creates a restoring force on the electrons to result in a localized resonance. This kind of resonance can be excited by direct light irradiation **[70]**.

The interaction of metallic nanostructures with electromagnetic fields can be described by a classical form of Maxwell's equations. Maxwell's equations are describe the electromagnetic field for a given system through four vectors strength of the electric field (E), the displacement (D), the strength of magnetic field (H), and the flux density (B) **[71]**.

$$\nabla . \vec{E} = \frac{\rho_e}{\epsilon_\circ} \qquad (2.2)$$

$$\nabla . \vec{B} = 0 \qquad (2.3)$$

$$\nabla \times \vec{E} = -\frac{\partial \vec{B}}{\partial t} \qquad (2.4)$$

$$\nabla \times \vec{B} = \mu_\circ \epsilon_\circ \frac{\partial \vec{E}}{\partial t} + \mu_\circ \vec{J} \qquad (2.5)$$

Where (ϵ_0) ,(μ_0): are the permittivity and the permeability of free space, (ρ_e): is the total charge density and ($\vec{J}$): is the total current density.

The incident external electric field excites the free electrons and displaces it from their normal positions in the metal lattice. Movement of oscillating free electron can be described by equation of motion **[72]**:

$$m_e \ddot{x} + m_e \gamma \dot{x} = -q_e E \qquad (2.6)$$

Where (m_e): is the free electron mass, (x): is the electron displacement, (q_e): is the electron charge and E is the external electric field, (γ): is electron damping factor.

The general solution of oscillating electric field is $E=E_0 e^{-i\omega t}$ so that the solution of equation (2.6) for given amplitude (x_0): is **[72]**:

$$x_\circ = \frac{q_e}{m_e(\omega^2 + i\omega\gamma)} E_\circ \qquad (2.7)$$

Where (ω): is the angular frequency. While in the case of (n) number of electrons a macroscopic polarization is rise $P=-nq_e x$ and given by:

$$P = \frac{n\, q_e^2}{m_e(\omega^2 + i\omega\gamma)} E \qquad (2.8)$$

The electric displacement (D) depends on the dielectric function of the free electron as:

$$D = \epsilon_\circ E + P \qquad (2.9)$$

So that equation (2.9) becomes:

$$D = \epsilon_\circ \left(1 - \frac{\omega_p^2}{(\omega^2 + i\omega\gamma)}\right) E \qquad (2.10)$$

The plasma frequency of the free electron is **[73]**:

$$\omega_p^2 = \frac{n\, q_e^2}{\epsilon_\circ m_e} \qquad (2.11)$$

The dielectric function of the free electron (ϵ_ω) is:

$$\epsilon_\omega = 1 - \frac{\omega_p^2}{\omega^2 + i\omega\gamma} \qquad (2.12)$$

The equation describes the behavior of plasmonic in a bulk metal using the Drude model.

For very small spherical metallic nanoparticles (compared to the wavelength of incident light), the nanoparticle polarisability (Pa): is **[74]**:

$$\mathrm{Pa} = 4\pi \mathrm{R}^3 \frac{\epsilon(\omega) - \epsilon_\mathrm{d}}{\epsilon(\omega) + 2\epsilon_\mathrm{d}} \qquad (2.13)$$

Where (R): is the nanoparticle radius, ϵ (ω): is the metal's dielectric function and (ϵ_d): is the dielectric function of the surrounding.

LSP resonance occurs when the polarisability of the nanoparticle reaches to maximum value i.e. ($\epsilon(\omega)+2\epsilon_d$) is minimized.

The optical cross section of the spherical nanoparticles enhances (strong scattering and absorption properties) under plasmonic conditions and given by **[75]**:

$$\sigma_{\mathrm{scs}} = \frac{\mathrm{k}^4}{6\pi} |\mathrm{Pa}|^2 \qquad (2.14)$$

$$\sigma_{\mathrm{acs}} = \mathrm{kIm}\ [\mathrm{Pa}] \qquad (2.15)$$

Where σ_{scs},σ_{acs} are the scattering and the absorption cross sections, and (k): is the wave vector of incident light **[75]**.

2.9 Excitation of SPs by light :

The dispersion relation of a free photon (k_{ph}) propagating in a dielectric medium (ε_2) is **[76]**:

$$\mathrm{k_{ph}} = \frac{\omega}{\mathrm{c}} \sqrt{\varepsilon_2} \qquad (2.16)$$

which is always smaller than the wave vector of SPs, (k_{sp}), propagating along an interface between the metal and the dielectric due to negative dielectric constant (ε_1) **[77]**:

$$\mathrm{k_{ph}} = \frac{\omega}{\mathrm{c}} \sqrt{\varepsilon_2} \ < \frac{\omega}{\mathrm{c}} \sqrt{\frac{\varepsilon_1 \varepsilon_2}{\varepsilon_1 + \varepsilon_2}} = \mathrm{k_{sp}} \qquad (2.17)$$

This dispersion relation is graphically shown in Figure (2-7). From this dispersion relation it is obvious that normal incident light cannot directly

couple with SPs and the momentum mismatch must be satisfied to couple the light with SPs **[76]**.

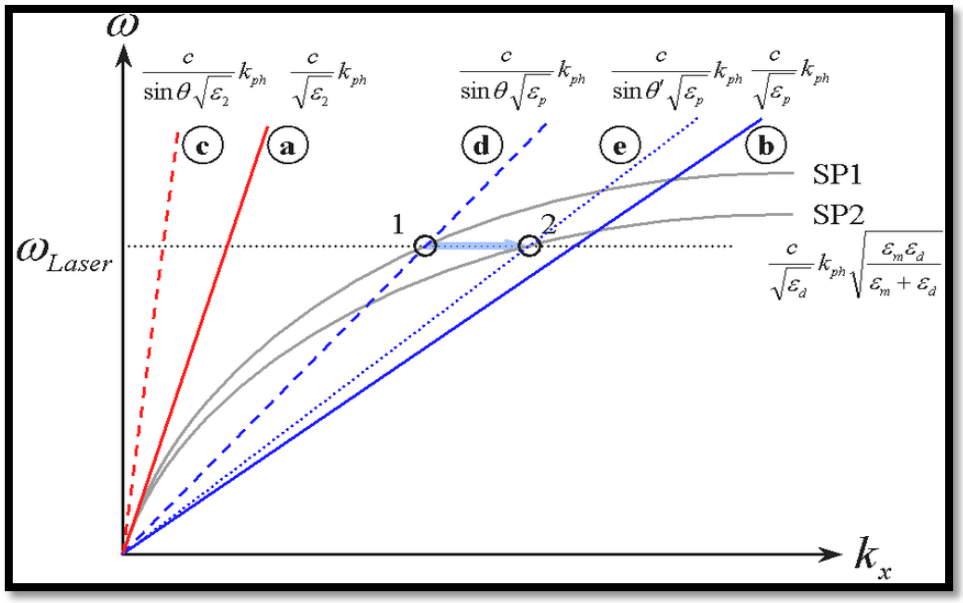

Figure (2-7): Dispersion relation of (a) free photons in a dielectric (red solid line), (b) free photons propagating in prism (blue solid line). (c) is x-component of free photons in a dielectric (red dashed line) and (d) and (e) are x-components of free photons in a prism (blue dashed line and dotted line), respectively. SP1 and SP2 are the dispersion curves of SPs before and after adsorption of an adlayer. 1 and 2 represent the momentum matching points before and after adsorption of an adlayer [77].

2.10 Attenuated total reflection method :

The attenuated total reflection (ATR) method is the widely techniques used to excite SPs. There are two (ATR) methods; the Otto configuration and the Kretschmann configuration, both are shown in Figure (2-8) **[78]**. Both principles are similar, with the exception of the prism location with respect to the metal layer. When an incident light is totally reflected at the bottom of a prism, an evanescent field occurs and this field excites SPs at the interface between a metal and dielectric. However, with the Otto configuration it is difficult to control the distance between a prism and a metal. Consequently, the Kretchmann configuration is used more often **[79]**.

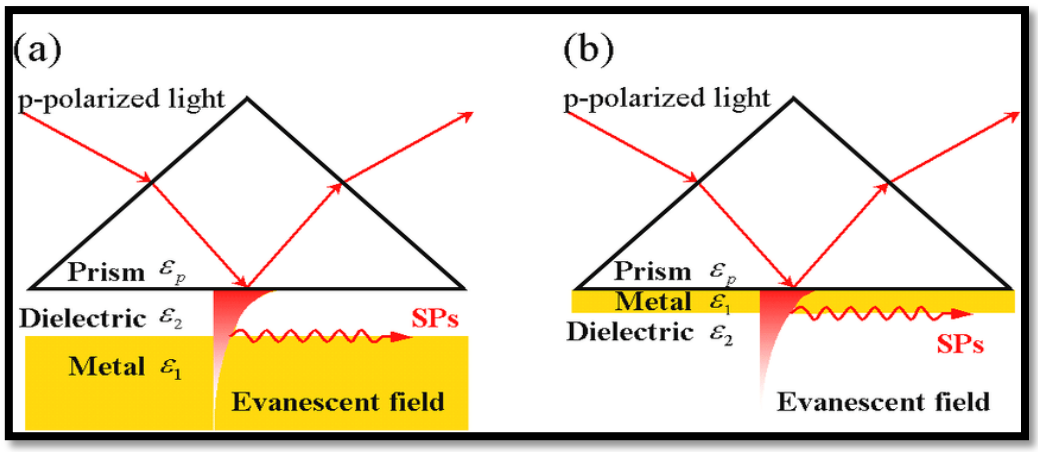

Figure (2-8): Configurations of the attenuated total reflection (ATR) method: (a) Otto configuration and (b) Kretschmann configuration [79].

The wavenumber of light is always smaller than that of SPs. A prism makes it possible to increase the wavenumber of light. If the p-polarized light is incident, the wavenumber of light in a prism is $\frac{\omega}{c}\sqrt{\varepsilon_p}$ and its projection on surface is $k_{ph}^{x} = \frac{\omega}{c}\sqrt{\varepsilon_p}\, sin\theta$ as shown in Figure (2-9). When this projection component, that is the wavenumber of evanescent photons, matches the wavenumber of SPs, SPs are excited **[80]**.

$$k_{ph}^{x} = \frac{\omega}{c}\sqrt{\varepsilon_p}\, sin\theta = \mathrm{k_{sp}} \qquad (2.18)$$

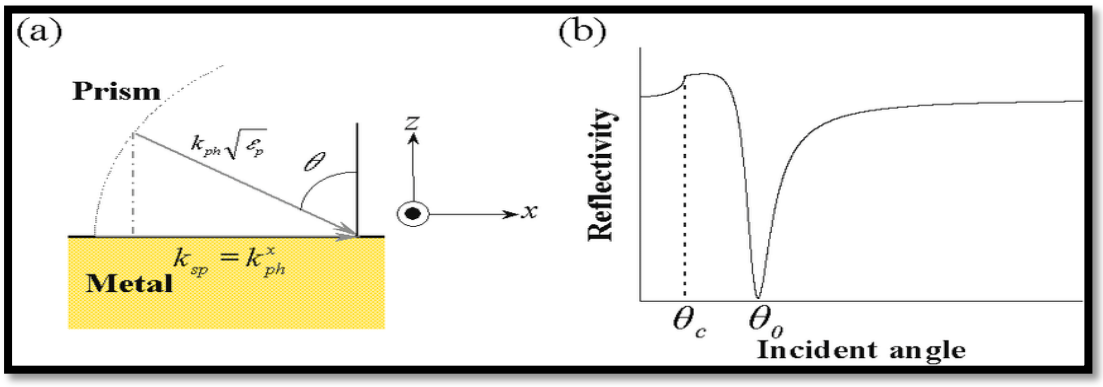

Figure (2-9): (a) A schematic of the momentum matching condition. K_{ph} , k_{ph}^{x} and k_{sp} are the numbers of incident light, x-component of incident light and surface plasmons, respectivelynt angle. (b) ATR scan curve. θc and θ_o are critical angle and resonance angle, respectively [80].

By adjusting the incident angle (θ) to match the wavenumber of the light and SPs [point 1 and 2 in Figure (2-7)], resonance conditions can be obtained. If the dielectric environment is changed, the momentum matching condition is also changed, resulting in the different resonance angle. If the reflectivity is recorded as a function of incident angle, excitation of SPs can be seen as shown in Figure (2-9, b) **[81]**.

2.11 Plasmon exciton coupling :

Controlling light-matter interaction plays a fundamental role in emerging optical phenomena, which have broad applications in optoelectronics, nonlinear optics, lasers, and spectroscopy **[82]**. Cavity quantum electrodynamics (QED) provides quantum mechanical description for these fundamental interactions in confined geometries **[83]**. When an atom is placed in an optical cavity, the resonant modes of the cavity are coupled with electronic transitions of the atom. Trapped ions in high-Q cavities **[84]**, Q-dots in photonic crystal cavities **[85]**, and organic materials with excitonic transitions in optical cavities **[86]** can be understood within the framework of cavity QED. Excitonic materials placed in a plasmonic cavity provide a new platform to study cavity QED **[87]**. Coupling between surface plasmons (SPs) on the metal surfaces **[88]** and excitons in optical materials results in a coupled quantum system **[89]**.

Strength of coupling between two oscillators can be classified in strong and weak coupling regimes. The strength of coupling is characterized by comparing the rate of energy transfer between the matter and the cavity and the decay rates of the individual states **[90]**. When the decay rate is significantly smaller than the rate of energy transfer, strong coupling regime is established **[91]**. Strong coupling between excitons

and SPs forms a coupled hybrid state, which arises when an exciton mode resonates with a plasmon mode **[87]**. Enhanced electromagnetic field of SPs and strong oscillator strength of excitons can provide the necessary conditions for strong coupling. In the weak plasmon-exciton coupling regime, the inherent nature of SPP and exciton modes are not modified and thereby increase the absorption or emission rates of the molecules **[92]**. However, when the coupling is considered to be strong, SPP and exciton modes are modified by forming new coupled modes and hence an anticrossing behavior is observed in the dispersion curve **[93]**. Anticrossing is observed at the energy where both bare plasmon and bare exciton modes resonate at the same frequency **[94]**. As it has been shown theoretically and experimentally, in the strong plasmon-exciton coupling regime, two newly formed energy states are separated by an energy value whose difference in energy is called the Rabi splitting energy. Rabi splitting energy is given by **[95]**:

$$\hbar\Omega_R = \sqrt{4\mathrm{V} - (\Upsilon_p - \Upsilon_e)^2} \qquad (2.19)$$

Where (V) is the coupling parameter,(Υ_p) and (Υ_e) are the line-widths (i.e., damping) of the bare plasmons and bare excitons, respectively. The strength of this interaction determines both the absorption and emission properties of molecules placed near plasmonic structures, effectively governing the optical properties of such a hybrid system **[96]**. Rabi splitting can be tuned in two ways; (i) by varying the excitonic properties of the matter like component (i.e. varying V or Υ_e), or (ii) by controlling the properties of the plasmonic system (i.e. varying Υ_p). Modification of excitonic properties has been demonstrated by varying the optical density of the excitonic system **[97]** on metal surfaces, as well as reversible switching between the weak and strong coupling regimes via a photochemical process, which changes the strength of the dipole moment

[93]. It has been shown that the thickness of the metal films (or the skin depth of the metal) affects the properties of the system under study and thereby control the amount of light absorbed or transmitted by the system **[98]**. For example, a nano-hole array perforated thick metal film greatly boost the transmission of the incident light **[98]**. Conversely, when the thickness of the nanostructured metal film is decreased to around the skin depth of the metal (~20 nm) opposite behavior has been observed, that is, transmission of the incident light is suppressed or, in other words, absorbance of the nanostructured film increases **[99]**. In earlier studies, it has been observed that when the metal film thickness is smaller than the penetration depth of the evanescent wave, absorbance of the metal film has been greatly increased **[100]**. In another study it has been shown that broad band critical coupling of the incident light can be achieved by adjusting the thickness of the metal film . In a similar way, critical coupling has been investigated in coupled molecular and plasmonic cavity arrays **[101]**. Lately, tuning plasmon-exciton coupling and hence the Rabi splitting energy in the strong coupling regime by controlling the plasmon damping has been presented **[94]**. However, plasmon-exciton coupling below the skin depth of the metal has not been studied. In this chapter, tuning of SP-exciton coupling by controlling the damping of the plasmonic component is demonstrated **[102]**. It is possible to tune the Rabi splitting energies ranging from (0 meV) to (150 meV) by varying the plasmonic layer thickness, which defines the damping of the plasmonic mode. Absorption enhancement of the molecules in the weak plasmon-exciton coupling regime is investigated **[103]**. Strength of the plasmon-exciton coupling has been controlled from the weak-coupling regime (exhibiting no anticrossing behavior) to the strong-coupling regime (exhibiting an anticrossing behavior) by plasmonic layer thickness **[90]**. In addition, concentration of the dye molecules is very critical and

determines the transition point from the weak-coupling regime to the strong-coupling regime. The ability to tune the SP-exciton coupling would make this system a promising candidate for a range of new applications **[104]**.

2.12 Fluorescence :

2.12.1 Characteristics of the fluorescence emission:

Fluorescence is a phenomenon that when a molecule is excited by absorption of a photon, it can return to the ground state with fluorescence emission. The various energy levels involved in the absorption and emission of light are presented by a Jablonski energy diagram as shown in Figure (2-10) **[105]**.

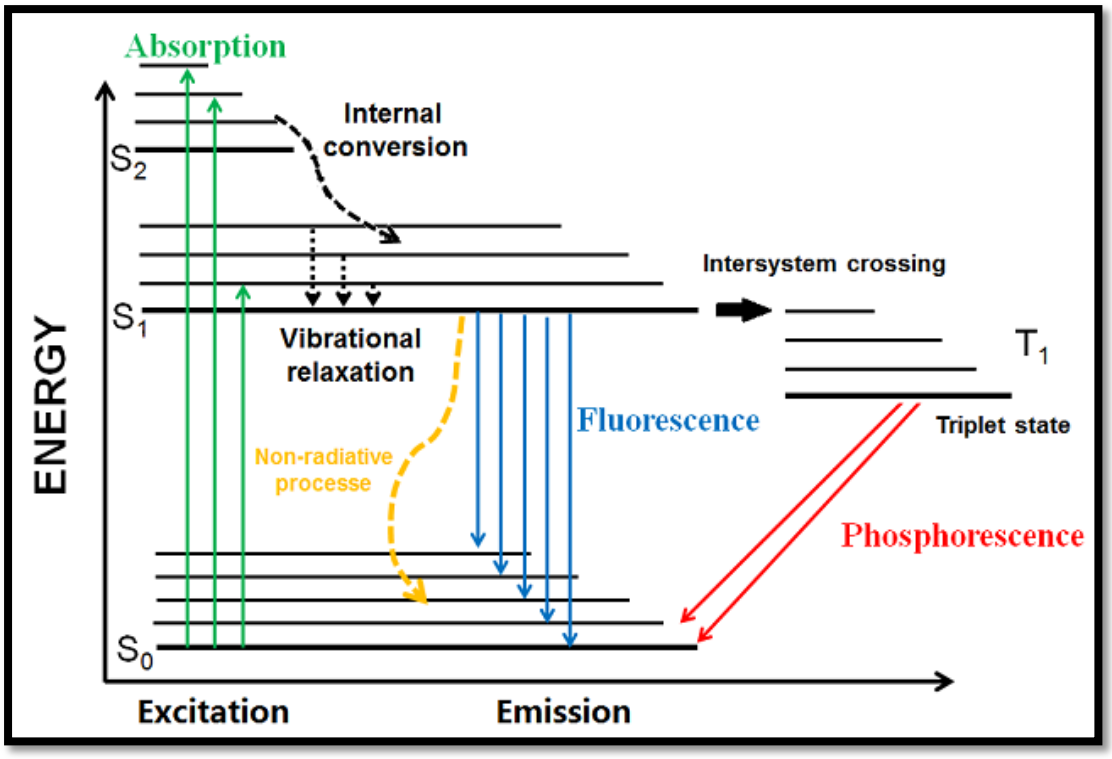

Figure (2-10): Jablonski energy diagram [105].

Three events occur that lead to the process of fluorescence emission: photon absorption, vibrational relaxation and fluorescence. When a molecule absorbs a photon, an electronic transition occurs and a molecule

in electronic grand state (S_o) can be brought to one of the vibrational state (S_1) **[106]**. This absorption process happens in femtoseconds (10^{-15} s). Once a molecule is excited to the vibrational state, vibrational relaxation of excited state electrons to the lowest state occurs in the range of (10^{-14} - 10^{-11}s. The final process, fluorescence that is emission of photons accompanying $S_1 \rightarrow S_0$, occurs in the range of (10^{-9}-10^{-7} s). The molecules undergoing electronic transitions that result in fluorescence are called fluorophores or dyes **[107]**.

An electron transition from the excited state to the ground state does not occur only with fluorescence emission, but also without fluorescence emission. The former process is radiative transition and the latter one is non-radiative transition **[108]**. This non-radiative transition can occur with their rate constants, such as internal conversion (IC, k_{IC}), intersystem crossing (ISC, k_{ICS}), quenching process (k_Q) and resonance energy transfer (RET, k_{RET}) which result in de-excitation of molecules and are related to the fluorescence quantum yield, thus giving an expression of the fluorescence quantum yield (Φ_F) which is the ratio of the number of emitted photons (k_F) to the number of absorbed photons **[108]**:

$$\Phi_F = \frac{k_F}{k_F + k_{IC} + k_{ISC} + k_Q + k_{RET}} \qquad (2.20)$$

Excitation leads to the population of higher electronic state, however the energy of fluorescence emission is smaller than that of excitation because of the energy loss in the excited state due to nonradiative relaxation. Therefore the fluorescence spectrum is located at higher wavelength than the absorption spectrum because molecules in the excited state lose energy due to non-radiation process. This gap between the absorption peak and the fluorescence peak is called Stokes shift **[109]**.

2.12.2 Fluorescence quenching and photobleaching:

Quenching and photobleaching are non-radiative processes to reduce the fluorescence quantum yield. Quenching process can be classified into collisional and static quenching. Collisional quenching occurs when the dyes in the excited state collide with other molecules, resulting in nonradiation relaxation **[110]**. Static quenching occurs when the dyes form a non-fluorescent complex with the quencher molecule in the ground state. In contrast to quenching, photobleaching occurs when a dye loses the ability to fluorescence due to photo-induced chemical damage. This process involves the interaction between dyes and molecular oxygen. Reducing the exposure time of fluorophores can avoid photobleaching **[111]**.

2.12.3 Resonance energy transfer:

Resonance energy transfer (RET) is another process that a donor transfers its excitation energy to an accepter without emission. When a donor and an accepter are separated by less than (10) nm, excitation energy of a donor can be transferred to an accepter. The transfer efficiency is defined as **[112]**:

$$\Phi_T = \frac{1}{1 + (r/R_0)^6} \qquad (2.21)$$

Where (r): is the distance between a donor and an accepter and (R_0): is the critical Förster radius. The transfer efficiency is 50% when the donor-accepter distance is equal to the critical Förster radius **[113]**.

2.12.4 Fluorescence at the metal/dielectric interface:

SPFS uses an evanescent field to excite dyes attached to the metal surface. Figure (2-11) summarizes major three decay channels depending on the distance for fluorophores near the metal surface **[114]**.

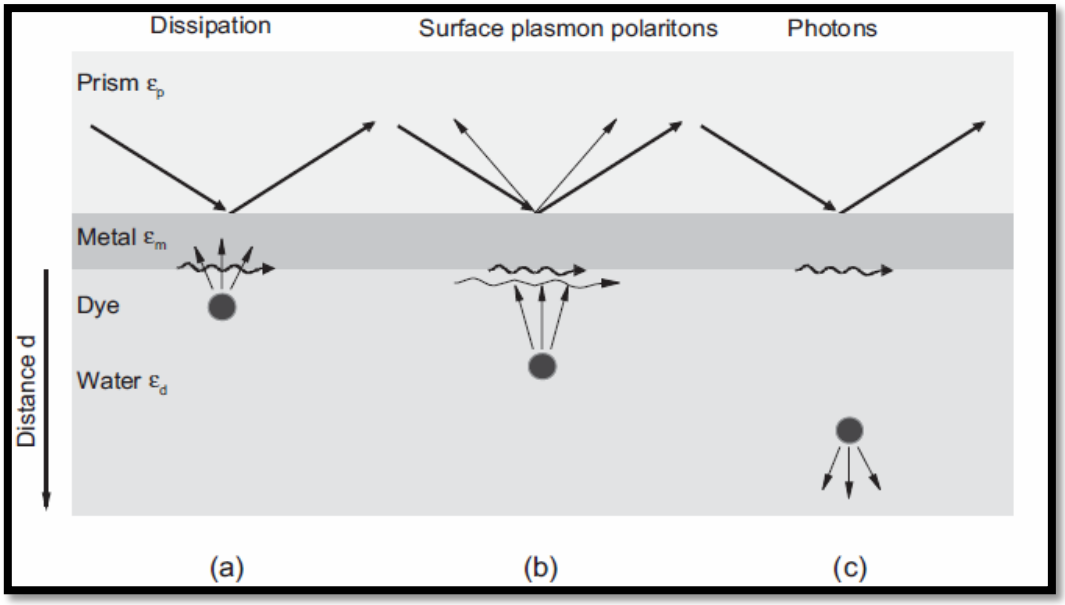

Figure (2-11): Schematic of three fluorescence decay channels depending on dye/metal distances [114].

If a dye is located very close to the metal surface within (10) nm, the fluorescence is quenched due to the dissipation of the energy into the metal as heat (Figure 2-11, a). Therefore non-radiative decay is dominant. In the distance regime below (20) nm, the fluorescence is coupled back to the metal and excites surface plasmons if the momentum matching coundition is satisfied via prism coupling **[115]**. At distance larger than (20) nm, free emission of photons is dominant.

2.12.5 Fluorescence life time:

Fluorescence lifetime (τ_F) can be defined as the average time of the particle residence in the molecular excited state until leaving it by photon emitting .(τ_F) can be described as the inverse of the decay rate as **[116]**:

$$\Gamma = \frac{1}{\tau_F} \qquad (2.22)$$

Where (Γ): is the decay rate. The above equation shows that the rapid rates causes an shortest lifetime **[116]**.

The main reason to rapid fluorescence lifetime (τ_F) decreasing in gain medium in specified cases , is attributed to the energy transition to quenching molecules **[117]**. The increasing particles concentration induces fast decaying of the fluorescence lifetime. A less internal transition radiation decreases the fluorescence lifetime **[118]**.The reduction of fluorescence lifetime causes a clear shift for the laser threshold to higher values . It is an important to note that the laser action has been occurred for gain modes of long lifetime **[119]**.

2.12.6 Quantum Yield:

The quantum yield (Φ) represents the number of absorption times the same photon by the random medium **[118]** . (Φ) can be given as the ratio of the number of photons emitted to the number of photons absorbed **[116]**. The probability of de-activity the excited molecular state by fluorescence mainly , can be named as the quantum yield **[120]**. A high values of quantum yield (Φ) can be obtained at low molecules concentration , while a less value of (Φ) verifies in presence of many quenching impurities or in cases of dye molecules dimerization **[121]**.(Φ) may be controlled by temperature variation for high scattering media of large thermal coefficient **[122]**.

2.13 Laser threshold :

The laser threshold is a very important factor of random lasing, and the threshold depends on the luminescence efficiency of the gain media, and the scattering mean free path of photons in the random media **[123]**. The lasing threshold reduced when the scattering mean free path is equal to or less than the stimulated emission wavelength **[124]**. The concentration of scatters can influence the threshold when increasing the

concentration of the scatters particles, and the lasing threshold decreased **[125]**. The lasing threshold also depends on the refractive index of the scatters compared to that of the surrounding media, and is reduced when the refractive index of the scatters is increased or the refractive index of surrounding media is decreased **[126]**. To reduce the lasing threshold in random laser, metal nanoparticles are used as the scatters, these nanoparticles can induce surface plasmon resonance, and spatially confine the light near the surface to enable a high gain. The metal nanoparticles have large scattering cross-section **[127]**.

When pumping the sample with a low power, is which less than the lasing threshold, a single peak of spontaneous emission will appear. While, when increasing the pump power, the emission decay time decreases quickly. Many spikes appeared due to the existence of large number of modes **[128]**.

3.1 Introduction :

This chapter presents the materials that used in the research, the method of preparing the samples, and the measuring devices that used in the study, in addition to a comprehensive scheme that indicate all the scientific steps that were followed in this research.

3.2 Chemical materials that used in the experimental part:

Raw material	Chemical Formula	Vendor	Purity
Rhodamine B (RhB)	$C_{28}H_{31}ClN_2O_3$ 479.02 g/mol	USA , Sigma - Aldrich	Without further purification
Silver	Ag	Germany , Sigma - Aldrich	99.9%
Silver nanowire	Ag NW	XFNANO	99.9%
Gold	Au	Germany , Sigma - Aldrich	99.9%
Distilled water	H_2O 18 g/mol	---	---
Polydimethylsiloxane (PDMS)	$(C_2H_6OSi)_n$	Germany , Sigma -Aldric	99%
polyvinylpyrrolidone (PVP)	$(C6H9NO)_n$	USA , Sigma - Aldrich	99%

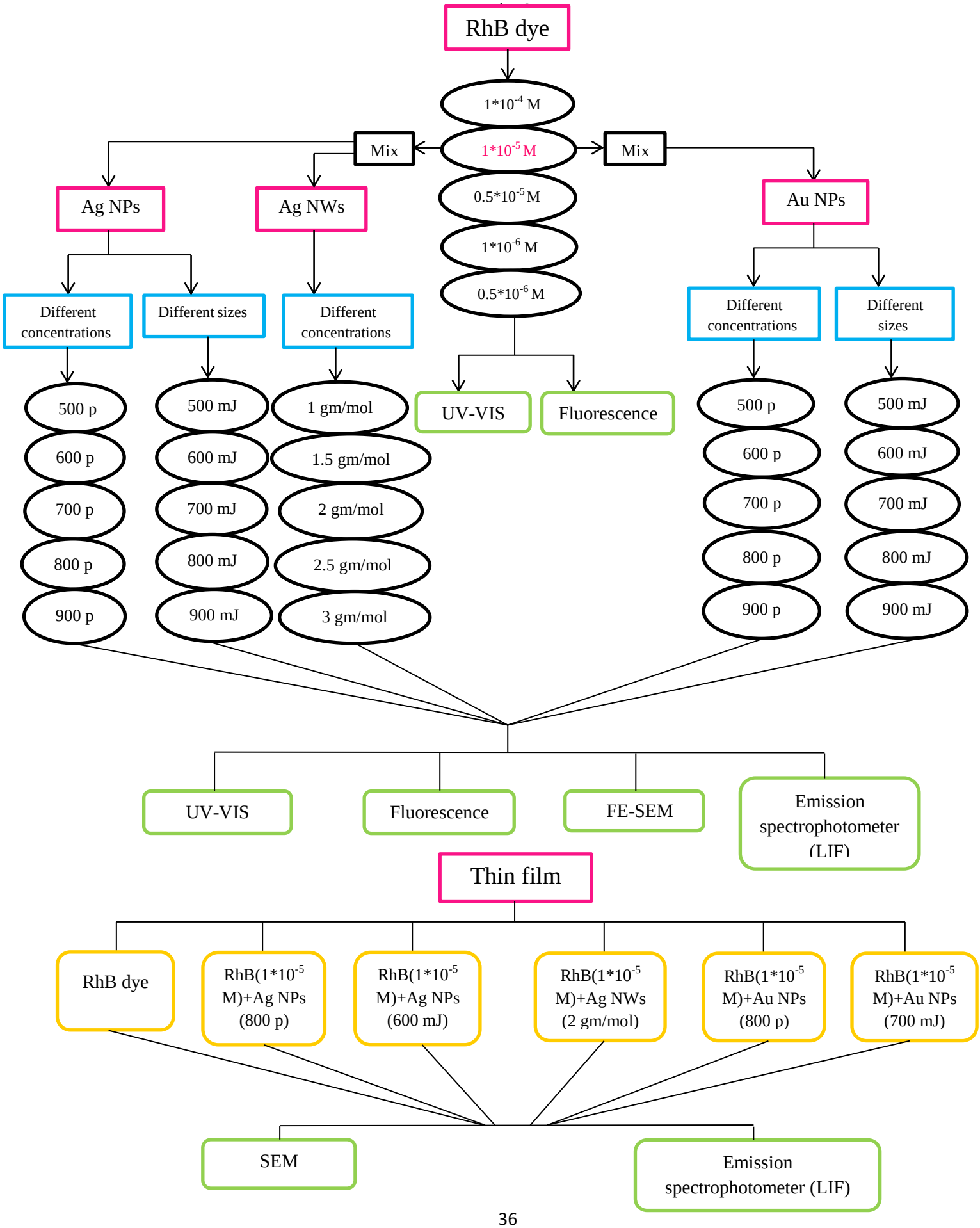
RhB dye
1*10-4 M
Mix
1*10-5 M
Mix
0.5*10-5 M
1*10-6 M
0.5*10-6 M
Ag NPs
Ag NWs
Au NPs
Different concentrations
Different sizes
Different concentrations
Different concentrations
Different sizes
500 p
600 p
700 p
800 p
900 p
500 mJ
600 mJ
700 mJ
800 mJ
900 mJ
1 gm/mol
1.5 gm/mol
2 gm/mol
2.5 gm/mol
3 gm/mol
UV-VIS
Fluorescence
500 p
600 p
700 p
800 p
900 p
500 mJ
600 mJ
700 mJ
800 mJ
900 mJ
UV-VIS
Fluorescence
FE-SEM
Emission spectrophotometer (LIF)
Thin film
RhB dye
RhB(1*10-5 M)+Ag NPs (800 p)
RhB(1*10-5 M)+Ag NPs (600 mJ)
RhB(1*10-5 M)+Ag NWs (2 gm/mol)
RhB(1*10-5 M)+Au NPs (800 p)
RhB(1*10-5 M)+Au NPs (700 mJ)
SEM
Emission spectrophotometer (LIF)

3.3 Dye preparation :

In this research, (Rh B dye) was used, whose chemical formula ($C_{28}H_{31}CIN_2O_3$), and molar mass (479.02 gm/mol) and appearance of red powder, it was dissolved (0.0099 gm) from the dye in (20 ml) of water to transform to a red solution, by this equation:

$$w = \frac{C \times V \times M}{1000} \dots\dots\dots\dots\dots\dots\dots\dots\dots\dots (1)$$

Where:

w: the dye weight (gm).

C: the dye concentration (M).

V: the solvent volume (ml).

M: the molecular weight of the solution (gm/mol).

To obtain different concentration of (Rh B), ($1*10^{-4}$, $1*10^{-5}$, $0.5*10^{-5}$, $1*10^{-6}$, $0.5*10^{-6}$) M ,it is used the dilution formula:

$$C_1 V_1 = C_2 V_2 \dots\dots\dots\dots\dots\dots\dots\dots\dots\dots (2)$$

Where:

C_1: the concentration of the original solution.

V_1: the volume of the original solution.

C_2: the concentration of the diluted solution.

V_2: the final volume of the diluted solution.

Figure (3-1) shows these concentrations. It was studied the absorption spectrum of these samples by using UV-VIS spectrometer, and then the emission spectrum by using fluorescence spectrometer.

Figure (3-1): A different concentration of RhB dye.

3.4 Ag and Au Nanoparticles preparation :

Two different kinds of noble metals NPs are prepared, such as Ag and Au NPs (Ag and Au target (>99.99% purity, Sigma Aldrich, Germany) with a thickness of (1) and (2) mm respectively, by laser ablation in liquids (LAL) method, figure (3-2) using second harmonic Q-switched Nd: YAG laser (532 nm) with a different pulse number (500, 600, 700, 800, 900) p, and then with a different pulse energies (500, 600, 700, 800, 900) mJ , the pulse width of (5) ns and repetition rate of (1–10) Hz. These samples are prepared at a fixed energy and variable repetition rate and a fixed repetition rate of (10) Hz. In the LAL setup, the laser light is focused on a rotated Au and Ag metal target in a deionized water (6 ml). The field emission scanning electron microscope (FE-SEM) is used to investigate the size and shape of the produced NPs. For obtaining the SPR response, UV–VIS absorption spectra of the samples were recorded.

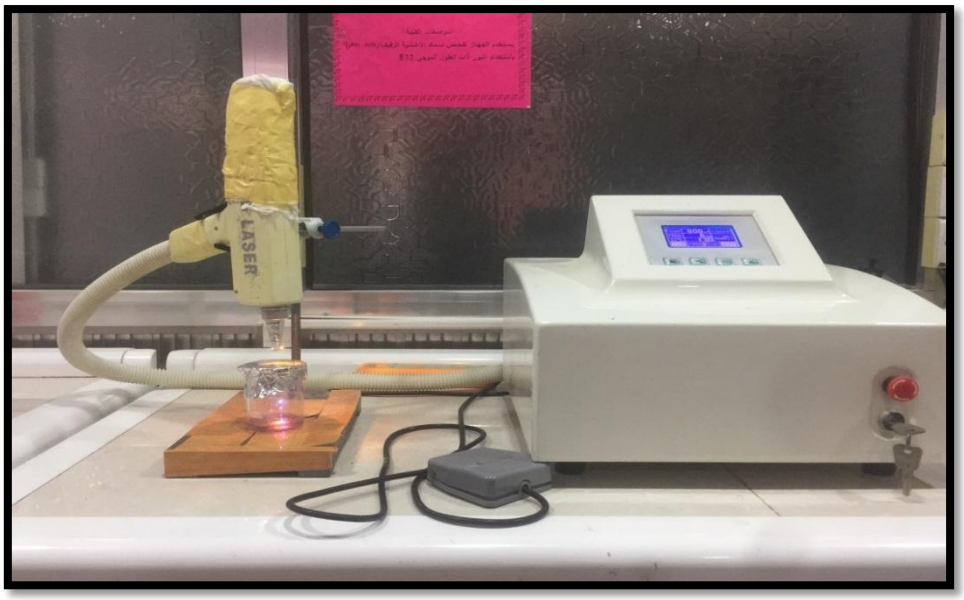

Figure (3-2): The experimental setup that is used for Ag and Au nanoparticles preparation by LAL.

3.4.1 Ag and Au Nanoparticles preparation with different concentrations :

To get different concentrations of Ag, Au NPs, it was changed the pulse number (500, 600, 700, 800, 900) p and keep the energy constant at (600 mJ), and studied the absorption spectrum, figure (3-3) (a) and (b).

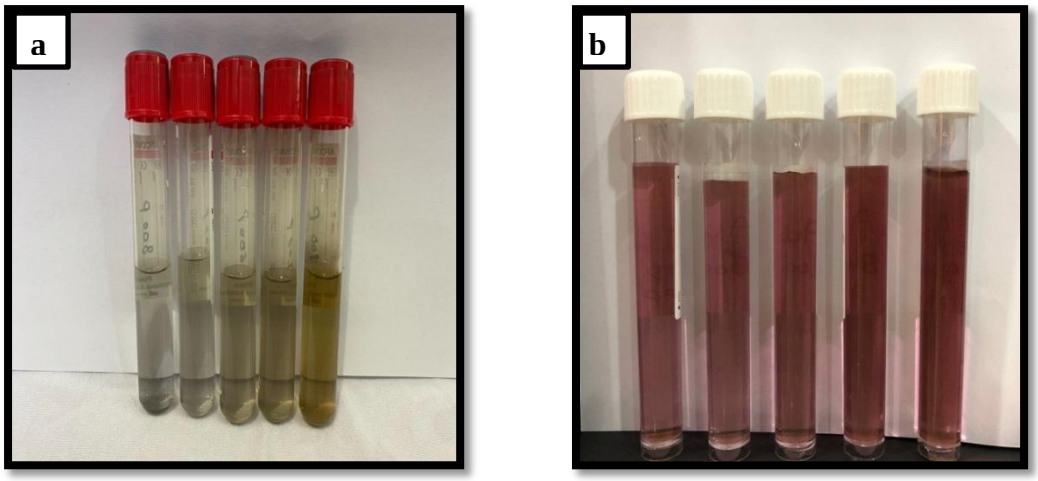

Figure (3-3): (a) Ag NPs, (b) Au NPs.

3.4.2 Ag and Au Nanoparticles preparation with different sizes :

To get different sizes of Ag NPs, it was changed the energy (500, 600, 700, 800, 900) mJ and keep the pulse number constant at (400 p), and studied the absorption spectrum, figure (3-4) (a) and (b).

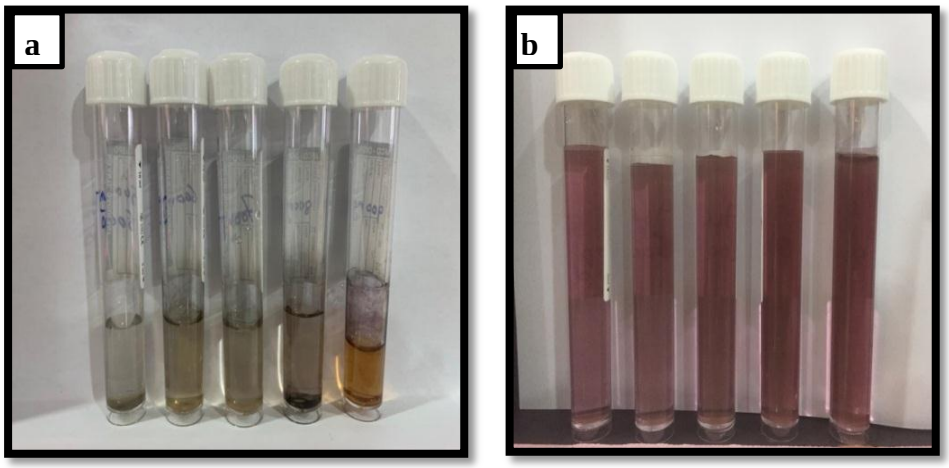

Figure (3-4): (a) Ag NPs, (b) Au NPs.

3.5 Ag NWs :

Silver nanowires (Ag NWs) are purchased from XFNANO with an average diameter of (90 nm) and length of (1) micron (500 mg dissolved in 25 ml water), where the concentration is (~ 0.2 M) It was used different concentration of Ag NWs (1, 1.5, 2, 2.5, 3) gm/mol, and studied the absorption spectrum.

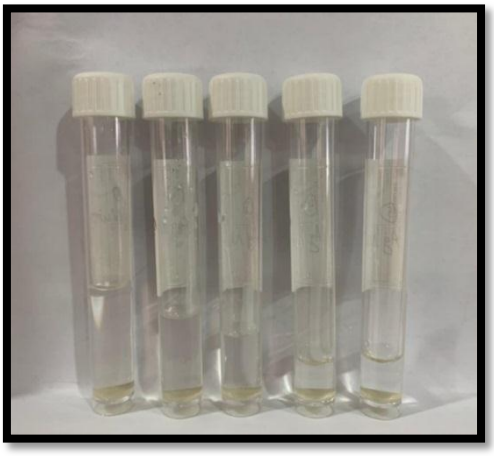

Figure (3-5): Different concentrations of Ag NWs.

3.6 Mixing (RhB with:Ag NPs, Ag NWs and Au NPs) :

(2 ml) of better concentration of RhB ($1*10^{-5}$ M) are mixed with (1 ml) of different concentration of Ag NPs, and studied the absorption, emission, and plasmonic spectrum.

Also, it was mixed (RhB with different sizes of Ag NPs), (RhB with different concentrations of Ag NWs), (RhB with different concentrations of Au NPs), (RhB with different sizes of Au NPs), in the same proportion as explained before, and studied the absorption, emission, and plasmonic spectrum.

3.7 Thin film preparation :

Two-dimensional charged coupled camera (CCD) were prepared as the main stamp. It was deposited RhB dye mixed with (50%) of gold nanoparticles, were employed as the active materials. RhB with different concentration and thicknesses has been deposited onto 2D nano grating.

3.7.1 Fabrication of RhB into 2D Nano grating :

It was studied a new multilayer structure that introduced as the main gain media including polydimethylsiloxane (PDMS) substrate/ Gold Nano rods covered by the Rhodamine B (RhB) as the first gain media and it was covered by PVP polymer.

First, Au NPs were prepared by laser ablation in the liquids (LAL) method by using the second harmonic of Q-switched Nd: YAG laser (pulse width of 5 ns and repetition rate of 10 Hz) with fixed energies per pulse. RhB dye ($1*10^{-5}$ M) was employed as an active material, and the Au NPs and RhB were mixed with the volume ratio of (50%) Au NPs and (50%) RhB. To obtain homogeneity, the mixed sample was stirred at the room temperature in an Ultrasonic bath for (20 min). In the next

procedure, a water solution of PVP was prepared with a concentration of (4.4) mg/mL. Two-dimensional plasmonic crystals were implemented as a periodic metallic structure to use its plasmonic band gap. In this process, a high-quality two-dimensional grating was extracted from the commercial grating of the cameras to make a mold. Then, PDMS and its curing agent with the aspect ratio of (10:1) were mixed and poured on the mold. For degassing, the mold was put in the vacuum to remove bubbles. Subsequently, the mold containing PDMS on its top was placed on the heater at the average temperature of (80°C) for about 1 hour. After cooling down, the patterned PDMS layer was removed from the mold using a scalpel, and after that, by soft lithography processes coating the surface of 2D with 30 nm gold layer as a plasmonic substance as shown in figure (3-6, a). Afterward, the chip was ready for covering the first dye, PVP, and last dye as follows. RhB of (200 nm) with (50%) Au NPs was spin-coated onto the 2D plasmonic nanostructure with the speed of (1500 rpm). Accordingly, PVP film was spin-coated onto the RhB layer at the speed of (2000 rpm). The thickness of the PVP layer was thinner than the above and below layers in order to excite the waveguide modes, as shown in figure (3-6, b).

Finally, the second harmonic generation of Nd: YAG laser was utilized to pump the samples and collect the lasing by the spectrometer to obtain the plasmon phenomenon.

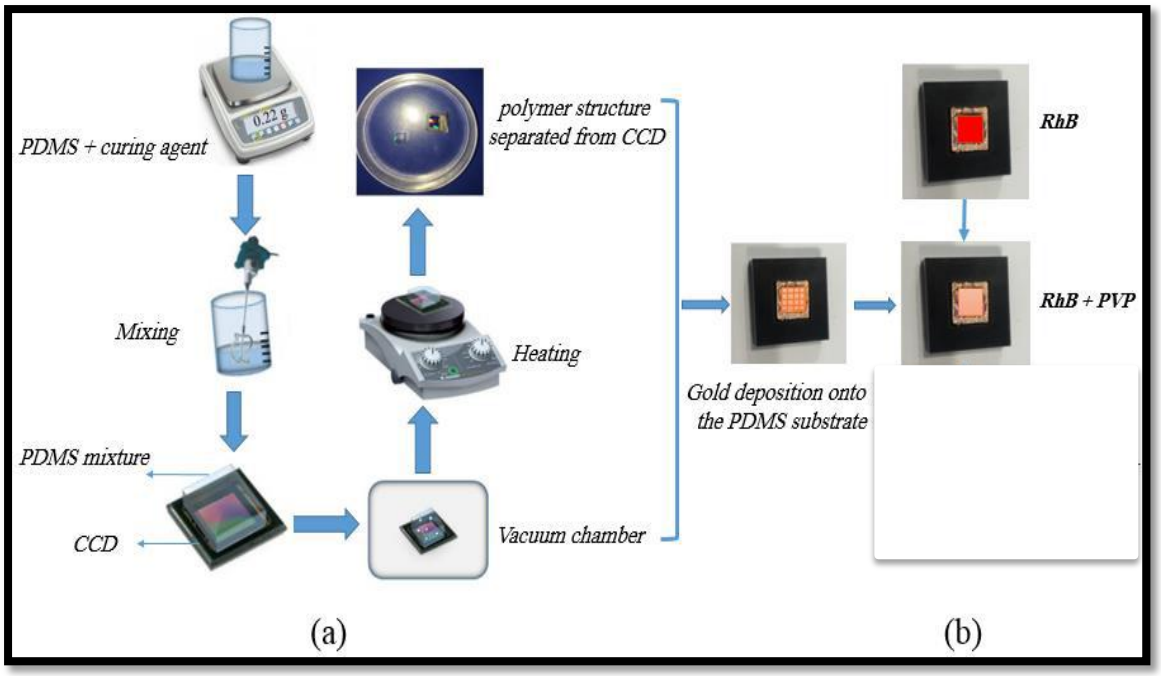

Figure (3-6): (a) Prepared sample after the deposition of gold onto the PDMS substrate and deposit onto 2D CCD, (b) Fabricated multilayer structure onto the substrate.

3.7.2 Fabrication of RhB with different concentrations into 2D nano grating :

Two-dimensional plexitonic structures have been prepared by nanoimprint lithography as a convenient technique of fabrication nanometer-scale patterning with low cost and high resolution. In this method, a thin layer of polydimethylsiloxane (PDMS) mixed with curing agent, which considered as a polymer in silicone elastomer and characterized by its high flexibility, was used as a substrate placed on camera's CCD forming the 2D nano-grating and allowing the deposition of a dye layer and finally (30 nm) gold layer on it (the details of these samples construction have been explained in (3.7.1).

Coating dyes, as exitonic subsystems, on 2D sample, done by spin coating. By this method, Rhodamin B (RhB) used here, can be combined

with polyvinylpyrrolidone (PVP), which can act as a polymer for increasing the viscosity.

Three samples were produced at different concentrations of RhB with one percent concentration of PVP. These solutions (composition) (0.44 mL) of RhB, were dissolved in methanol with concentration (10^{-3}, 10^{-4} and 10^{-5} M), with (4.4 mg/ml) of PVP. In this situation, spin coating take place optimally with (3000) round per minute (rpm), (30 seconds) concomitant (20 μL) of dye solutions. The schematic diagram of the final 2D sample is shown in figure (3-7).

Finally, to get the plasmonic phenomenon, it was used the second harmonic generation of Nd: YAG laser to pump the samples and get the emission spectra by the emission spectrophotometer (LIF).

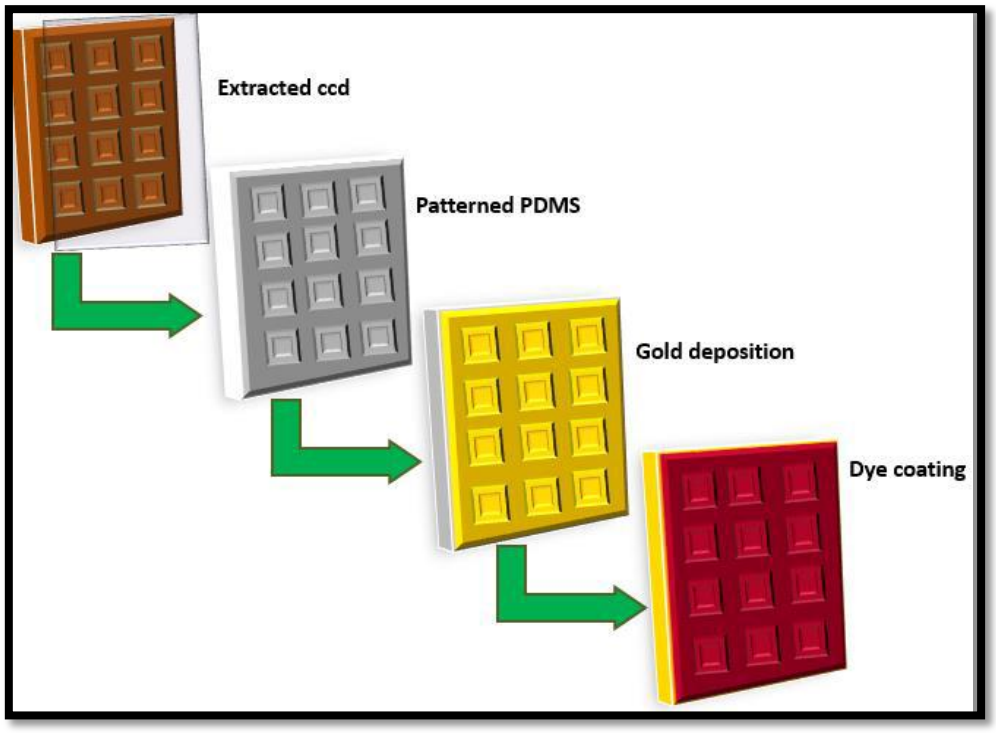

Figure (3-7): Schematic diagram of construction processes 2D plexcitonic structures.

3.8 The experimental devises :

In this research, various devises are used in order to study the improvement of the laser output of the laser active media (dye lasers).

3.8.1 UV-VIS spectrometer :

The absorption spectrum was measured by using (UV-VIS spectrometer). This spectrometer covers a wide range of the electromagnetic spectrum, from (UV to NIR). The figure (3-8) represents the device that contain two excitation sources:

(a) Deuterium lamp: that covers the range of wavelengths (190-360) nm.
(b) Tungesten lamp: that covers the range of wavelengths (360-1100) nm.

It is possible to use the both lamps to cover the ranges (UV-VIS) spectrum. The device contain a monochromator to select the wavelength that excite the sample, also it contain a grating, filters according to the desired wavelength, and a detector from a type of (PMT), and power supply. The idea of measurement depends on the basis of separation the incident beam into two beams, one of them passes through the sample, and the other to the solvent that represents the reference.

Finally, the device record the absorption spectrum to the samples.

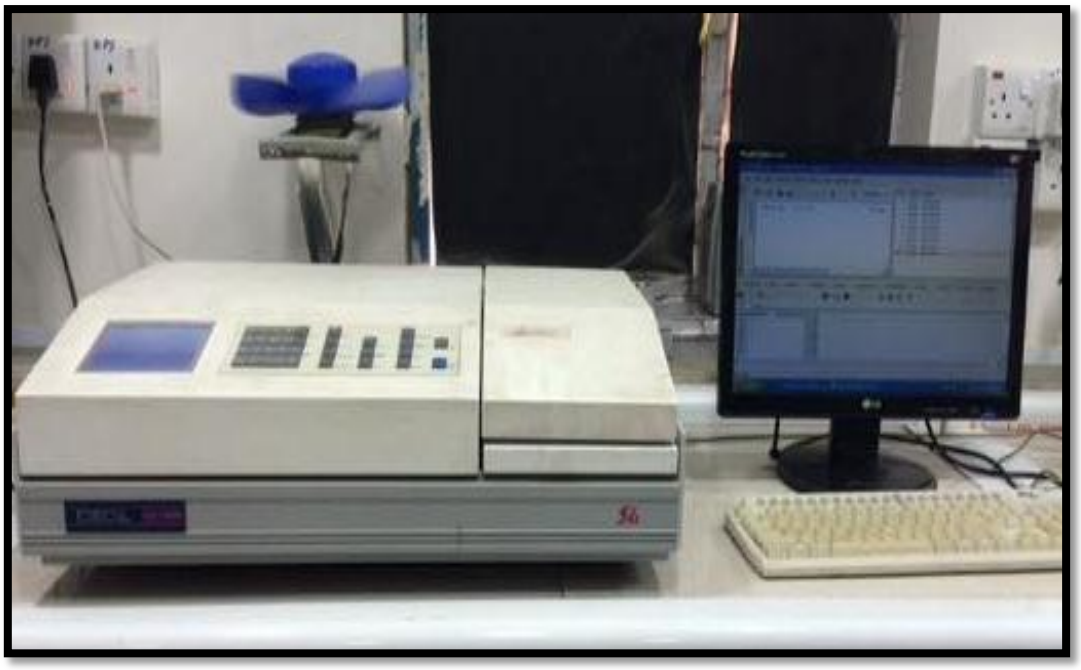

Figure (3-8): UV-VIS spectrometer.

3.8.2 Fluorescence spectrometer :

The emission spectrum was measured by using the fluorescence spectrometer, from a type of (F96PRO), figure (3-9) represent it.

It contains a light source of (xenon arc lamp 150 watt), excitation and emission spectrum rate of (200-700) nm, scanning rate of (200,400,600) nm/min, detector of high sensitivity photomultiplier tube (PMT), and computer.

Figure (3-9): Fluorescence spectrometer.

3.8.3 Emission spectrophotometer (laser induced fluorescence) (LIF) :

Laser Induced Fluorescence (LIF) is an optical spectroscopic technique where a sample is excited with a laser, and the fluorescence emitted by the sample is subsequently captured by a photodetector. LIF can be understood as a class of fluorescence spectroscopy where the usual lamp excitation is replaced by a laser source. Whilst lasers are now routinely used as excitation sources in photoluminescence spectrometers.

To obtain a plasmon spectrum to these samples, (532 nm) Nd:YAG pulsed laser was used with a repetition rate of (10 Hz), and a pulse width of (5) ns during (30) seconds for sample illumination as shown in figure (3-10). In this experimental setup, the sample was exposed to pulsed laser with and without external AC voltage, and the emission light were collected by the computer-connected spectrometer in (40) degree relative to the pumping direction.

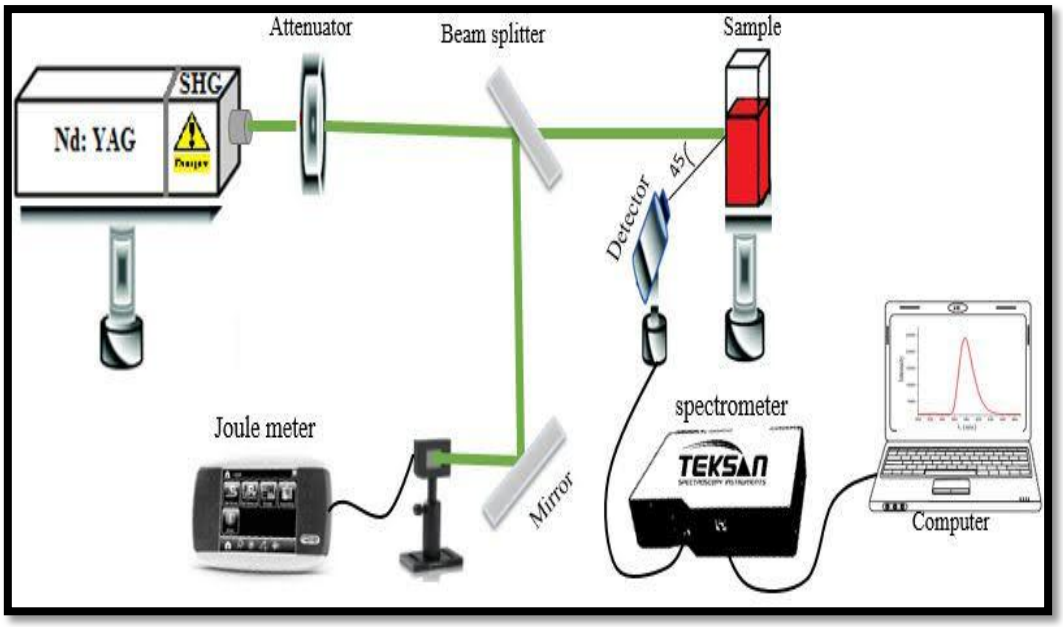

Figure (3-10): Emission spectrophotometer (LIF).

3.8.4 Field Emission Scanning Electron Microscope (FESEM) :

It is a type of electron microscope that produces images of a sample by scanning the surface with a focused beam of electrons. The electrons interact with atoms in the sample, producing various signals that contain information about the surface topography and composition of the sample.

By field emission scanning electron microscopy (FE-SEM) the topography of prepared films was studied and also investigate the nanoparticles shape, size. It was used the field emission scanning electron microscopy (FE-SEM) of (ΣIGMA, JSM-7610F, Carl Zeiss, Germany) image operating at an accelerating voltage of (10 kV). And also, it is used (FE-SEM) model of (MIRA TESCAN) operating at an accelerating voltage of (25 kV), as shown in figure (3-11).

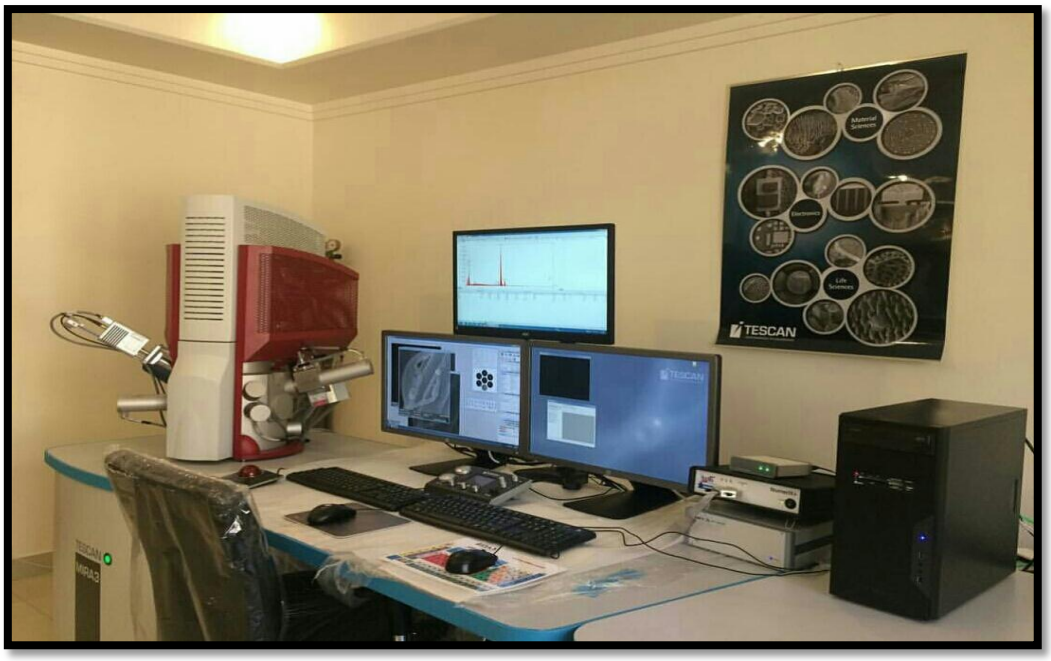

Figure (3-11): Schematic of a: FE-SEM device.

Before the test, all the samples must be cleaned and dried. The time of FE-SEM takes about (4 to 5) minutes to reach the operational vacuum is (10^{-5}) mbar. And as it is known, when it wanted to test the particle size, the scanning electron microscopy electron beam will produces charges on the top surface of the sample, which cannot access a high image resolution, and thus size of the particle cannot be measured, this problem can be eliminated by covering the top surface of the sample with a gold coating to assist the discharging of the top surface charge.

4.1 Introduction :

This chapter presents the results obtained from mixing (RhB with Ag NPs, Ag NWs, Au NPs), and studied the absorption spectrum of these samples by using UV-VIS spectrometer, the emission spectrum by using fluorescence spectrometer, and then the plasmonic spectrum by using the emission spectrophotometer (LIF).

Also, studied 2D nano grating deposited with (RhB with Ag NPs, Ag NWs, Au NPs) and studied the localized surface plasmon and surface plasmon polariton.

4.2 Spectral properties of RhB, Ag NPs and Ag NWs:

4.2.1 Absorption spectra of Rhodamine B dye:

Figure (4-1) represents the absorption spectra of RhB dye with different concentrations. It was noted that by increasing the concentrations of the dye, that leads to an increase in the absorbance peak, related wavelength and the bandwidth of the absorption spectra. Where, noted that the absorption of RhB at (553 nm), and the best absorbance at the concentration ($1*10^{-5}$ M). The behavior of the absorption spectra with the increasing of dye concentration can explained as the highest values of the dye molecules in the lower energy level consolidates the absorption probability per time ,so the largest contribution by molecules in absorption appears in the wide absorption band width.

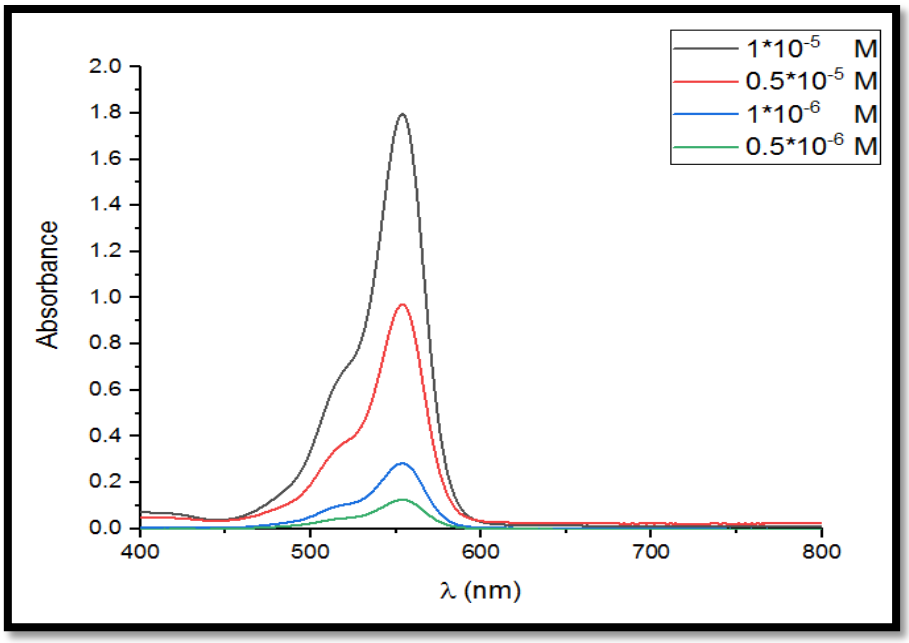

Figure (4-1): Absorption spectra of RhB dye with different concentrations.

4.2.2 Fluorescence spectra of Rhodamine B dye:

The fluorescence spectrum of RhB dye is studied with different concentrations, represented in figure (4-2). It was noted that by increasing the concentration of the dye, the emission spectra will increase, and got the red shift. The emission spectra was sharply decreased at the concentrations ($1*10^{-5}$,$1*10^{-4}$ M) because of quenching process that refers to any process which decreases the fluorescence intensity, many dyes undergo self-quenching, which can decrease the brightness of the dye for fluorescence spectroscopy.

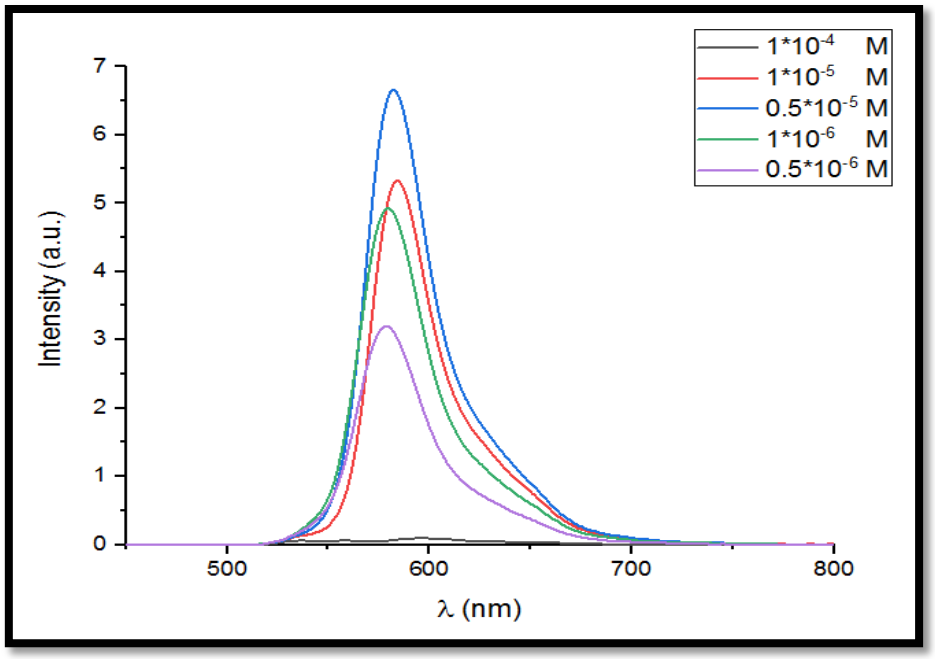

Figure (4-2): Fluorescence spectra of RhB dye with different concentrations.

4.2.3 Structure characterizations of metallic nanoparticles :

The Field Emission Scanning Electron Microscopes (FE-SEM) of NPs and NWs which dropped onto the glass slide show, the formation of Ag and Au nanoparticles of different concentration (different pulses) of size range (30-50) nm, figure (3-4, a,b,e,f), Ag, Au NPs for different sizes (differet energies) of size range (100-200) nm, figure (3-4, c,d,g,h) , and Ag NWs of the concentration (1,2,3 gm/mol), figure (4-3, i,j,k).

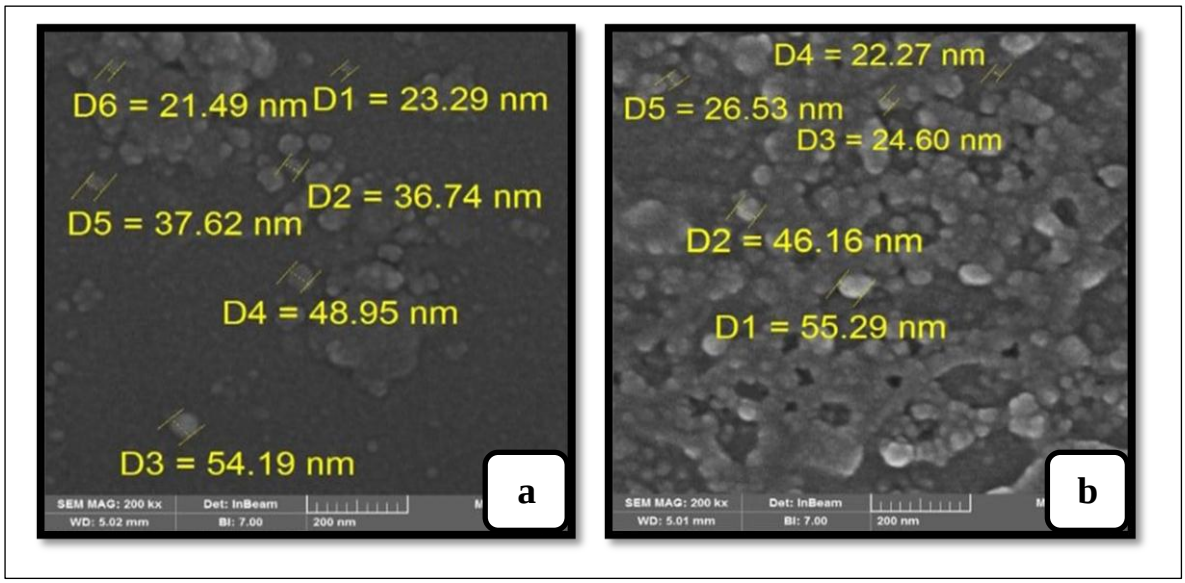

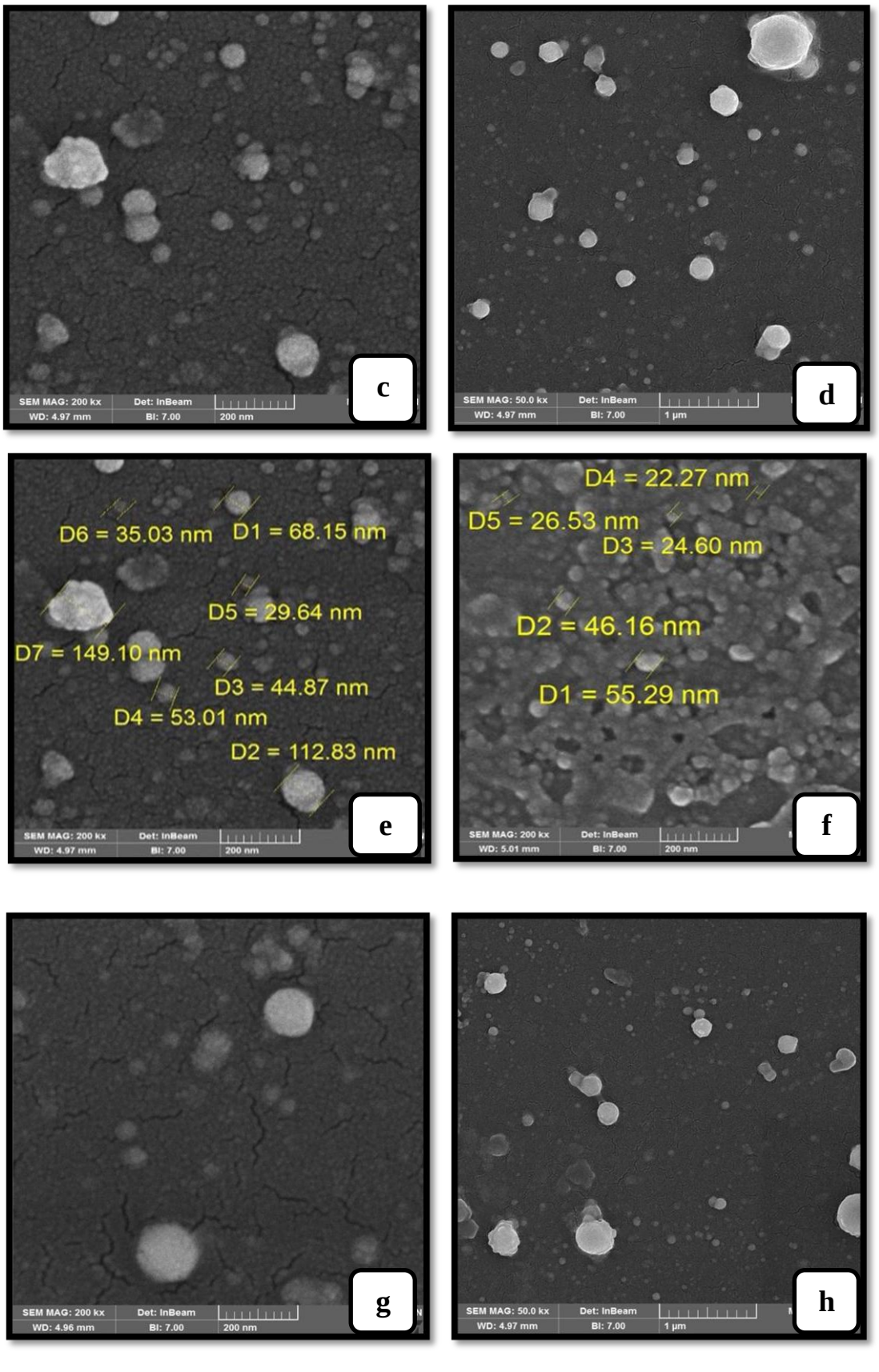
SEM MAG: 200 kx
Det: InBeam
WD: 4.97 mm
BI: 7.00
200 nm
c
SEM MAG: 50.0 kx
Det: InBeam
WD: 4.97 mm
BI: 7.00
1 µm
d
D6 = 35.03 nm
D1 = 68.15 nm
D5 = 29.64 nm
D7 = 149.10 nm
D3 = 44.87 nm
D4 = 53.01 nm
D2 = 112.83 nm
SEM MAG: 200 kx
Det: InBeam
WD: 4.97 mm
BI: 7.00
200 nm
e
D4 = 22.27 nm
D5 = 26.53 nm
D3 = 24.60 nm
D2 = 46.16 nm
D1 = 55.29 nm
SEM MAG: 200 kx
Det: InBeam
WD: 5.01 mm
BI: 7.00
200 nm
f
SEM MAG: 200 kx
Det: InBeam
WD: 4.96 mm
BI: 7.00
200 nm
g
SEM MAG: 50.0 kx
Det: InBeam
WD: 4.97 mm
BI: 7.00
1 µm
h

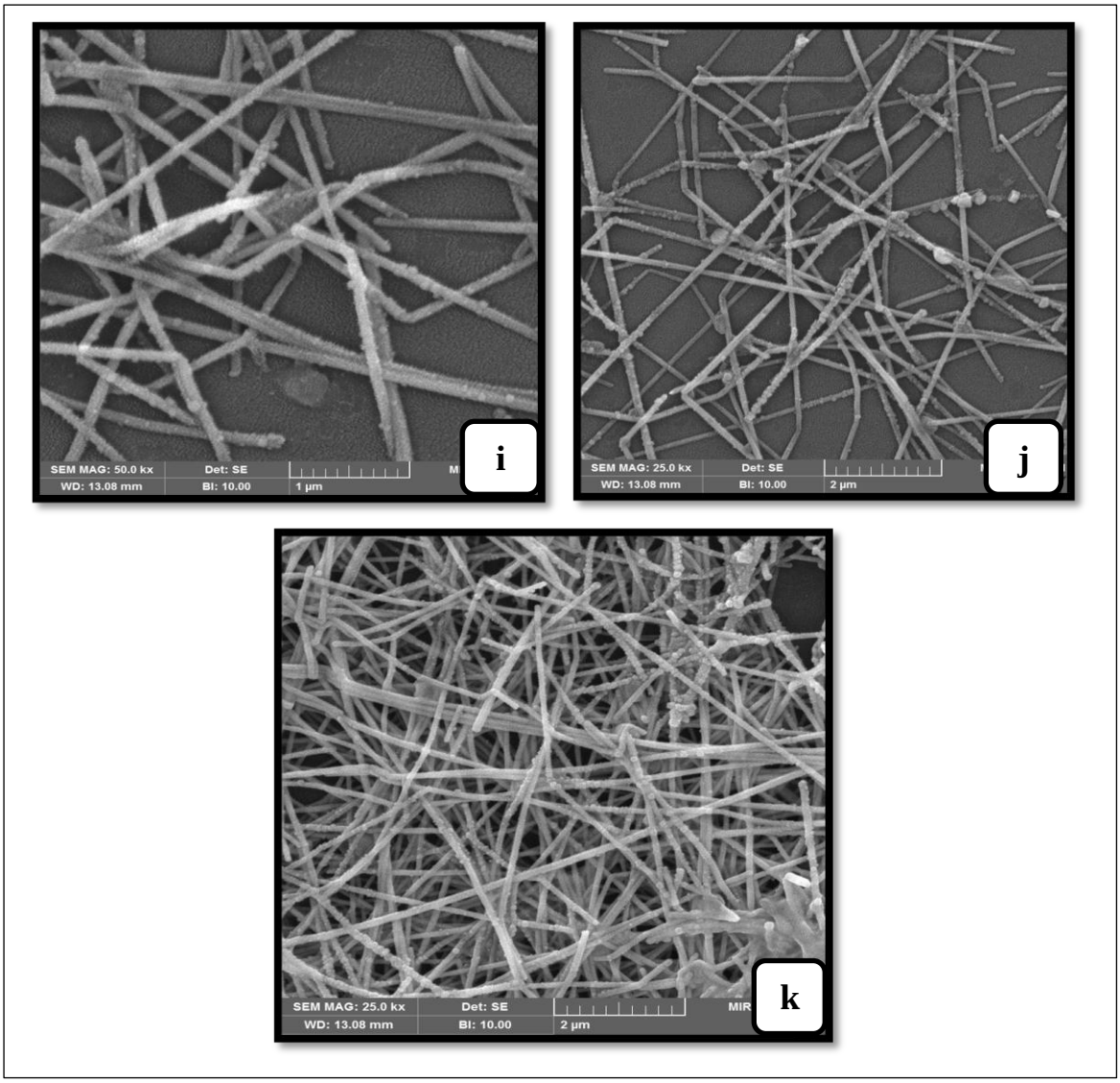

Figure (4-3): FE-SEM image of Ag NPs (a: 500 p, b: 900 p, c: 500 mJ, d: 900 mJ) , Au NPs (e: 500 p, f: 900 p, g: 500 mJ, h: 900 mJ) and Ag NWs (i: 1 gm/mol, j: 2 gm/mol, 3 gm/mol).

4.2.4 Absorption spectra of Ag NPs with different concentrations :

It is clear in figure (4-4), that the absorption spectra of Ag NPs with different concentrations. It was noted that by keeping the energy constant at (600 mJ) , and changing the number of pulses (500, 600, 700, 800, 900) p, that helps to get a different concentration of Ag NPs. Where, noted that the absorption of Ag NPs at (395 nm), It is obvious that

increasing of absorption spectra due to the increases of Ag NPs concentration, and noted that the absorbance increased significantly at the last concentration due to the large increase in the concentration of the nanoparticles.

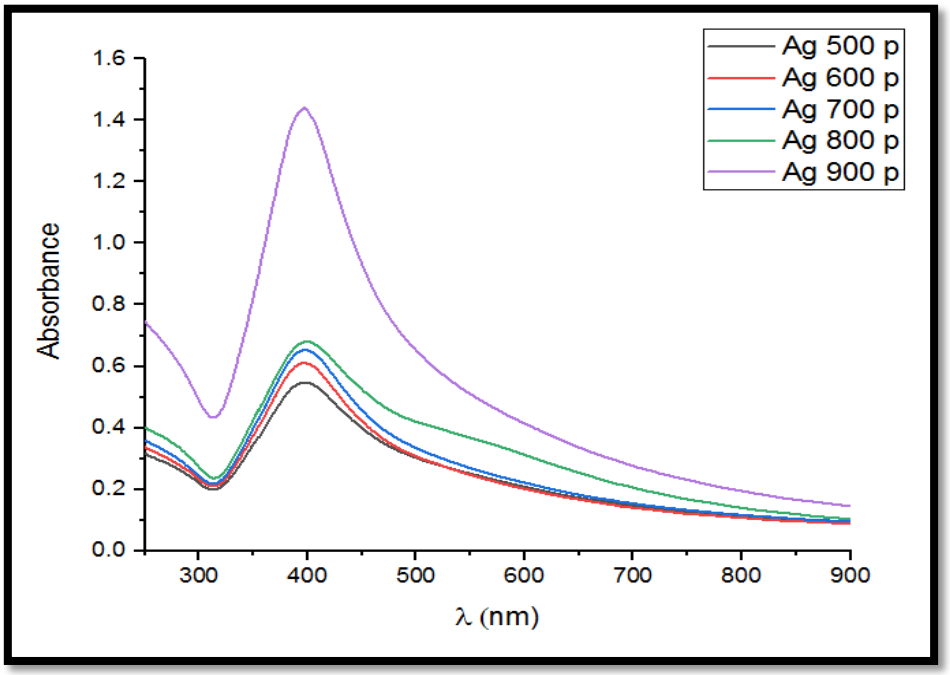

Figure (4-4): Absorption spectra of Ag NPs with different concentrations.

4.2.5 Absorption spectra of RhB mixed with different concentrations of Ag NPs:

The better concentration of RhB dye ($1*10^{-5}$M) was chosen to mix with different concentrations of Ag NPs, figure (4-5) represents the absorption spectra of this mixture. It shows that by adding the nanoparticles to the dye, leads to a decrease in the absorption band width due to the highest contribution of the lower energy particles in absorption, in the same time lowest contribution of dyes in absorption, also, the enhancement of lasing emission in the samples containing Ag NPs is attributed to the increase of the local field in the vicinity of the silver NPs. Noted that the effect of increasing the concentration of NPs on the

dye is obvious in the mixture RhB ($1*10^{-5}$ M) + Ag NPs (900 p), got a high absorption of the Ag NPs at (395 nm).

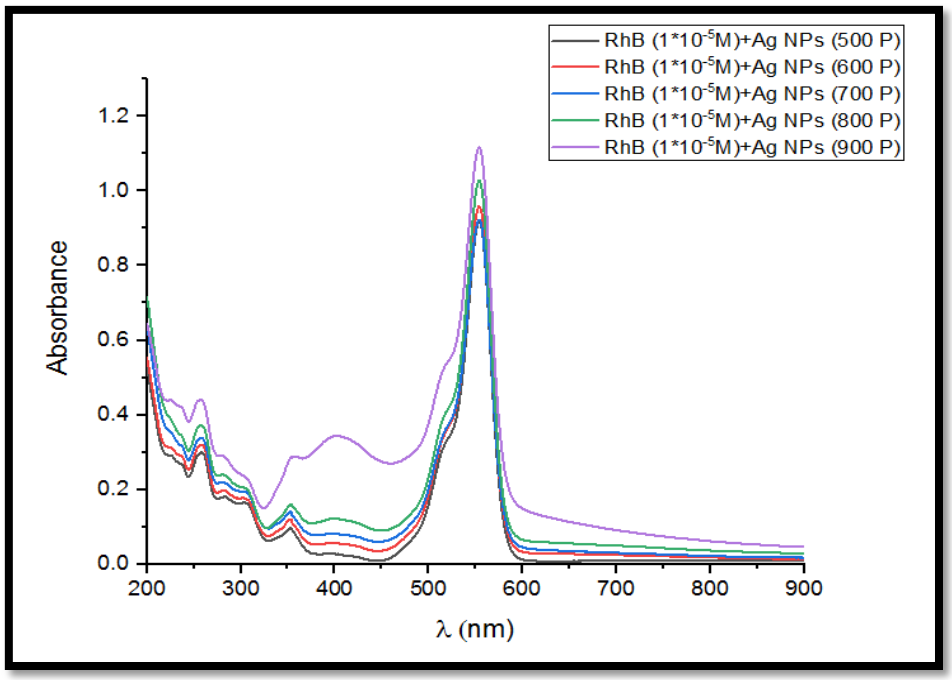

Figure (4-5): Absorption spectrum of RhB dye ($1*10^{-5}$ M) mixed with different concentrations of Ag NPs.

4.2.6 Fluorescence spectra of Rhodamine B mixed with different concentrations of Ag NPs:

The fluorescence spectra of RhB dye ($1*10^{-5}$M) mixed with a different concentrations of Ag NPs represented in figure (4-6). It was noted that by increasing the concentration of Ag NPs that mixed with RhB dye, the emission spectra will increase, and got the blue shift. The quenching process is appeared at (RhB+ concentration of Ag NPs at 900 p), due to reaching the saturation limit, which led to decrease in the fluorescence.

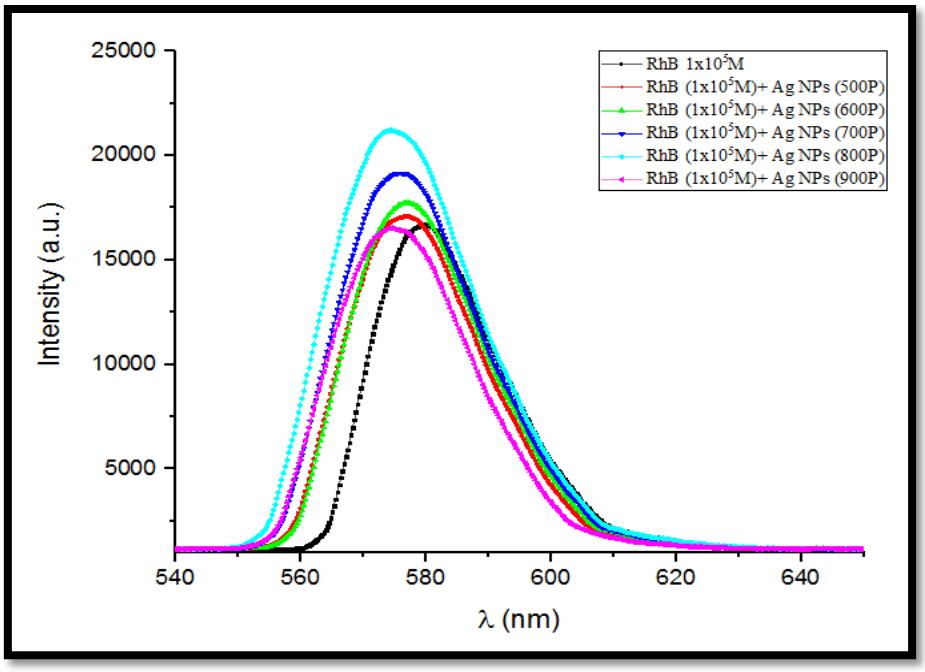

Figure (4-6): Fluorescence spectra of RhB dye ($1*10^{-5}$M) mixed with different concentrations of Ag NPs.

4.2.7 Plasmonic phenomenon in emission spectra (LIF) of (Rhodamine B dye) and RhB mixed with different concentrations of Ag NPs:

The emission spectra of RhB dye ($1*10^{-5}$ M) represented in figure (4-7, a), it shown that the highest intensity was (10000 a.u.). However, the plasmonic phenomenon is clear in the emission spectra of the mixture of RhB dye ($1*10^{-5}$ M) with the Ag NPs in different pulses, shown in figure (4-7) (b, c, d, e, f). It was showed the plasmonic that is an optical phenomena that results from interaction of conduction free electrons of noble metal nanoparticles with electromagnetic waves (especially at visible optical frequencies) and collective oscillation called as surface plasmon, nevertheless, figure (4-7) (b, c, d, e, f) show the intensity of the final peak as a function of pump energy, where, the highest intensity at figure (4-7,b) (lower concentration of Ag NPs mixed with RhB dye) is

(16000 a.u),while, at figure (4-7,c) the intensity was increased (25000 a.u), and then the intensity continued to increase at figures (4-7,d,e), (33000, 50000 a.u) respectively. Finally, the quenching process is clear in figure (4-7,f), where the intensity decreased to be (16000 a.u). This shows that the increase in the concentration of Ag NPs leads to increase the plasmonic intensity, and the localized surface plasmon phenomenon of the emission spectrum is appear.

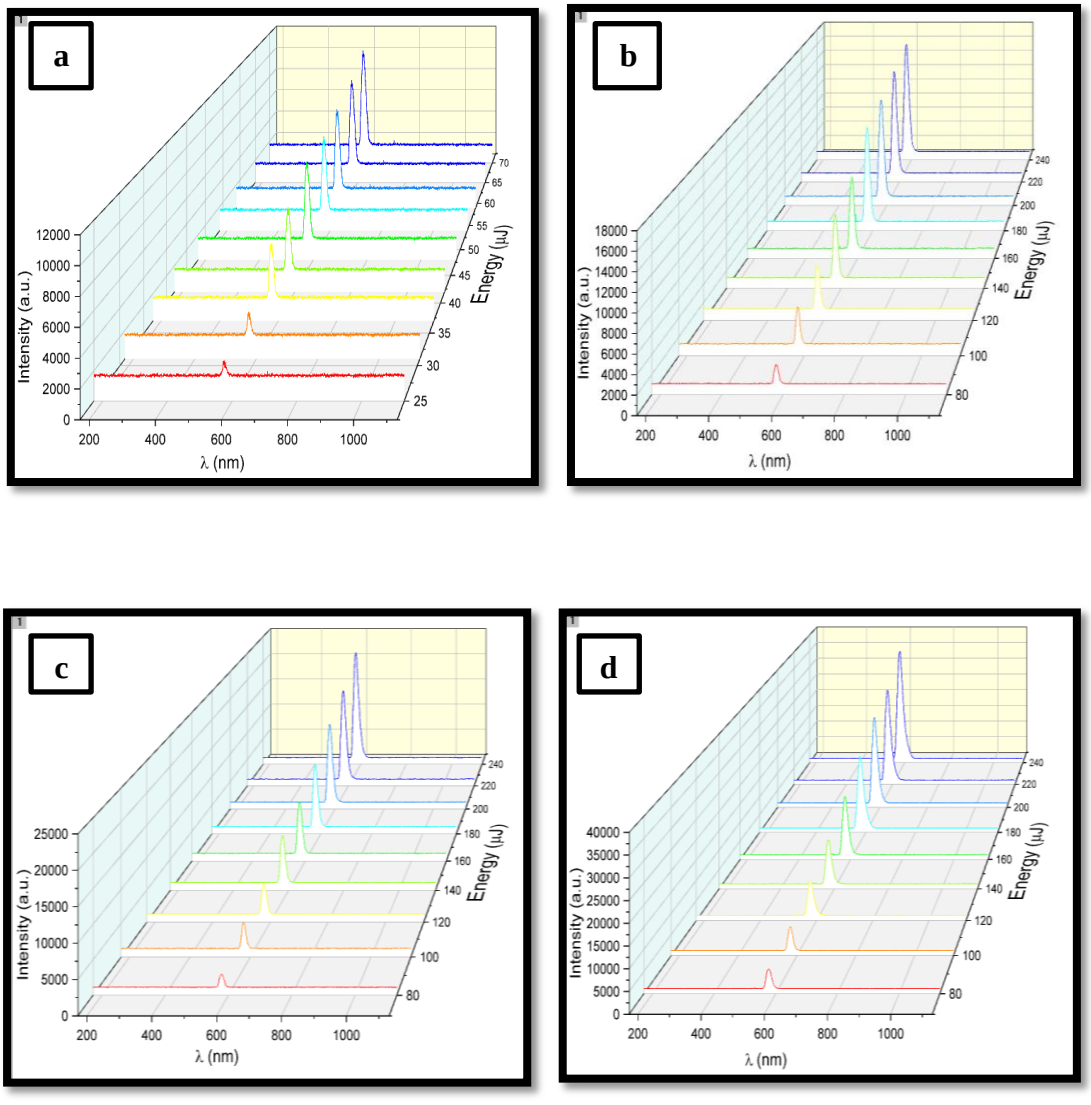

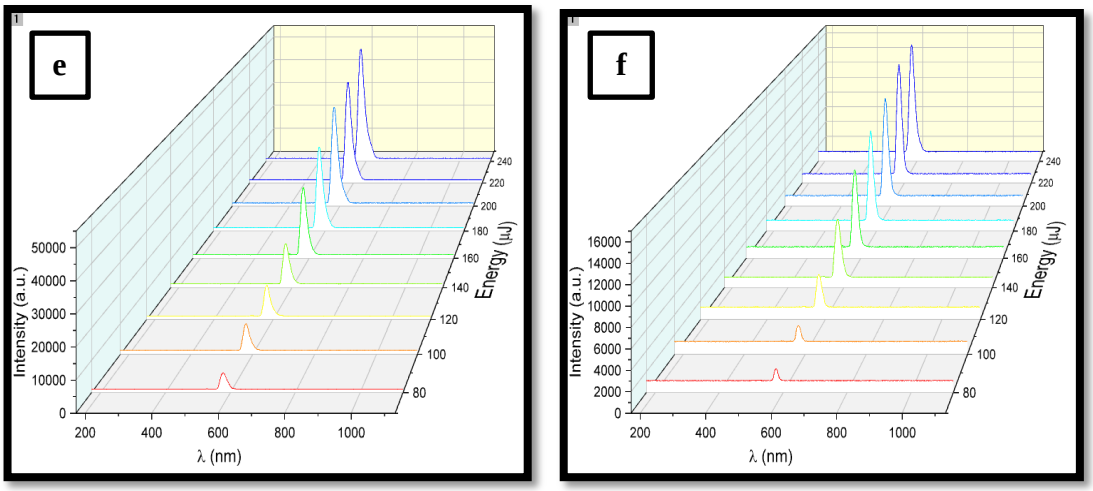

Figure (4-7): Emission spectra (LIF) of (a) RhB dye ($1*10^{-5}$M) only, and RhB dye ($1*10^{-5}$M) mixed with Ag NPs at (b) 500 p , (c) 600 p , (d) 700 p, (e) 800 p ,(f) 900 p.

The threshold of all above samples (RhB dye $1*10^{-5}$ M) and (RhB dye $1*10^{-5}$ M mixed with different concentrations of Ag NPs) is clear in figure (4-8), where the threshold of RhB dye is (42 µJ) and the threshold of the lowest concentration (500 p) is (42 µJ), while the threshold of (800 p) is (31 µJ), this shows that the threshold is decreases by increasing the concentration of Ag NPs. While, the quenching is clear at (900 p) to be (42 µJ) due to the increasing of the NPs overwhelms the dye fluorescence. Noted that when the sample was RhB dye only, the intensity was low and the threshold was large, while, by adding the nanoparticles to the dye, the intensity was increased but the threshold was decreased. Table (4-1) represents the parameters characteristics of RhB dye ($1*10^{-5}$ M), and RhB ($1*10^{-5}$ M) mixed with different concentrations of Ag NPs.

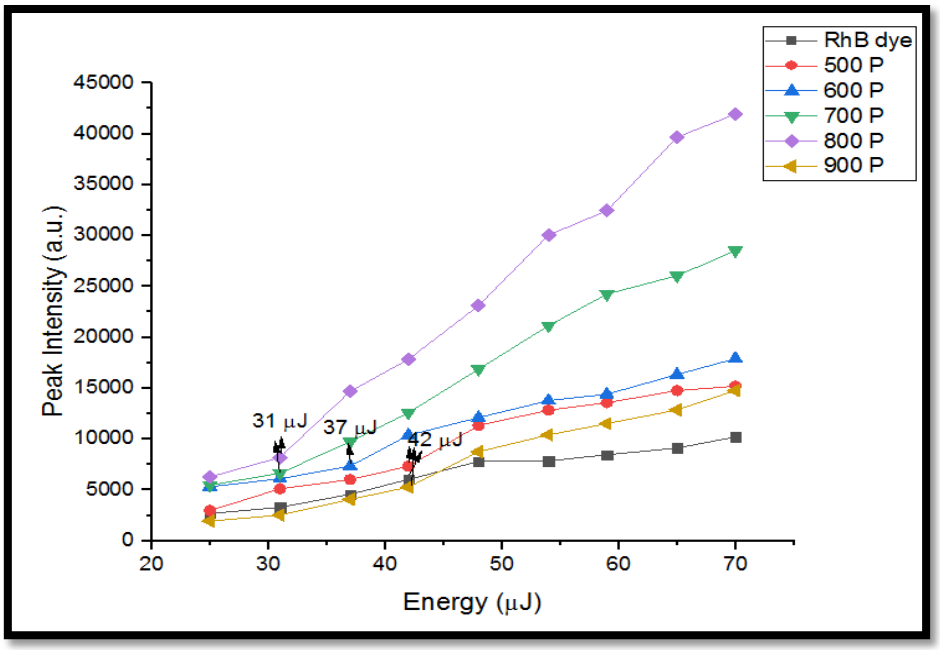

Figure (4-8): Threshold of (RhB dye 1*10^{-5}M) and (RhB dye 1*10^{-5}M mixed with different concentrations of Ag NPs).

Table (4-1): The parameters characteristics of RhB dye (1*10^{-5} M), and RhB (1*10^{-5} M) mixed with different concentrations of Ag NPs.

Samples	Lasing threshold (µJ)	Intensity (a.u.)
RhB dye (1*10^{-5}M)	42	10000
RhB(1*10^{-5}M) + Ag NPs (500 p)	42	16000
RhB(1*10^{-5}M) + Ag NPs (600 p)	37	25000
RhB(1*10^{-5}M) + Ag NPs (700 p)	31	33000
RhB(1*10^{-5}M) + Ag NPs (800 p)	31	50000
RhB(1*10^{-5}M) + Ag NPs (900 p)	42	16000

4.2.8 Absorption spectra of Ag NPs with different sizes :

The absorption spectra of Ag NPs with different sizes is clear in figure (4-9). It was noted that by changing the energy (500, 600, 700, 800, 900) mJ, and keep the pulse number constant at (400 p), that leads to increase the absorption spectra. Noted that the absorbance increased significantly at the last concentration due to the large increase in the size of the nanoparticles.

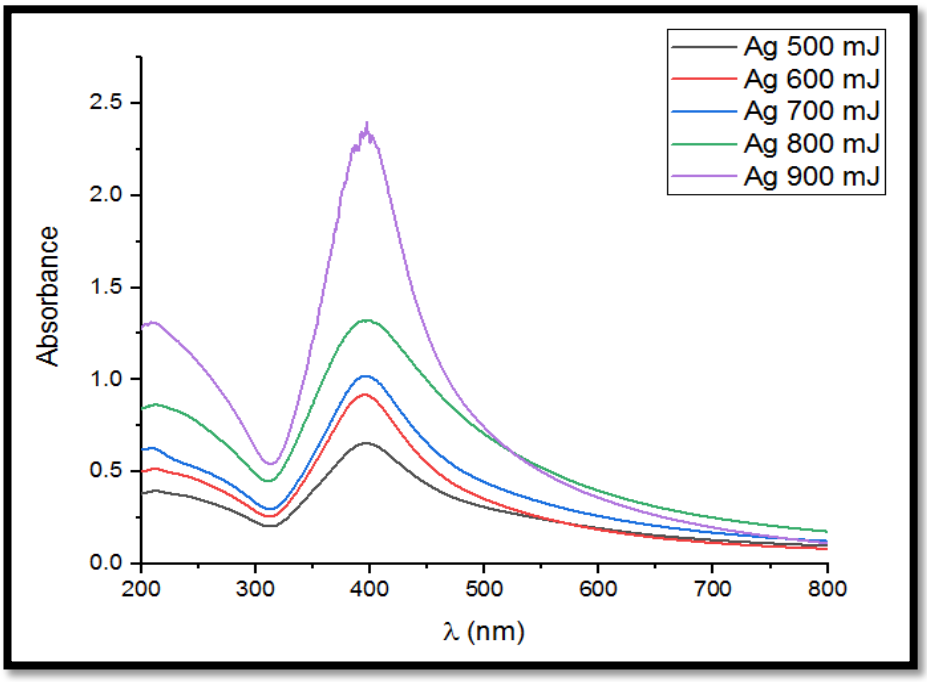

Figure (4-9): Absorption spectra of Ag NPs with different sizes.

4.2.9 Absorption spectra of RhB mixed with different sizes of Ag NPs:

The absorption spectra of RhB dye (best concentration $1*10^{-5}$ M) mixed with different concentrations of Ag NPs represented in figure (4-10). It is obvious that by adding the nanoparticles to the dye, that leads to increase in the absorption spectra, except the last mixture (RhB $1*10^{-5}$ M

+ Ag NPs 900 mJ) decreased because of the increase in the nanoparticles size.

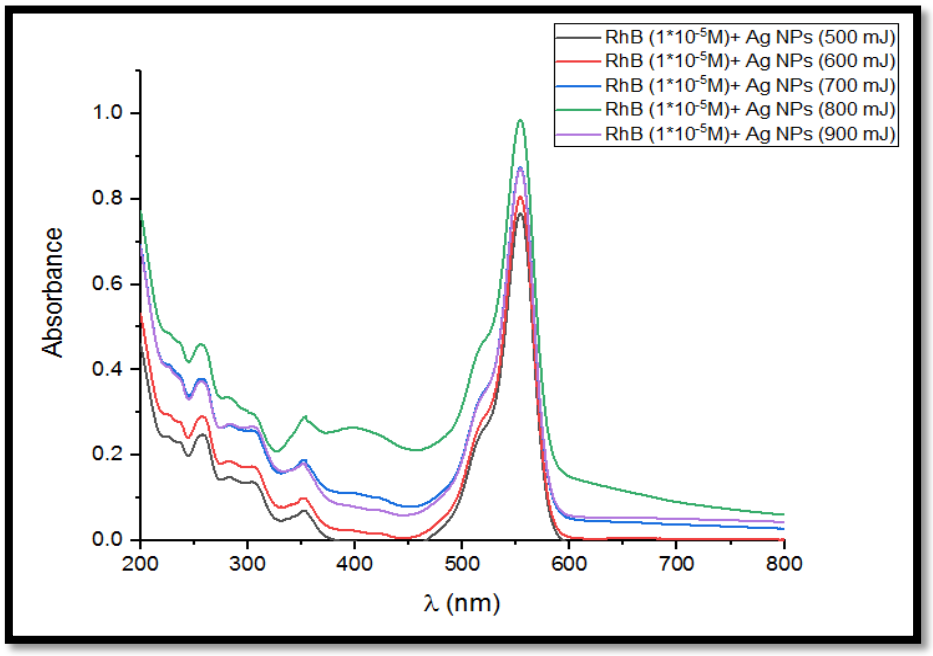

Figure (4-10): Absorption spectra of RhB dye ($1*10^{-5}$ M) mixed with different sizes of Ag NPs.

4.2.10 Fluorescence spectra of Rhodamine B mixed different sizes with Ag NPs:

The fluorescence spectra of RhB dye ($1*10^{-5}$M) mixed with a different sizes of Ag NPs represented in figure (4-11). It was noted that by increasing the sizes of Ag NPs that mixed with RhB dye, the emission spectrum will increase, while these spectra are decreased at (RhB $1*10^{-5}$ M + Ag NPs 700 mJ), (RhB $1*10^{-5}$ M + Ag NPs 800 mJ) (RhB $1*10^{-5}$ M + Ag NPs 900 mJ), because of the increase in the nanoparticles size. Indicate that the lasing properties (threshold for lasing, emission intensity) strongly depend on the size of the nanoparticles.

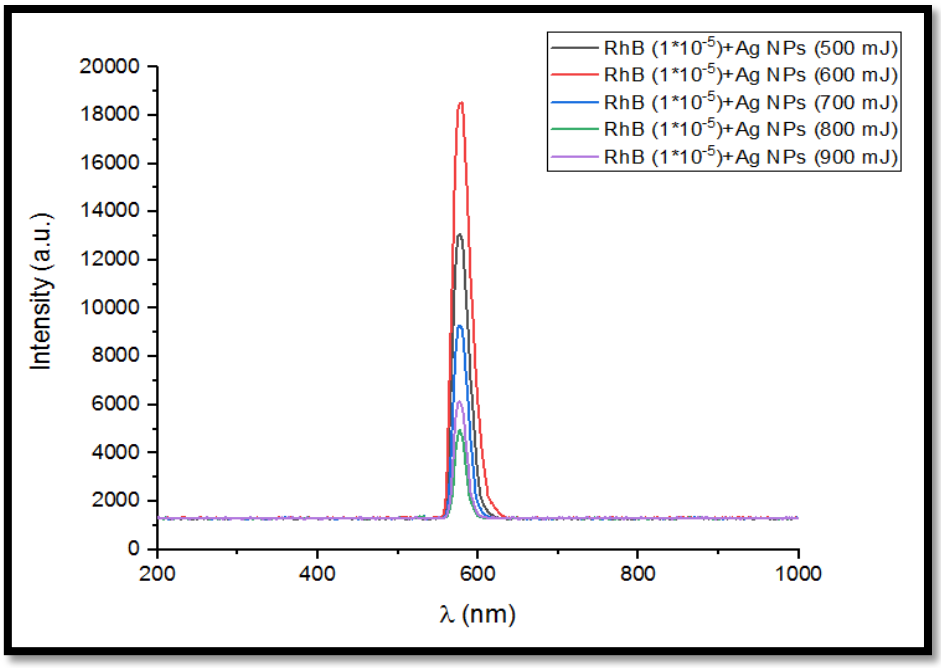

Figure (4-11): Fluorescence spectrum of RhB dye ($1*10^{-5}$M) mixed with a different sizes of Ag NPs.

4.2.11 Plasmonic phenomenon in emission spectra (LIF) of Rhodamine B mixed with different sizes of Ag NPs:

The plasmonic effect appears in the emission spectra of the mixture of RhB dye ($1*10^{-5}$ M) with the Ag NPs in different energies, shown in figure (4-12) (a, b, c, d, e), where the intensity of the final peak as a function of pump energy. The higher intensity at figure (4-12,a) (smaller size of Ag NPs mixed with RhB dye) is (9000 a.u.), while, at figure (4-12, b) the intensity was increased (14000 a.u), but, at energies (700, 800, 900 mJ) the intensity was decreased (11000, 10000, 7000) a.u. , figures (4-12, c, d, e) respectively. These observations are attributed to the enhanced scattering and absorption of silver nanoparticles and increased spectral overlap between the dye fluorescence spectra and the silver extinction spectrum, which induces localized surface plasmons and resonance energy transfer.

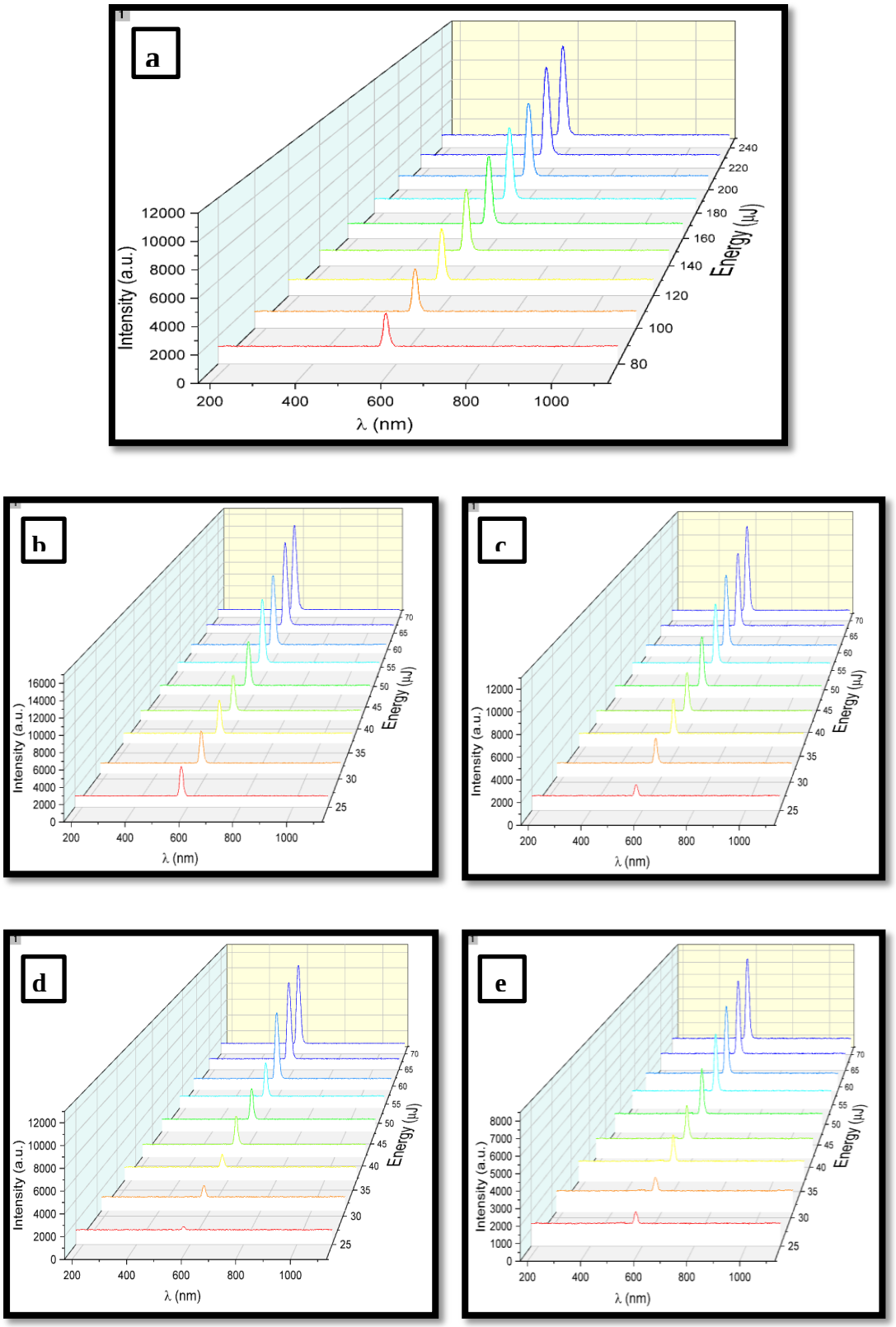

Figure (4-12): Emission spectrum (LIF) of RhB dye ($1*10^{-5}$M) mixed with Ag NPs at (a) 500 mJ , (b) 600 mJ , (c) 700 mJ, (d) 800 mJ ,(e) 900 mJ.

Figure (4-13) represents the threshold of all above samples (RhB dye $1*10^{-5}$ M mixed with different sizes of Ag NPs), where the threshold of the lowest concentration (500 mJ) is (37 µJ), while the threshold of (600 mJ) is (31 µJ), this shows that the threshold is decreases by increasing the size of Ag NPs to a certain limit, after that the threshold begins to increase due to the increase in the size of the nanoparticles from the required limit, and this is called the quenching process. Table (4-2) represents the parameters characteristics of RhB ($1*10^{-5}$ M) mixed with different sizes of Ag NPs.

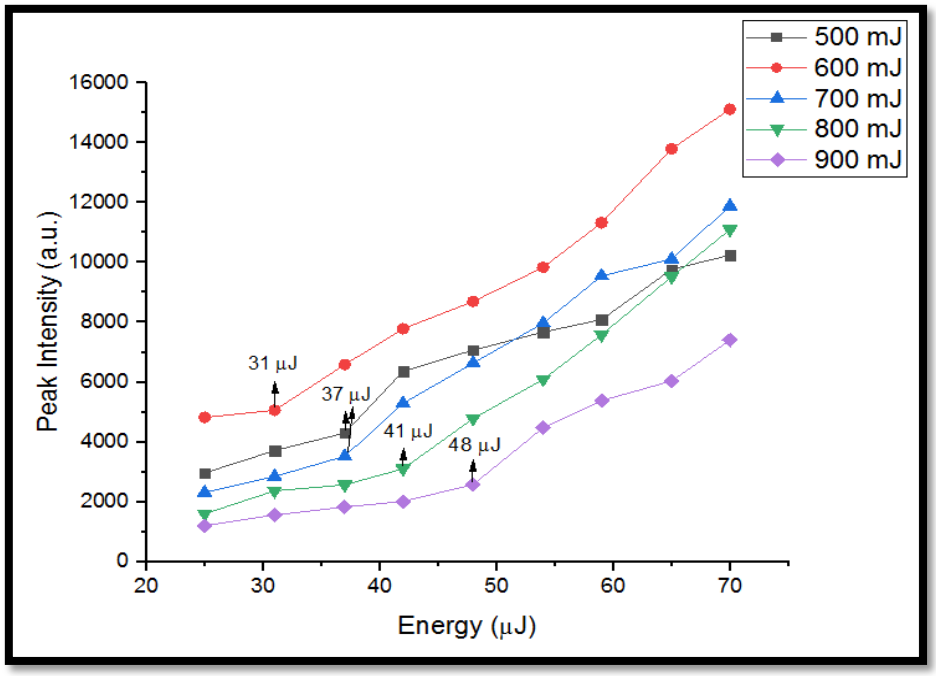

Figure (4-13): Threshold of (RhB dye $1*10^{-5}$M mixed with different sizes of Ag NPs).

Table (4-2): The parameters characteristics of RhB ($1*10^{-5}$ M) mixed with different sizes of Ag NPs.

Samples	Lasing threshold (µJ)	Intensity (a.u.)
RhB($1*10^{-5}$M)+ Ag NPs(500 mJ)	37	9000
RhB($1*10^{-5}$M)+ Ag NPs(600 mJ)	31	14000
RhB($1*10^{-5}$M)+ Ag NPs(700 mJ)	37	11000
RhB($1*10^{-5}$M)+ Ag NPs(800 mJ)	41	10000
RhB($1*10^{-5}$M)+ Ag NPs(900 mJ)	48	7000

4.2.12 Absorption spectra of Ag NWs with different concentrations :

Five concentrations of Ag NWs were used (1, 1.5, 2, 2.5, 3) gm/mol, figure (4-14) represents the absorption spectra of these concentrations, where, it was noted that by increasing the concentration of Ag NWs, that leads to increase the absorption spectra. It contains two characteristic plasmon absorption bands at about (350) and (373) nm; they correspond to the transverse and longitudinal plasmon bands, respectively. The absorption signal at (350 nm) is due to the scattering and the absorption of light spreading along the short axis of the nanowire. The absorption band at (373 nm), on the other hand, is caused by the same process, but along the long axis of the nanowire.

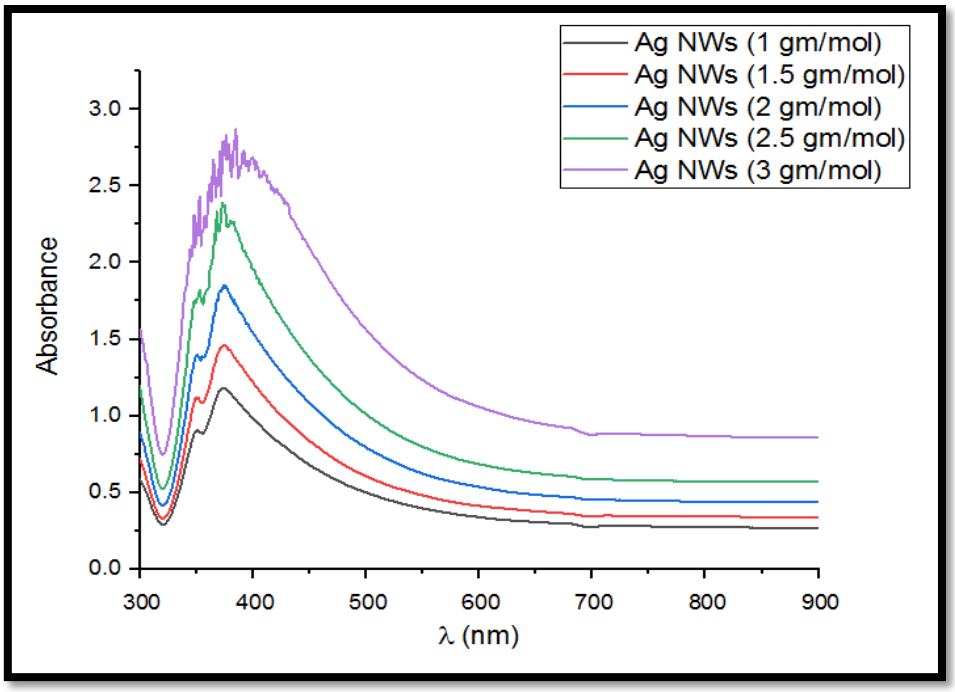

Figure (4-14): Absorption spectra of Ag NWs with different concentrations.

4.2.13 Absorption spectra of RhB mixed with different concentrations of Ag NWs:

The best concentration of RhB dye was mixed with different concentrations of Ag NWs, where, figure (4-15) represents the absorption spectrum of this mixture. It is obvious that by adding the nanowires to the dye, that leads to increase in the absorption spectrum. Noted that the effect of increasing the concentration of NWs on the dye is obvious in the mixture RhB ($1*10^{-5}$ M) + Ag NWs (3 gm/mol), and the highest absorption of the Ag NWs in this mixture was at the wavelengths of (350 and 373 nm).

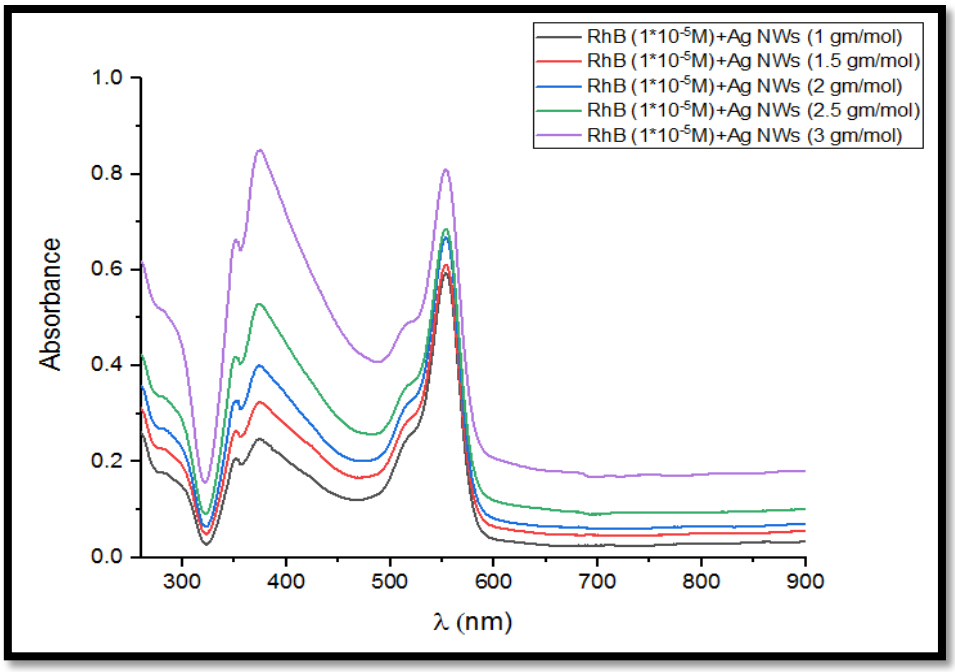

Figure (4-15): Absorption spectra of RhB dye ($1*10^{-5}$ M) mixed with a different concentrations of Ag NWs.

4.2.14 Fluorescence spectra of RhB mixed with different concentrations of Ag NWs:

Figure (4-16) represents the fluorescence spectra of the mixture (RhB $1*10^{-5}$ M + different concentrations of Ag NWs). It is clear that by increasing the Ag NWs that leads to increase the emission spectra, while, the quenching happened at the last two spectra (RhB $1*10^{-5}$ M+ Ag NWs 2.5 gm/mol) and (RhB $1*10^{-5}$ M+ Ag NWs 3 gm/mol).

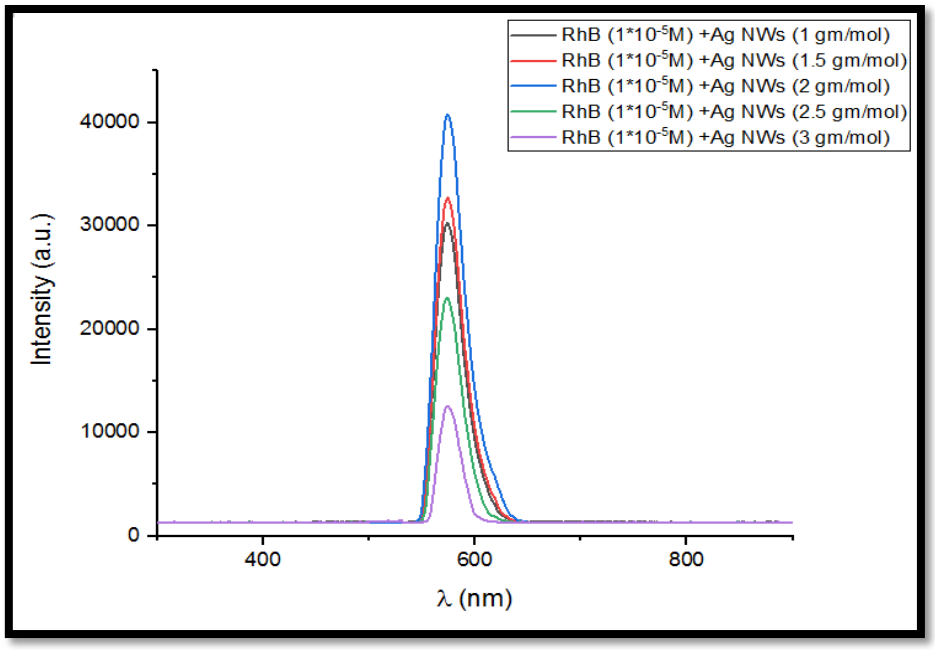

Figure (4-16): Fluorescence spectra of RhB dye ($1*10^{-5}$M) mixed with different concentrations of Ag NWs.

4.2.15 Surface plasmon polariton phenomenon in emission spectra (LIF) of RhB mixed with different concentrations of Ag NWs:

Figure (4-17) represents the intensity as a function of pump energy. Surface plasmon polariton phenomenon is appears in the mixture of RhB ($1*10^{-5}$ M) with Ag NWs with different concentrations, where, the higher intensity at figure (4-17, a) (lower concentration of Ag NWs mixed with RhB dye) is (23000 a.u),while, at figure (4-17, b) the intensity was increased (25000 a.u), and then the intensity continued to increase at figure (4-17, c), (33000 a.u.). Finally, the quenching process is clear in figure (4-17, d,e), where the intensity decreased to be (19000,17000) a.u. respectively, that achieved the phenomenon of surface plasmon polariton. It was shown that the spectral center position of the plasmonic emission can be tuned by changing the shape of the Ag nanoparticles.

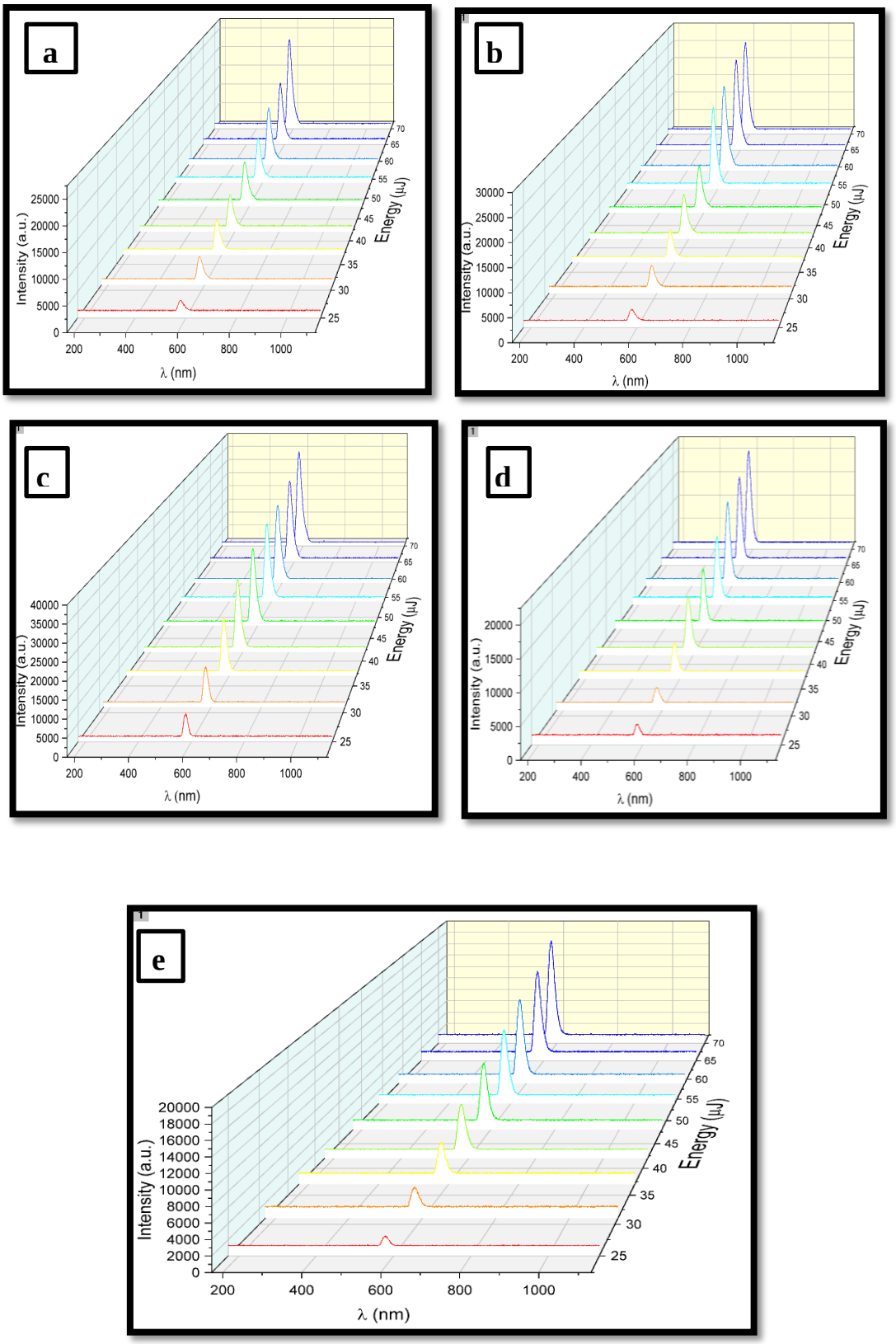

Figure (4-17): Emission spectrum of RhB dye ($1*10^{-5}$M) mixed with Ag NWs at (a) 10 % Ag NWs, (b) 20 % Ag NWs, (c) 30 % Ag NWs, (d) 40 % Ag NWs,(e) 50 % Ag NWs.

The threshold of all above samples (RhB dye $1*10^{-5}$ M mixed with different concentrations of Ag NWs) is clear in figure (4-18), where the threshold is decreases by increasing the concentration of Ag NWs, where the threshold of the lowest concentration (1 gm/mol) is (42 µJ), while the threshold of (2 gm/mol) is (31 µJ). Table (4-3) represents the parameters characteristics of RhB ($1*10^{-5}$ M) mixed with different concentrations of Ag NWs.

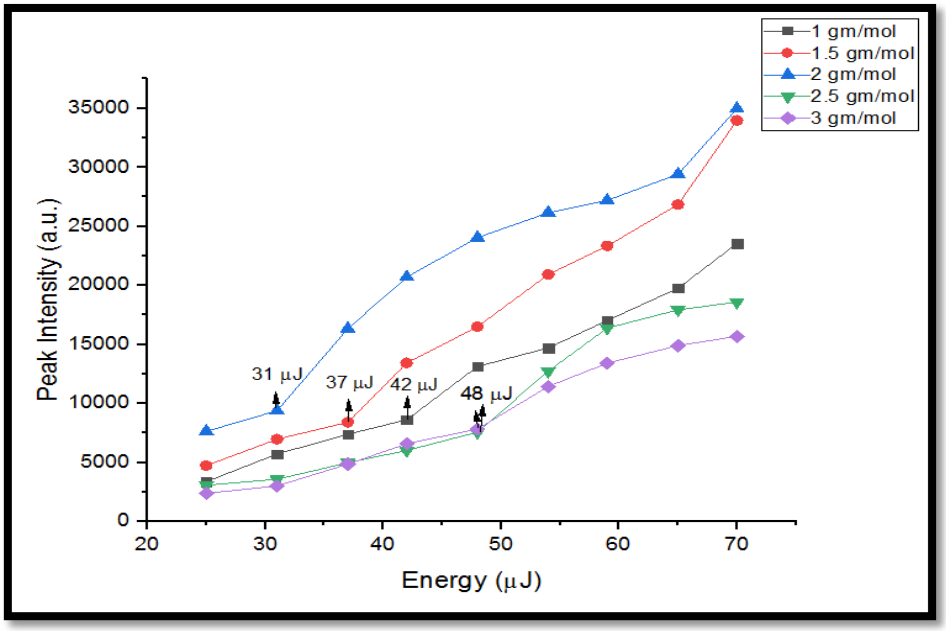

Figure (4-18): Threshold of (RhB dye $1*10^{-5}$M mixed with different concentrations of Ag NWs).

Table (4-3): The parameters characteristics of RhB ($1*10^{-5}$ M) mixed with different concentrations of Ag NWs.

Samples	Lasing threshold (µJ)	Intensity (a.u.)
RhB($1*10^{-5}$M) +Ag NWs (1gm/mol)	42	23000
RhB($1*10^{-5}$M) +Ag NWs (1.5gm/mol)	37	25000
RhB($1*10^{-5}$M) +Ag NWs (2gm/mol)	31	33000
RhB($1*10^{-5}$M) +Ag NWs (2.5gm/mol)	48	19000
RhB($1*10^{-5}$M) +Ag NWs (3gm/mol)	48	17000

4.3 Spectral properties of RhB and Au NPs:

4.3.1 Absorption spectra of Au NPs with different concentrations :

To get different concentrations of Au NPs, by keeping the energy constant at (600 mJ), and changing the number of pulses (500, 600, 700, 800, 900) p. Where, noted that the absorption of Au NPs at (525 nm), It is clear in figure (4-19) that by increasing Au NPs concentration, the absorption spectra will increase.

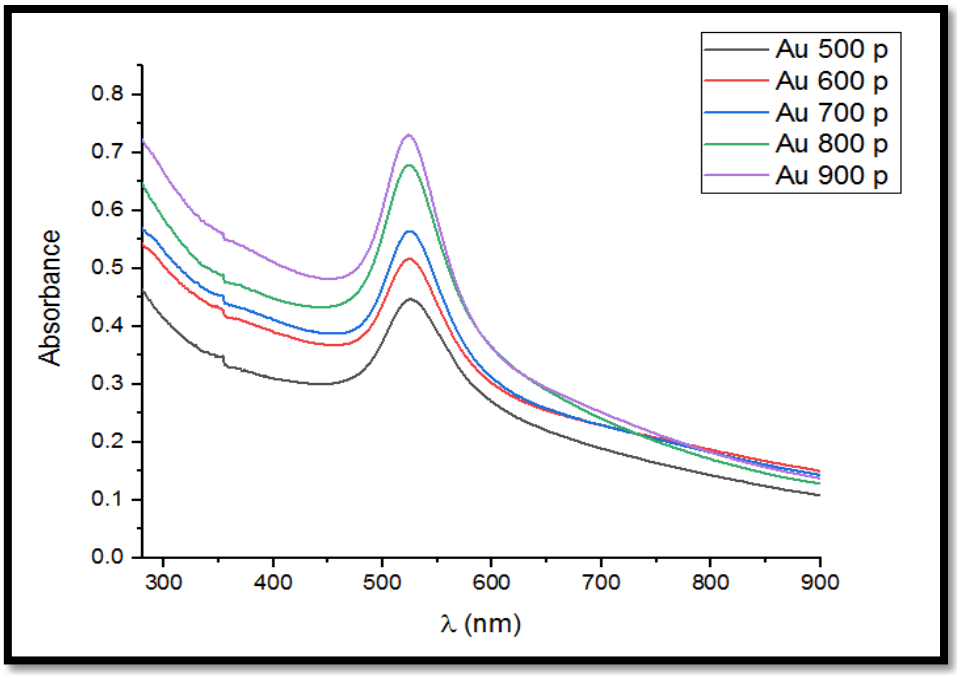

Figure (4-19): Absorption spectra of Au NPs with different concentrations.

4.3.2 Absorption spectra of RhB mixed with different concentrations of Au NPs:

The best concentration of RhB dye ($1*10^{-5}$ M) was mixed with different concentrations of Au NPs, where, figure (4-20) represents that by adding the nanoparticles to the dye, leads to the enhancement of lasing emission. The influence of the local field enhancement mechanism depends on the distance between Au NP and a dye molecule, which is directly related to NP density.

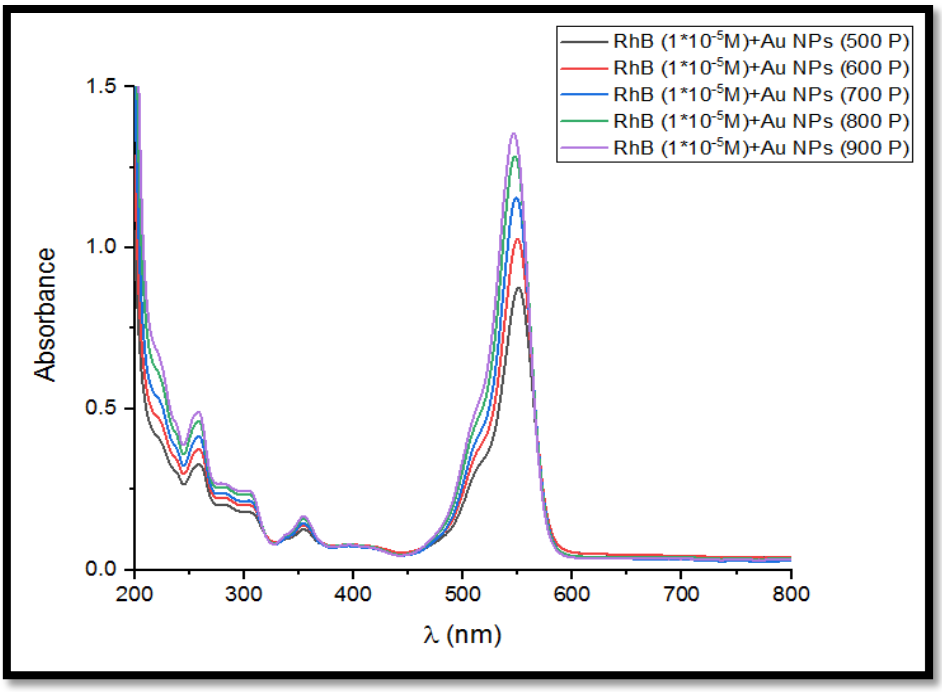

Figure (4-20): Absorption spectra of RhB dye ($1*10^{-5}$ M) mixed with different concentrations of Au NPs.

4.3.3 Fluorescence spectra of RhB mixed with different concentrations of Au NPs:

The fluorescence spectra of RhB dye ($1*10^{-5}$M) mixed with a different concentrations of Au NPs represented in figure (4-21). It was noted that by increasing the concentration of Au NPs that mixed with RhB dye, the emission spectra will increase, and the quenching process is appeared at (RhB+ concentration of Au NPs at 900 p).

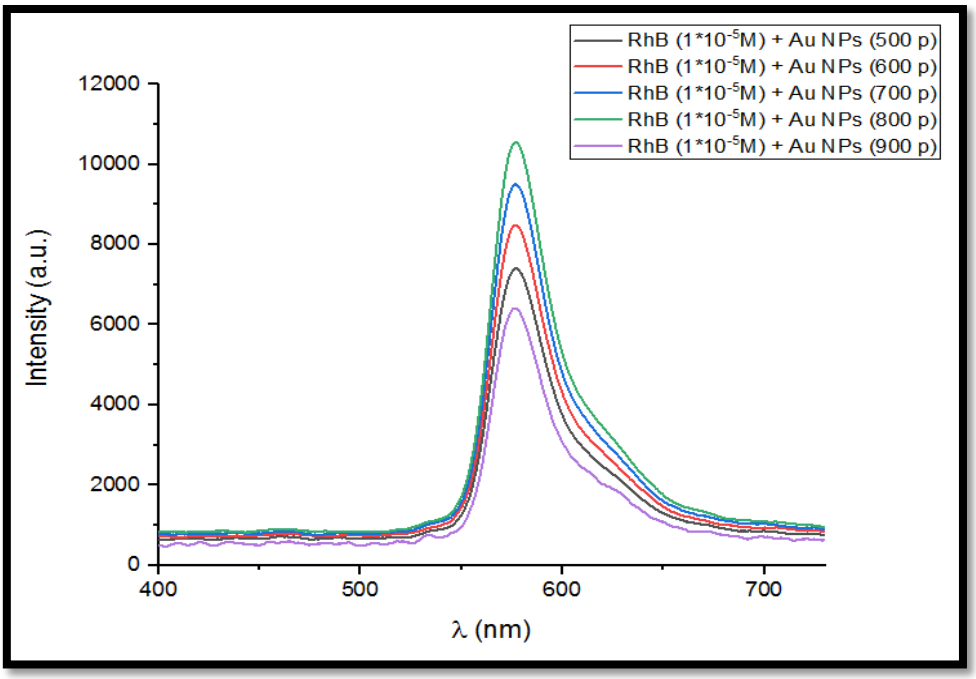

Figure (4-21): Fluorescence spectra of RhB dye ($1*10^{-5}$M) mixed with different concentrations of Au NPs.

4.3.4 Plasmonic phenomenon in emission spectra (LIF) of RhB mixed with different concentrations of Au NPs:

The plasmonic phenomenon of the emission spectra is appear, figure (4-22) (a, b, c, d, e) shows the intensity of the final peak as a function of pump energy, where, the higher intensity at figure (4-22, a) (lower concentration of Au NPs mixed with RhB dye) is (28000 a.u), and the intensity continued to increase at figures (4-22, b, c), (35000, 38000 a.u) respectively. Finally, the quenching process is clear in figure (4-22, d, e), where the intensity decreased to be (30000 and 15000 a.u) respectively. This shows that the increase in the concentration of Au NPs leads to increase the enhancement of the emission spectra.

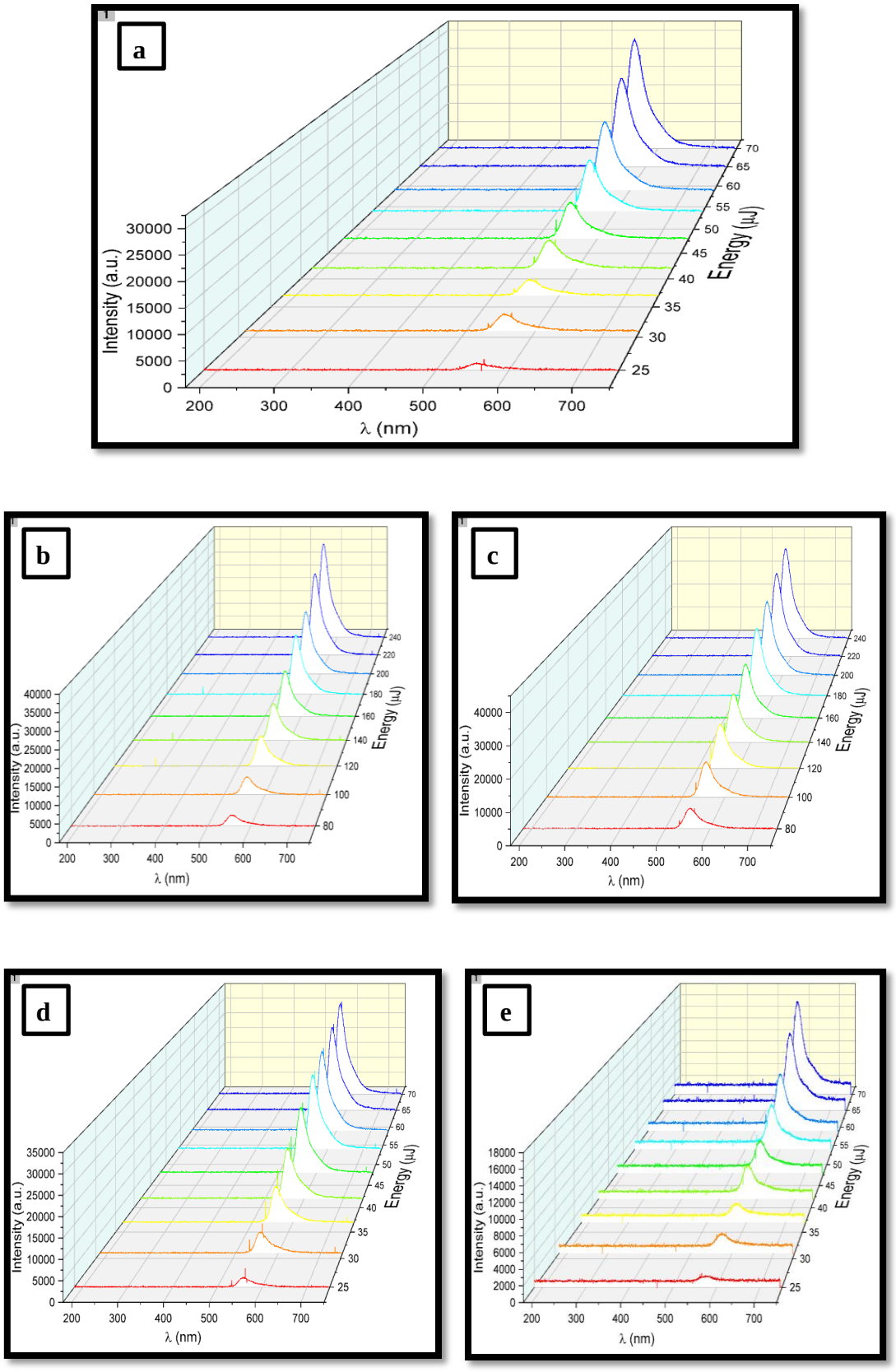

Figure (4-22): Emission spectra of RhB dye(1*10^{-5}M) mixed with Au NPs at (a) 500 p , (b) 600 p , (c) 700 p, (d) 800 p ,(e) 900 p.

The threshold of all above samples (RhB dye $1*10^{-5}$ M mixed with different concentrations of Au NPs) is clear in figure (4-23), where the threshold of the lowest concentration (500 p) is (42 µJ), while the threshold of (700 p) is (31 µJ), this shows that the threshold is decreases by increasing the concentration of Au NPs. While, the quenching is clear at (800, 900) p due to the increasing of the NPs overwhelms the dye fluorescence. Table (4-4) represents the parameters characteristics of RhB ($1*10^{-5}$ M) mixed with different concentrations of Au NPs.

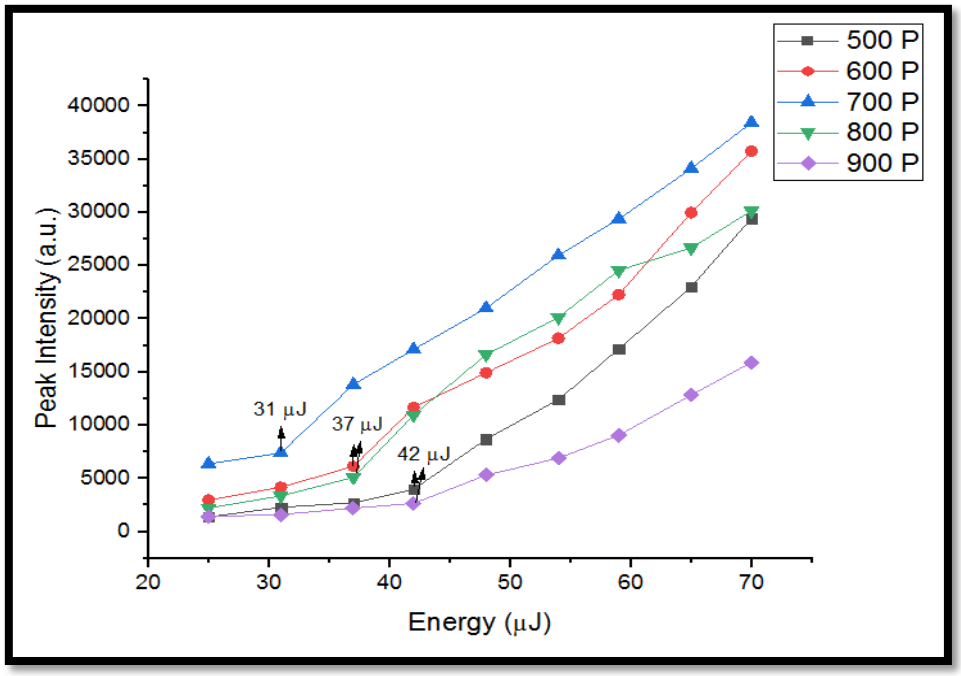

Figure (4-23): Threshold of (RhB dye $1*10^{-5}$M mixed with different concentrations of Au NPs).

Table (4-4): The parameters characteristics of RhB ($1*10^{-5}$ M) mixed with different concentrations of Au NPs.

Samples	Lasing threshold (µJ)	Intensity (a.u.)
RhB($1*10^{-5}$M) + Au NPs (500 p)	42	28000
RhB($1*10^{-5}$M) + Au NPs (600 p)	37	35000
RhB($1*10^{-5}$M) + Au NPs (700 p)	31	38000
RhB($1*10^{-5}$M) + Au NPs (800 p)	37	30000
RhB($1*10^{-5}$M) + Au NPs (900 p)	42	15000

4.3.5 Absorption spectra of Au NPs with different sizes:

The absorption spectra of Au NPs with different sizes is clear in figure (4-24). It was noted that by changing the energy (500, 600, 700, 800, 900) mJ, and keep the pulse number constant at (400 p),where, by increasing the energy, that leads to increase the absorption spectra.

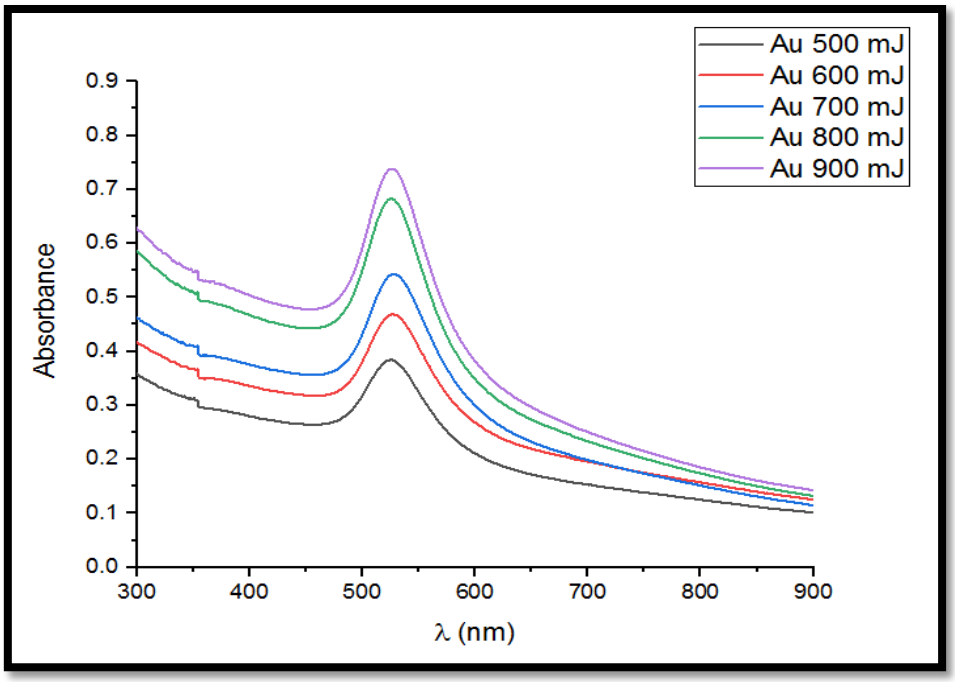

Figure (4-24): Absorption spectra of Au NPs with different sizes.

4.3.6 Absorption spectra of RhB mixed with different sizes of Au NPs:

The absorption spectra of RhB dye (best concentration $1*10^{-5}$ M) mixed with different sizes of Au NPs represented in figure (4-25). It is obvious that by adding the nanoparticles to the dye, that leads to increase in the absorption spectra.

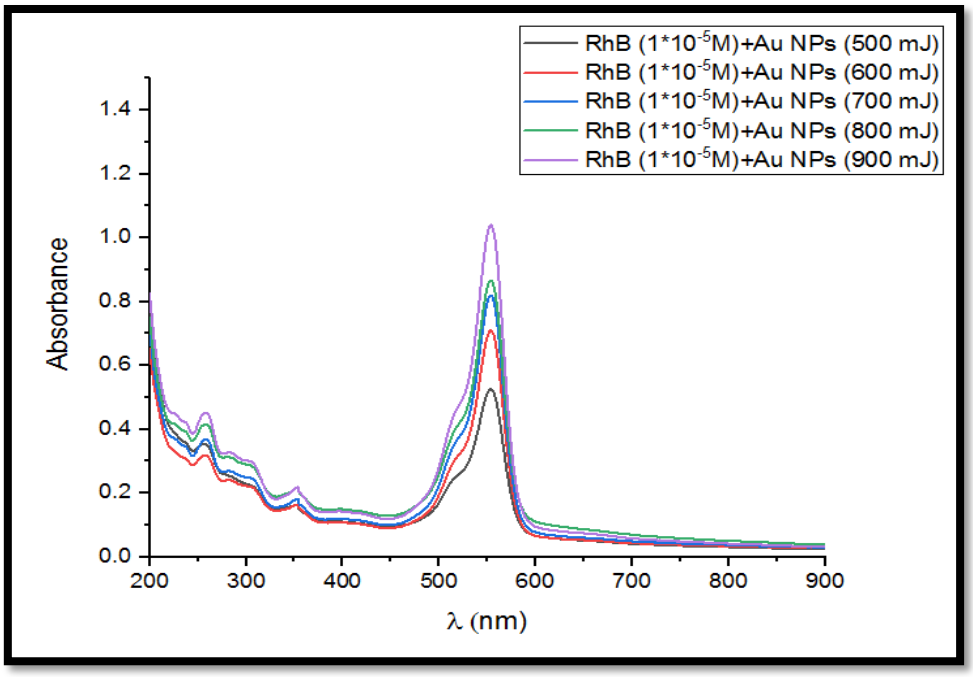

Figure (4-25): Absorption spectra of RhB dye ($1*10^{-5}$ M) mixed with different sizes of Au NPs.

4.3.7 Fluorescence spectra of RhB mixed with different sizes of Au NPs:

It is obvious from the figure (4-26) that the fluorescence spectra increased by increases the size of Au NPs to a threshold limit, then the quenching process occurred at (RhB $1*10^{-5}$ M + Au NPs 800 mJ), (RhB $1*10^{-5}$ M + Au NPs 900 mJ), that leads to decrease in the spectra due to the large size of the gold nanoparticles.

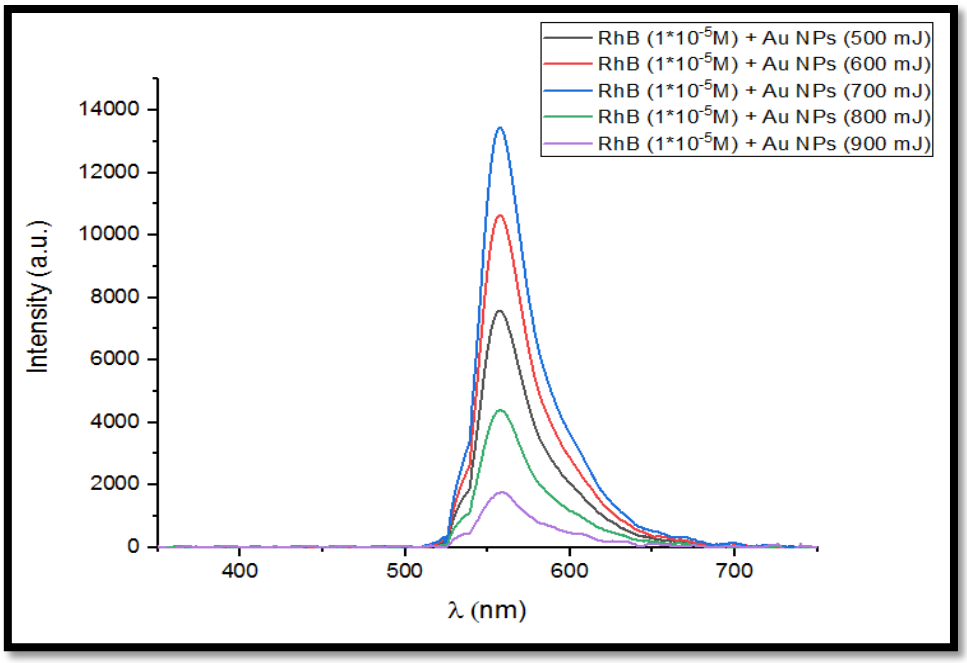

Figure (4-26): Fluorescence spectra of RhB dye ($1*10^{-5}$M) mixed with a different sizes of Au NPs.

4.3.8 Plasmonic phenomenon in emission spectra (LIF) of RhB mixed with different sizes of Au NPs:

Figure (4-27) (a, b, c, d, e) represents the emission spectra (LIF) of the mixture (RhB $1*10^{-5}$ M+ Au NPs with different sizes), got the plasmonic effect by using second harmonic generation of Nd:YAG laser, the enhancement of the gain is clear from the increasing of the peak intensity by increase the energy, where, the higher intensity at figure (4-27, a) (smaller size of Au NPs mixed with RhB dye) is (9000 a.u), and the intensity continued to increase at figures (4-27, b, c), (10500, 11000 a.u) respectively. Finally, the quenching process is clear in figure (4-27, d, e), where the intensity decreased to be (7000 and 5500 a.u) respectively.

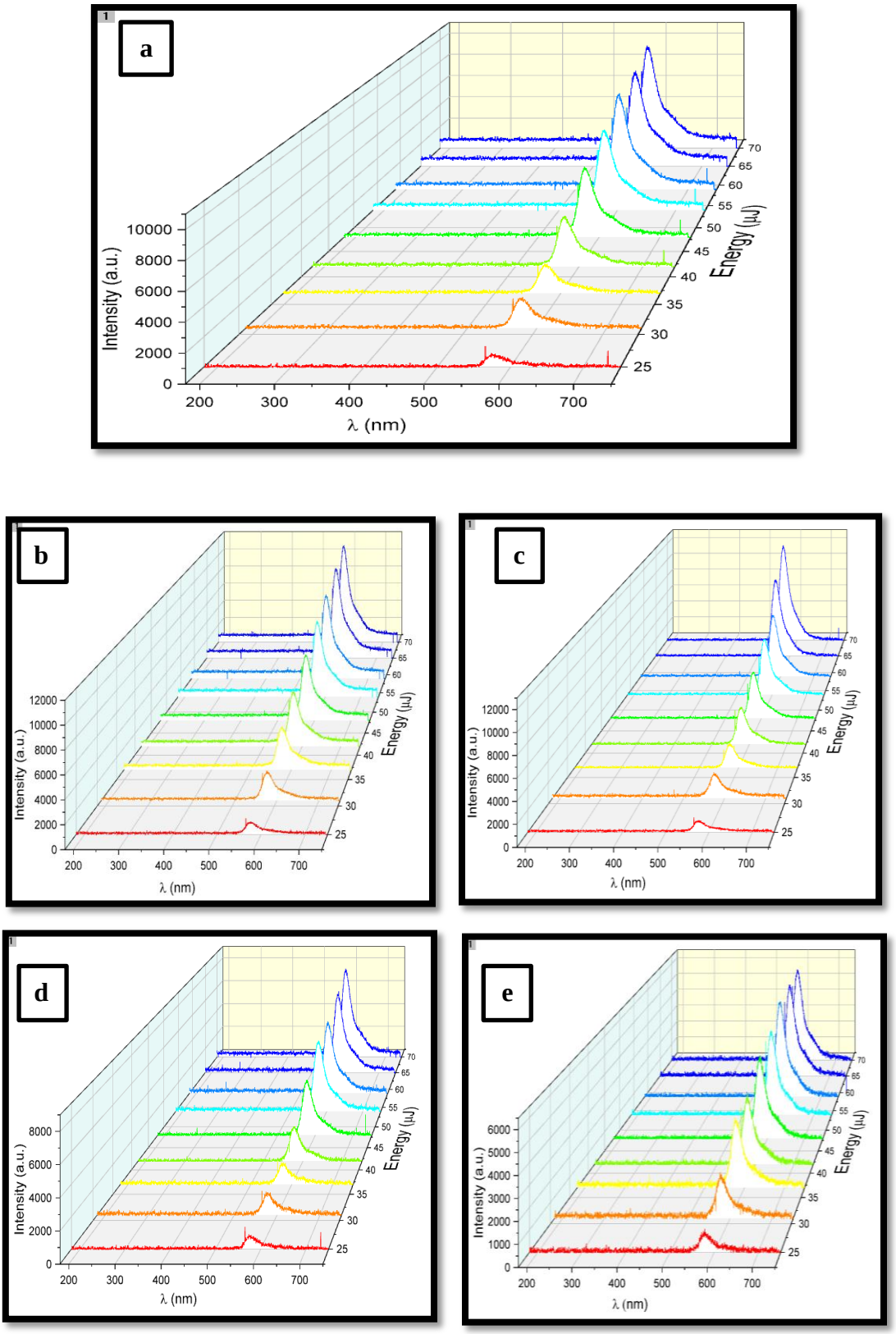

Figure (4-27): Emission spectra (LIF) of RhB dye ($1*10^{-5}$M) mixed with Au NPs at (a) 500 mJ , (b) 600 mJ , (c) 700 mJ, (d) 800 mJ ,(e) 900 mJ.

Figure (4-28) represents the threshold of all above samples (RhB dye $1*10^{-5}$ M mixed with different sizes of Au NPs), where the threshold of the lowest concentration (500 mJ) is (42 µJ), while the threshold of (700 mJ) is (31 µJ), this shows that the threshold is decreases by increasing the size of Ag NPs. While, the quenchi ng is clear at (800, 900) mJ. Table (4-5) represents the parameters characteristics of RhB ($1*10^{-5}$ M) mixed with different sizes of Au NPs.

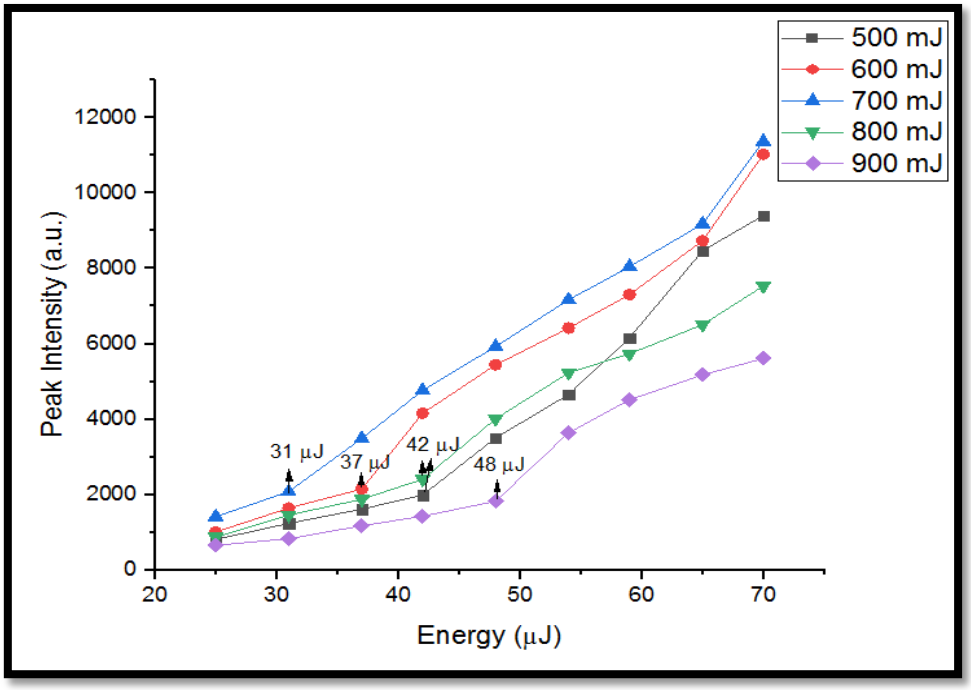

Figure (4-28): Threshold of (RhB dye $1*10^{-5}$M mixed with different sizes of Au NPs).

Table (4-5): The parameters characteristics of RhB ($1*10^{-5}$ M) mixed with different sizes of Au NPs.

Samples	Lasing threshold (µJ)	Intensity (a.u.)
RhB($1*10^{-5}$M)+ Au NPs(500 mJ)	42	9000
RhB($1*10^{-5}$M)+ Au NPs(600 mJ)	37	10500
RhB($1*10^{-5}$M)+ Au NPs(700 mJ)	31	11000
RhB($1*10^{-5}$M)+ Au NPs(800 mJ)	42	7000
RhB($1*10^{-5}$M)+ Au NPs(900 mJ)	48	5500

4.4 Structure characterizations of the thin film samples :

The SEM image of 2D plasmonic structures top surface fabricated samples that have been prepared as explained in the previous chapter, the behavior of gold nanoparticles is arranged in a periodic array for 2D grating samples. It is worth noting that periodic arrays of metallic nanoparticles can exhibit extremely narrow extinction line shaping excitations called surface lattice resonances (SLRs). SLRs are a result of the coupling between localized surface plasmon resonances (LSPRs) coming from metallic nano-rods in the sample associated with individual nanoparticles and diffractive orders (DOs) present in periodic structures. The diffraction coupling occurs when nanostructures are spaced with the optical path length between the neighboring particles equals to an integer multiple of the incident wavelength. Shown in figure (4-29).

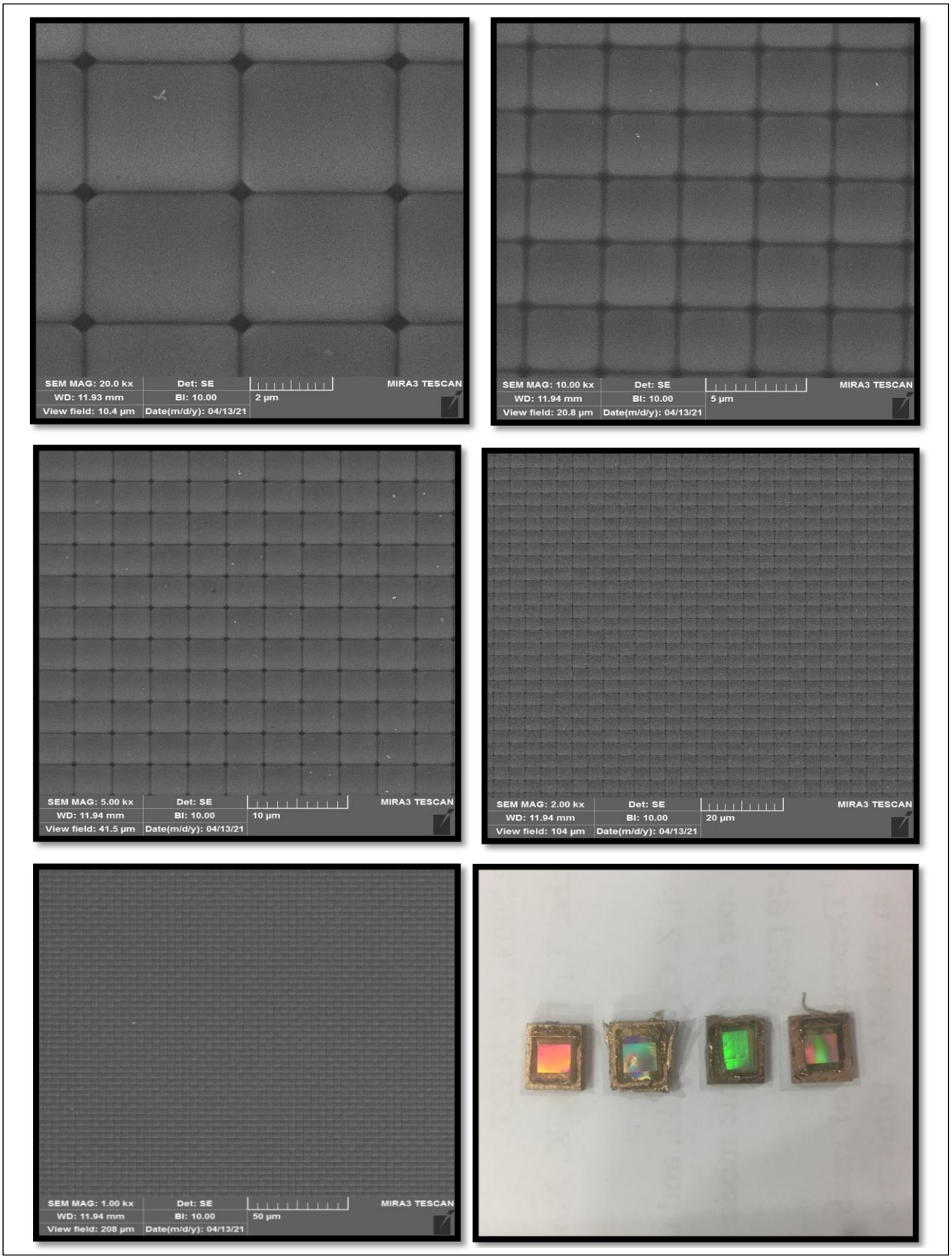

Figure (4-29): The SEM image of 2D plasmonic structures top surface fabricated samples.

4.4.1 Plasmonic phenomenon in emission spectra (LIF) of RhB deposited on the 2D nano grating:

Rhodamine B ($1*10^{-5}$ M) was deposited on the 2D nano grating that have been fabricated as explained in the previous chapter. The plasmonic spectra was studied by using the spectrophotometer, where, the highest intensity is (22000 a.u.) as shown in figure (4-30).

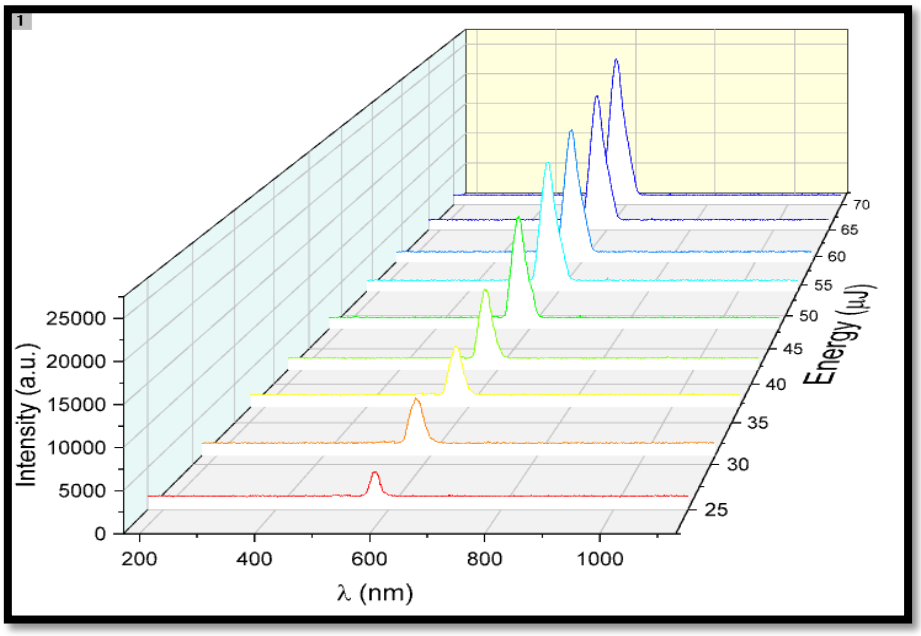

Figure (4-30): Emission spectra (LIF) of RhB dye ($1*10^{-5}$M) deposited on the 2D nano grating.

4.4.2 Plasmonic phenomenon in emission spectra (LIF) of (RhB $1*10^{-5}$ M+Ag NPs 800 p) deposited on the 2D nano grating:

In the case of (RhB $1*10^{-5}$ M+Ag NPs 800 p) deposition on the 2D nano grating, the highest intensity was increased to be (37000 a.u.) as shown in figure (4-31). It attributes to the strong plasmonic scattering by the Ag NPs and the high quality confinement by the polymer membrane.

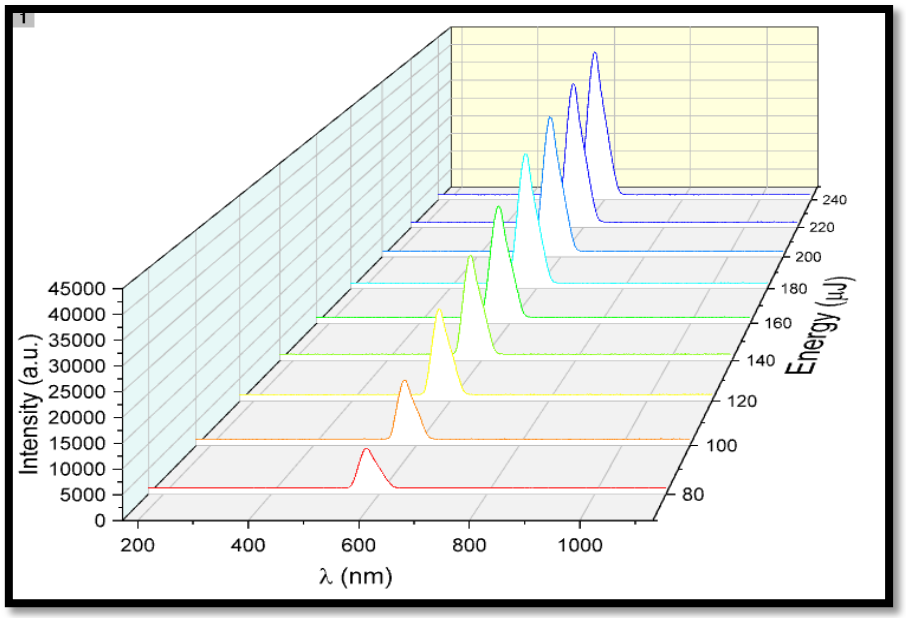

Figure (4-31): Emission spectra (LIF) of (RhB 1*10^{-5} M+Ag NPs 800 p) deposited on the thin film.

In comparing between (highest intensity and lowest threshold) for the values of the dye and the thin film (RhB 1*10^{-5} M + Ag NPs 800 p) and (RhB 1*10^{-5} M + Ag NPs 800 p) respectively , it was noted that at the thin film the intensity increased while the threshold was decreased, where the threshold of the thin film is (31 µJ), while the threshold of the dye is (37 µJ). As compared with (RhB dye 1*10^{-5} M) deposited on the thin film, noted that the intensity was decreased but the threshold was increased to be (42 µJ) , this shows that NPs enhanced the active media where the intensity was increased and the threshold was decreased, and the best result was in the thin film, represented in figure below.

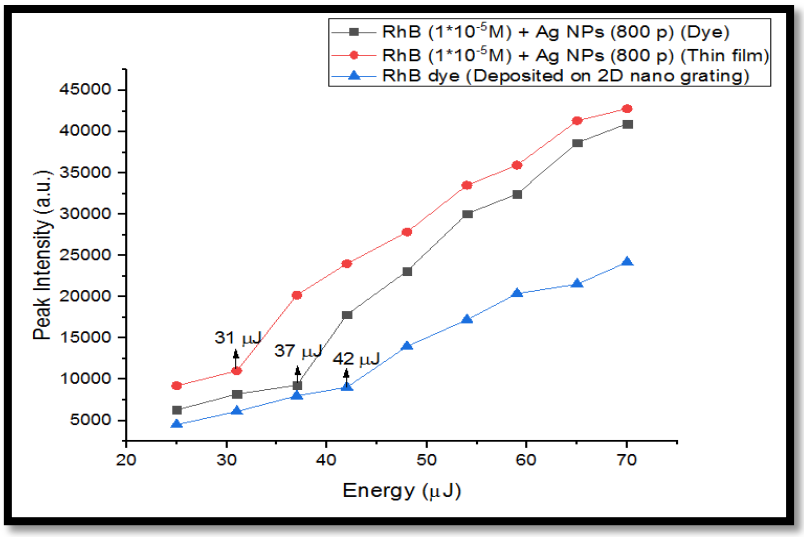

Figure (4-32): Threshold of RhB (1*10^{-5} M) deposited on the 2D nano grating , and RhB (1*10^{-5} M) mixed with Ag NPs (800 p) for the dye and the thin film.

4.4.3 Plasmonic phenomenon in emission spectra (LIF) of (RhB 1*10^{-5} M+Ag NPs 600 mJ) deposited on the 2D nano grating:

When the 2D nano grating deposited by (RhB 1*10^{-5} M+Ag NPs 600 mJ), the intensity was also increased to be (45000 a.u.) as shown in figure (4-33).

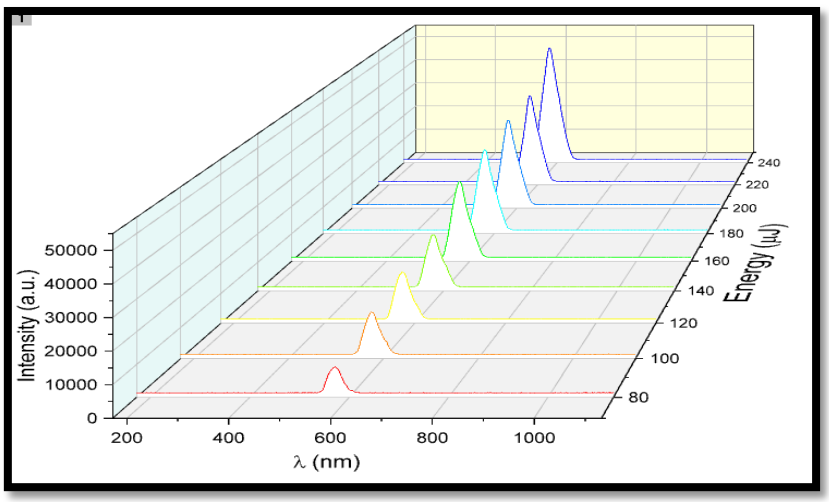

Figure (4-33): Emission spectra (LIF) of (RhB 1*10^{-5} M+Ag NPs 600 mJ) deposited on the thin film.

The highest intensity and lowest threshold for the values of the dye and the thin film (RhB 1*10^{-5} M + Ag NPs 600 mJ) and (RhB 1*10^{-5} M + Ag NPs 600 mJ) respectively, as comparing between the dye and the thin film threshold, noted that at the thin film the intensity increased while the threshold was decreased, where the threshold of the thin film is (31 µJ), while the threshold of the dye is (37 µJ), represented in figure (4-34).

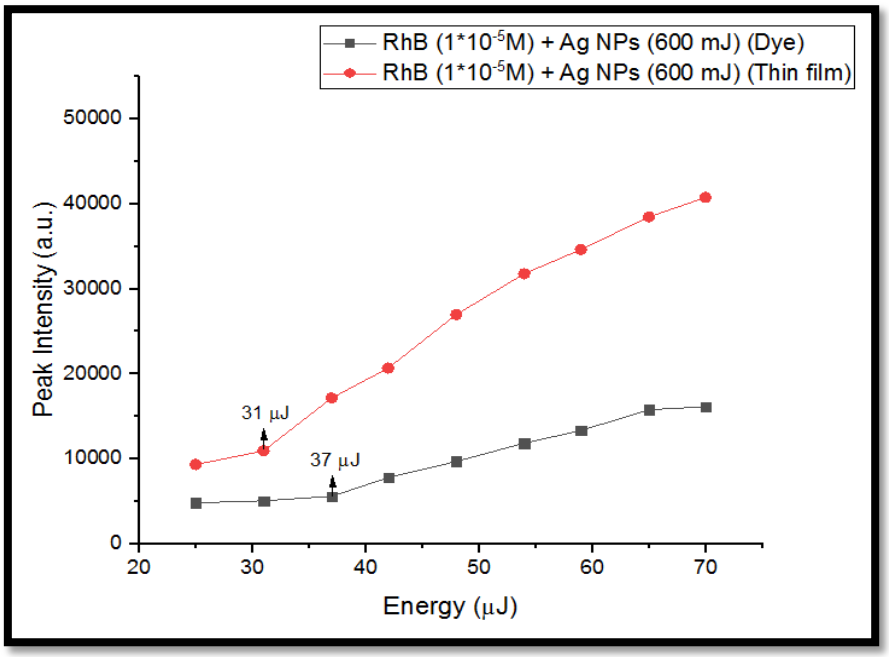

Figure (4-34): Threshold of RhB (1*10^{-5} M) mixed with Ag NPs (600 mJ) for the dye and the thin film.

4.4.4 Plasmonic phenomenon in emission spectra (LIF) of (RhB 1*10^{-5} M+Ag NWs 2 gm/mol) deposited on the 2D nano grating:

In the case of (RhB 1*10^{-5} M+Ag NWs 2 gm/mol) deposition, the intensity was (44000 a.u.), figure (4-35).

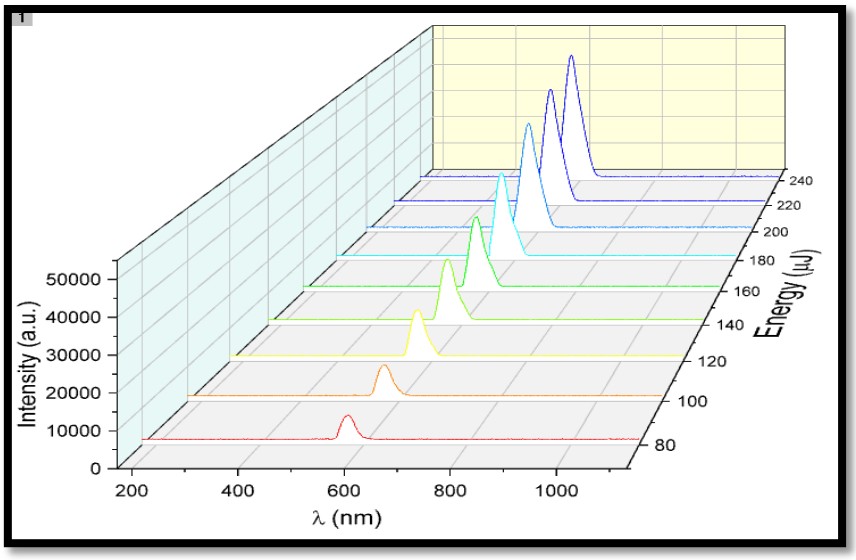

Figure (4-35): Emission spectra (LIF) of (RhB 1*10^{-5} M+Ag NWs 2 gm/mol) deposited on the 2D nano grating.

For mixing the dye with Ag NWs, and comparing between the dye and the thin film threshold for (RhB 1*10^{-5} M + Ag NWs 2 gm/mol) and (RhB 1*10^{-5} M + Ag NWs 2 gm/mol) respactively, noted that at the thin film the intensity increased while the threshold was decreased, where the threshold of the thin film is (31 µJ), while the threshold of the dye is (37 µJ), represented in figure (4-36).

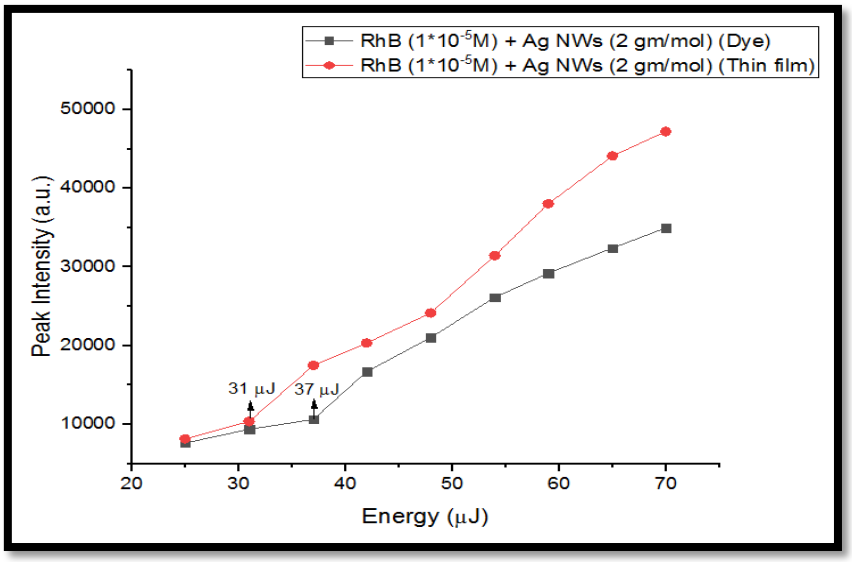

Figure (4-36): Threshold of RhB (1*10^{-5} M) mixed with Ag NWs (2 gm/mol) for the dye and the thin film.

4.4.5 Plasmonic phenomenon in emission spectra (LIF) of (RhB 1*10^{-5} M+Au NPs 800 p) deposited on the 2D nano grating:

Figure (4-37) below represents the plasmonic spectra in the case of Au NPs deposition (RhB 1*10^{-5} M+Au NPs 800 p), noted that the emission spectra was increased to be (48000 a.u.).

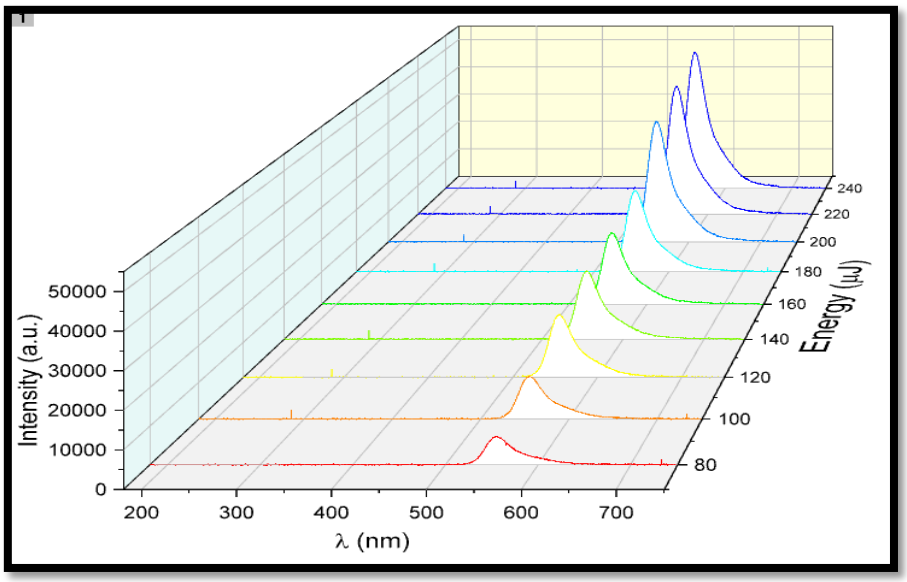

Figure (4-37): Emission spectra (LIF) of (RhB 1*10^{-5} M+Au NPs 800 p) deposited on the 2D nano grating.

In comparing between (highest intensity and lowest threshold) for the values of the dye and the thin film (RhB 1*10^{-5} M + Au NPs 700 p) and (RhB 1*10^{-5} M + Au NPs 800 p) respectively , it was noted that at the thin film the intensity increased while the threshold was the same in both cases, the dye and the thin film (31 μJ), illustrated in figure (4-38).

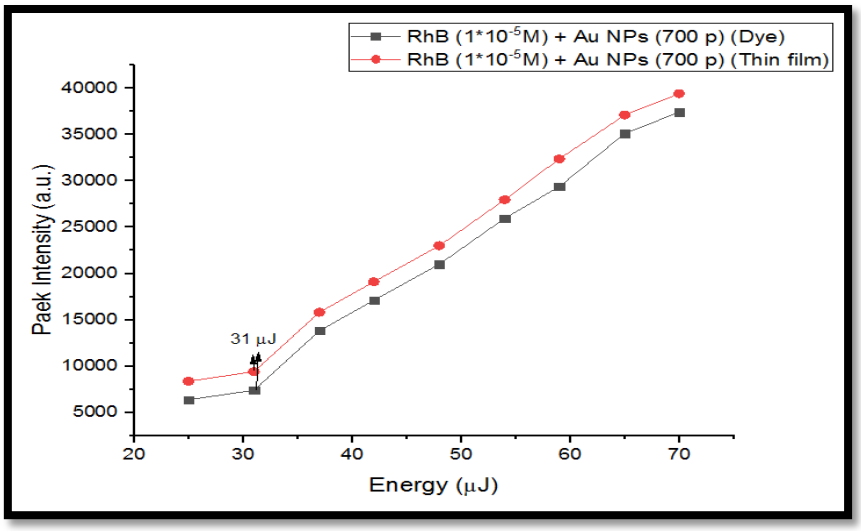

Figure (4-38): Threshold of RhB (1*10^{-5} M) mixed with Au NPs (800 p) for the dye and the thin film.

4.4.6 Plasmonic phenomenon in emission spectra (LIF) of (RhB 1*10^{-5} M+Au NPs 700 mJ) deposited on the 2D nano grating:

When the 2D nano grating deposited by (RhB 1*10^{-5} M+Au NPs 700 mJ), the intensity was also increased to be (50000 a.u.) as shown in figure (4-39).

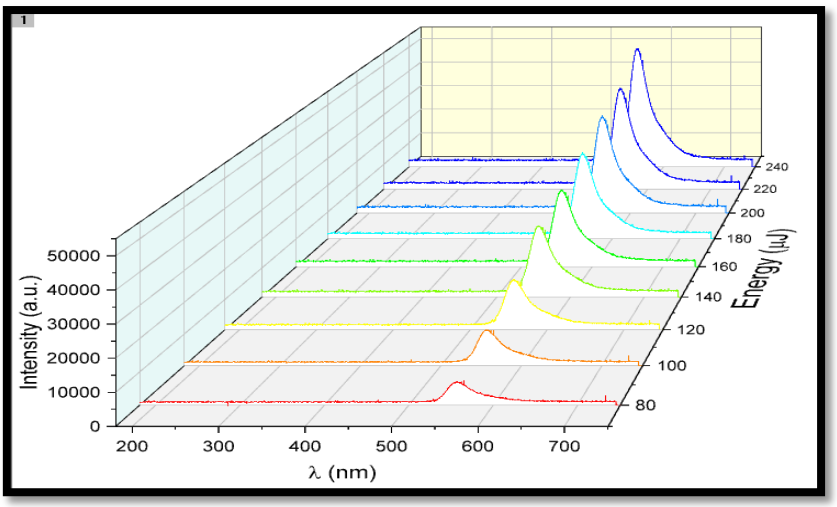

Figure (4-39): Emission spectra of (RhB 1*10^{-5} M+Au NPs 700 mJ) deposited on the 2D nano grating.

The highest intensity and lowest threshold for the values of the dye and the thin film (RhB $1*10^{-5}$ M + Au NPs 700 mJ) and (RhB $1*10^{-5}$ M + Au NPs 700 mJ) respectively, as comparing between the dye and the thin film threshold, noted that at the thin film the intensity increased while the threshold was the same in both cases, the dye and the thin film (31 µJ), illustrated in figure (4-40). Table (4-6) represents the parameters characteristics of the thin film Deposited by RhB ($1*10^{-5}$ M) and (RhB $1*10^{-5}$ M mixed with Ag NPs, Ag NWs, and Au NPs).

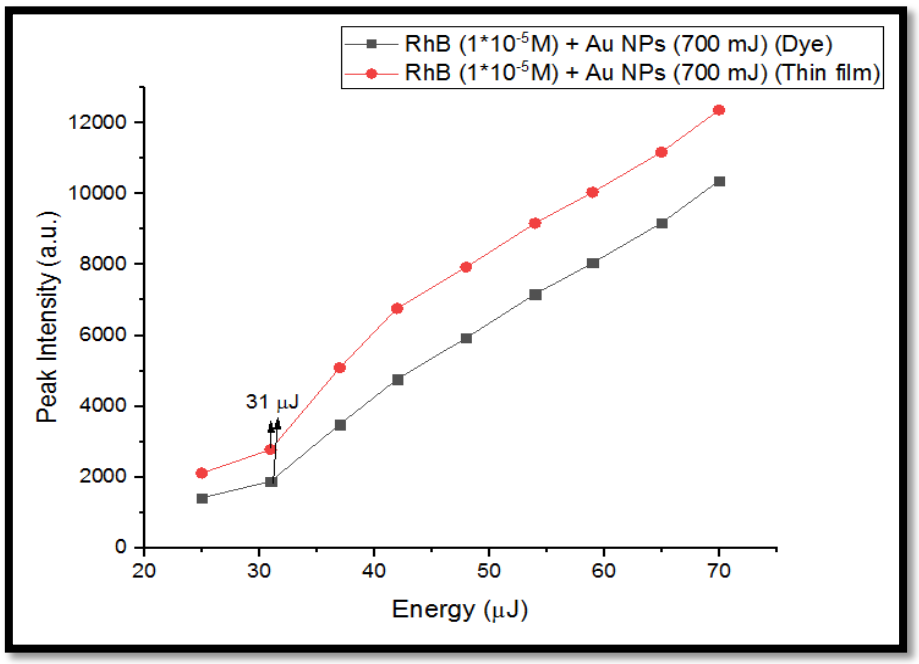

Figure (4-40): Threshold of RhB ($1*10^{-5}$ M) mixed with Au NPs (700 mJ) for the dye and the thin film.

Table (4-6): The parameters characteristics of the 2D nano grating deposited by RhB ($1*10^{-5}$ M) and (RhB $1*10^{-5}$ M mixed with Ag NPs, Ag NWs, and Au NPs).

Samples	Lasing threshold (μJ)	Intensity (a.u.)
RhB ($1*10^{-5}$M)	42	22000
RhB($1*10^{-5}$M)+ Ag NPs(800 p)	31	37000
RhB($1*10^{-5}$M)+ Ag NPs(600 mJ)	31	45000
RhB($1*10^{-5}$M)+ Ag NWs(2 gm/mol)	31	44000
RhB($1*10^{-5}$M)+ Au NPs(800 p)	31	48000
RhB($1*10^{-5}$M)+ Au NPs(700 mJ)	31	50000

It was noted that the emission intensity is enhanced by depositing the nanoparticles or nanowires on the thin film, which leads to the confinement of the rays within the effective medium, and this leads to an increase in the reflections that affect the energy gap, which improve the emission spectra to the active medium, and that emission spectra got from the thin film was better and more enhanced than the spectra that got from the mixture of the dye with NPs or NWs.

5.1 Conclusions :

1) For the RhB dye, the emission spectra increased by increasing the concentration of the dye, but it was sharply decreased at the concentrations ($1*10^{-5}$,$1*10^{-4}$ M) because of quenching process.

2) Noted that the increasing of the dye concentration led to a red shift, while the increasing of Ag NPs concentration in the dye led to a blue shift.

3) It was found that by adding NPs or NWs to the dye that helps to increase the intensity, that achieved by increasing the concentrations of (Ag NPs, Ag NWs, and Au NPs), the intensity was increased.

4) It was noted that by increasing the sizes of Ag NPs that mixed with RhB dye, the emission spectrum will increase, indicate that the lasing properties (threshold for lasing, emission intensity) strongly depend on the size of the nanoparticles.

5) Shows that the threshold is decreases by increasing the concentration of Ag NPs, Ag NWs, and Au NPs.

6) In comparing between the dye and the thin film (intensity and threshold), noted that at the thin film, the intensity increased while the threshold was decreased.

7) Got the localized surface plasmon in emission spectra (LIF) for the mixtue of RhB ($1*10^{-5}$ M) with (Ag NPs and AuNPs).

8) Surface plasmon polariton phenomenon appears in emission spectra (LIF) for the mixture of RhB ($1*10^{-5}$ M) with Ag NWs with different concentrations.

9) For the thin film, the plasmonic phenomenon in emission spectra (LIF) of RhB mixed with (Ag NPs, Ag NWs, and AuNPs) was achieved.

10) Indicated that the lowest plasmonic intensity was (5500 a.u.) for RhB ($1*10^{-5}$ M)+Au NPs (900 mJ) while the highest intensity was (50000 a.u.)

for RhB ($1*10^{-5}$ M)+Ag NPs (800 p), and for the 2D nano grating that deposited with RhB ($1*10^{-5}$ M)+Au NPs (700 mJ).

11) It was noted that the emission intensity is enhanced by depositing the nanoparticles or nanowires on the thin film, which leads to the confinement of the rays within the effective medium, and this leads to an increase in the reflections that affect the energy gap, which improve the emission spectra to the active medium, and that emission spectra got from the thin film was better and more enhanced than the spectra that got from the mixture of the dye with NPs or NWs.

5.2 Future works :

1) Studying the effect of dye laser emission spectrum by using surface plasmon resonance phenomena in other energy ranges like (UV or IR).

2) Studying the effect of the different surface plasmon phenomena on samples prepared from layers of different dyes, polymers and nanomaterials.

3) An applied study of the prepared samples and their use in different life sensors.

4) Studying the effect of surface plasmon resonance phenomenon and its interaction with Raman scattering on the laser induce emission spectrum (LIF) of different laser dyes.

References:

[1] Ann M**,** "Definition and Determination in Medieval Arabic Grammatical Thought." *The Foundations of Arabic Linguistics IV*, 2019, 253-273. doi:10.1163/9789004389694_016.

[2] Roberts, Mildred B. "Sykes, Peter. A guidebook to mechanism in organic chemistry (3rd ed.). New York: John Wiley & Sons, Inc., 1970 (301 pages)." *Science Education* 57, no. 1 (1973), 100-100. doi:10.1002/sce.3730570128.

[3] Dice, G. D., S. Mujumdar, and A. Y. Elezzabi. "Plasmonically enhanced diffusive and subdiffusive metal nanoparticle-dye random laser." *Applied Physics Letters* 86, no. 13 (2005), 131105. doi:10.1063/1.1894590.

[4] Popov, O., A. Zilbershtein, and D. Davidov. "Random lasing from dye-gold nanoparticles in polymer films: Enhanced gain at the surface-plasmon-resonance wavelength." *Applied Physics Letters* 89, no. 19 (2006), 191116. doi:10.1063/1.2364857.

[5] Kabashin, A. V., and M. Meunier. "Visible photoluminescence from nanostructured Si-based layers produced by air optical breakdown on silicon." *Applied Physics Letters* 82, no. 10 (2003), 1619-1621. doi:10.1063/1.1557752.

[6] Meng, Xiangeng, Koji Fujita, Shunsuke Murai, Tomohiko Matoba, and Katsuhisa Tanaka. "Plasmonically Controlled Lasing Resonance with Metallic−Dielectric Core−Shell Nanoparticles." *Nano Letters* 11, no. 3 (2011), 1374-1378. doi:10.1021/nl200030h.

[7] Lakowicz, Joseph R., Joanna Malicka, Ignacy Gryczynski, Zygmunt Gryczynski, and Chris D. Geddes. "Radiative decay engineering: the role of photonic mode density in biotechnology." *Journal of Physics D:*

Applied Physics 36, no. 14 (2003), R240-R249. doi:10.1088/0022-3727/36/14/203.

[8] Dominguez, Christian T., Rogério L. Maltez, Roberto M. Dos Reis, Luciana S. De Melo, Cid B. De Araújo, and Anderson S. Gomes. "Dependence of random laser emission on silver nanoparticle density in PMMA films containing rhodamine 6G." *Journal of the Optical Society of America B* 28, no. 5 (2011), 1118. doi:10.1364/josab.28.001118.

[9] Popov, O., A. Zilbershtein, and D. Davidov. "Enhanced amplified emission induced by surface plasmons on gold nanoparticles in polymer film random lasers." *Polymers for Advanced Technologies* 18, no. 9 (2007), 751-755. doi:10.1002/pat.938.

[10] Aslan, Kadir, Ignacy Gryczynski, Joanna Malicka, Evgenia Matveeva, Joseph R. Lakowicz, and Chris D. Geddes. "Metal-enhanced fluorescence: an emerging tool in biotechnology." *Current Opinion in Biotechnology* 16, no. 1 (2005), 55-62. doi:10.1016/j.copbio.2005.01.001.

[11] Tam, Felicia, Glenn P. Goodrich, Bruce R. Johnson, and Naomi J. Halas. "Plasmonic Enhancement of Molecular Fluorescence." *Nano Letters* 7, no. 2 (2007), 496-501. doi:10.1021/nl062901x.

[12] O. Popov, A. Zilbershtein and D. Davidov. " Enhanced amplified emission induced by surface plasmons on gold nanoparticles in polymer film random lasers " (2007), John Wiley & Sons, Ltd, doi: 10.1002/pat.938.

[13] Xiangeng Meng, Koji Fujita, Shunsuke Murai, and Katsuhisa Tanaka. " Coherent random lasers in weakly scattering polymer films containing silver nanoparticles ", (2009), the American Physical Society,doi: 10.1103/PhysRevA.79.053817.

[14] Murai, Shunsuke, Koji Fujita, Xiangeng Meng, and Katsuhisa Tanaka. "Random Dispersion of Metal Nanoparticles Can Form a Laser

Cavity." Chemistry Letters 39, no. 6 (2010), 532-537. doi:10.1246/cl.2010.532.

[15] Christian Tolentino Dominguez, Rogério L. Maltez, Roberto M. S. dos Reis, Luciana S. A. de Melo, Cid B. de Araújo, and Anderson S. L. Gomes. " Dependence of random laser emission on silver nanoparticle density in PMMA films containing rhodamine 6G " Optical Society of America, (2011), J. Opt. Soc. Am. B / Vol. 28, No. 5.

[16] Wang, Cih-Su, Hsia-Yu Lin, Jian-Ming Lin, and Yang-Fang Chen. " Surface-Plasmon-Enhanced Ultraviolet Random Lasing from ZnO Nanowires Assisted by Pt Nanoparticles." Applied Physics Express 5, no. 6 (2012), 062003. doi:10.1143/apex.5.062003.

[17] Bhupesh Kumar, S. K. S. Patel and N. S. Gajbhiye, and Raj K. Thareja. " Random laser action with nanostructures in a dye solution " (2013), laser Institute of America.

[18] García-Ramiro, B., M. A. Illarramendi, S. García-Revilla, R. Balda, D. Levy, M. Zayat, and J. Fernández. " Lasing threshold of one- and two-photon-pumped dye-doped silica powder." (2014), Applied Physics B 117, no. 4 1135-1140. doi:10.1007/s00340-014-5936-5.

[19] Shuya Ning, Zhaoxin Wu, Hua Dong, Lin Ma, Bo Jiao, Lei Ding, Liping Ding, Fanghui Zhang. " The enhanced random lasing from dye-doped polymer films with different-sized silver nanoparticles " Elsevier, (2015), doi.org/10.1016/j.orgel.2015.12.021.

[20] Wan Zakiah Wan Ismail, Thanh Phong Vo, Ewa M Goldys and Judith M Dawes. " Plasmonic enhancement of Rhodamine dye random lasers" 2015, doi:10.1088/1054-660X/25/8/085001.

[21] Jiajia Yin, Guoying Feng, Shouhuan Zhou, Hong Zhang, Shutong Wang & Hua Zhang. " The shape effect of Au particles on random laser action in disordered media of Rh6G dye doped with PMMA polymer " Journal of Modern Optics, (2016), doi: 10.1080/09500340.2016.1184338.

[22] Tianrui Zhai, Zhiyang Xu, Xiaofeng Wu, Yimeng Wang, Feifei Liu, and Xinping Zhang. " Ultra-thin plasmonic random lasers " (2016), Optical Society of America, doi:10.1364/OE.24.000437.

[23] Tianrui Zhai, Zhiyang Xu, Songtao Li, and Xinping Zhang. " Red-green-blue plasmonic random laser " (2017), Optical Society of America, doi.org/10.1364/OE.25.002100.

[24] Ernesto Jiménez-Villar, Iran F. da Silva,Valdeci Mestre, Niklaus U. Wetter, Cefe Lopez, Paulo C. de Oliveira, Wagner M. Faustino, and Gilberto F. de Sá. " Random Lasing at Localization Transition in a Colloidal Suspension (TiO2@Silica) " (2017), American Chemical Society,doi: 10.1021/acsomega.7b00086.

[25] N. Asgari, S.M. Hamidi. " Exciton-plasmon coupling in two-dimensional plexitonic nano grating " (2018), Optical Materials, /doi.org/10.1016/j.optmat.2018.05.011.

[26] N. Asgari, S.M. Hamidi. " Fantastic exciton-plasmon coupling in dye-doped poly (vinyl pyrrolidone) /gold one-dimensional nano-grating ", (2018), Superlattices and Microstructures, doi.org/10.1016/j.spmi.2018.09.019.

[27] S. F. Haddawi, M. Mirahmadi , H. Mbarak, A. K. Kodeary, M. Ghasemi , S. M. Hamidi. " Footprint of plexcitonic states in low‑power green–blue plasmonic random laser " (2019), Applied Physics A, doi.org/10.1007/s00339-019-3139-y.

[28] S.F. Haddawi, Hammad R. Humud, S.M. Hamidi. " Signature of plasmonic nanoparticles in multi-wavelength low power random lasing " (2020), Elsevier, doi.org/10.1016/j.optlastec.2019.105770.

[29] S A Suheil, N S Shnan and Qussay Mohammed Salman . " The Plasmon Effects of AgNPs on Wave Guide Consisting of Polymers Mixed with Rhodamine Dyes " (2021), Journal of Physics: Conference Series.

[30] NRoostaei, HMbarak, S Almasi Monfared and SMHamidi. " Plasmonic wideband and tunable absorber based on semi etalon nano structure in the visible region " (2021), Phys. Scr. 96 , 035805 , doi.org/10.1088/1402-4896/abdbf6.

[31] Saddam F. Haddawi, Hammad R. Humud, Sakineh Almasi Monfared & S. M. Hamidi. " Two-dimensional plasmonic multilayer as an efficient tool for low power random lasing applications " (2021), Taylor & Francis, doi.org/10.1080/17455030.2021.1943563.

[32] Sahar, E., D. Treves, and I. Wieder. "Fluorescence quenching in laser dyes by absorption from an excited singlet state." *Optics Communications* 16, no. 1 (1976), 124-127. doi:10.1016/0030-4018(76)90066-3.

[33] Petukhov, V. A., M. B. Popov, and A. I. Krymova. "Determination of the quantum efficiency of the fluorescence of the solutions of organic dyes by diffraction on a thermal phase grating induced by laser radiation." *Soviet Journal of Quantum Electronics* 16, no. 4 (1986), 503-509. doi:10.1070/qe1986v016n04abeh006528.

[34] Peterson, O. G., J. P. Webb, W. C. McColgin, and J. H. Eberly. "Organic Dye Laser Threshold." *Journal of Applied Physics* 42, no. 5 (1971), 1917-1928. doi:10.1063/1.1660468.

[35] Johnston,, T.F., and F.J. Duarte. "Lasers, Dye." *Encyclopedia of Physical Science and Technology*, 2003, 315-359. doi:10.1016/b0-12-227410-5/00365-3.

[36] Li, Zhenyu, Zhaoyu Zhang, Axel Scherer, and Demetri Psaltis. "Optofluidic Microring Dye Laser." *2007 Digest of the IEEE/LEOS Summer Topical Meetings*, 2007. doi:10.1109/leosst.2007.4288336.

[37] Suzuki, HIiroshi. "Relations between Electronic Absorption Spectra and Geometry of Molecules. Biphenyl and Related Compounds." *Electronic Absorption Spectra and Geometry of Organic Molecules*, 1967, 261-292. doi:10.1016/b978-0-12-395557-9.50015-x.

[38] López Arbeloa, F., T. López Arbeloa, I. López Arbeloa, A. Costela, I. García-Moreno, J.M. Figuera, F. Amat-Guerri, and R. Sastre. "Relations between photophysical and lasing properties of rhodamines in solid polymeric matrices." *Applied Physics B: Lasers and Optics* 64, no. 6 (1997), 651-657. doi:10.1007/s003400050228.

[39] Stepanov, B. I., and A. N. Rubinov. "Effect of strokes shift on the operating frequency of lasers." *Journal of Applied Spectroscopy* 4, no. 3 (1966), 159-163. doi:10.1007/bf00612141.

[40] Bezrodnyi, V. I., M. V. Bondar, G. Y. Kozak, O. V. Przhonskaya, and E. A. Tikhonov. "Dye-activated polymer media for frequency-tunable lasers (review)." *Journal of Applied Spectroscopy* 50, no. 5 (1989), 441-455. doi:10.1007/bf00664400.

[41] Caldwell, Dennis. "Advances in radiation chemistry. Vol. 4. Edited by: M. Burton and J. L. Magee. Published by: Wiley-Interscience, John Wiley & Sons, Inc. New York, 1974." *International Journal of Quantum Chemistry* 9, no. 4 (1975), 755-757. doi:10.1002/qua.560090416.

[42] Svelto, Orazio. "Types of Lasers." *Principles of Lasers*, 1989, 287-377. doi:10.1007/978-1-4615-7670-9_6.

[43] Yang, Fuyong, Ying Chu, Lei Huo, Yang Yang, Yang Liu, and Jinglin Liu. "Preparation of uniform rhodamine B-doped SiO2/TiO2 composite microspheres." *Journal of Solid State Chemistry* 179, no. 2 (2006), 457-463. doi:10.1016/j.jssc.2005.11.006.

[44] Arbeloa, I.Lopez, and K.K. Rohatgi-Mukherjee. "Solvent effect on photophysics of the molecular forms of rhodamine B. Solvation models and spectroscopic parameters." Chemical Physics Letters 128, no. 5-6 (1986), 474-479. doi:10.1016/0009-2614(86)80656-x.

[45] Contreras, J.E., E.A. Rodriguez, and J. Taha-Tijerina. "Nanotechnology applications for electrical transformers—A review." *Electric Power Systems Research* 143 (2017), 573-584. doi:10.1016/j.epsr.2016.10.058.

[46] Berube, David, Christopher Cummings, Michael Cacciatore, Dietram Scheufele, and Jason Kalin. "Characteristics and classification of nanoparticles: Expert Delphi survey." *Nanotoxicology* 5, no. 2 (2010), 236-243. doi:10.3109/17435390.2010.521633.

[47] Tiwari, Jitendra N., Rajanish N. Tiwari, and Kwang S. Kim. "Zero-dimensional, one-dimensional, two-dimensional and three-dimensional nanostructured materials for advanced electrochemical energy devices." *Progress in Materials Science* 57, no. 4 (2012), 724-803. doi:10.1016/j.pmatsci.2011.08.003.

[48] Piquemal, Jean-Yves, Emmanuel Briot, and Jean-Marie Bregeault. "ChemInform Abstract: Preparation of Materials in the Presence of Hydrogen Peroxide: From Discrete or “Zero-Dimensional” Objects to Bulk Materials." *ChemInform* 44, no. 9 (2013), no-no. doi:10.1002/chin.201309194.

[49] Yeap, Swee P. "Permanent agglomerates in powdered nanoparticles: Formation and future prospects." *Powder Technology* 323 (2018), 51-59. doi:10.1016/j.powtec.2017.09.042.

[50] Gubicza, Jenő. "Defect Structure in Bulk Nanomaterials Processed by Severe Plastic Deformation." *Defect Structure and Properties of Nanomaterials*, 2017, 59-93. doi:10.1016/b978-0-08-101917-7.00003-7.

[51] Zhang, Haijun, Naoki Toshima, Kanako Takasaki, and Mitsutaka Okumura. "Preparation of Agcore/Aushell bimetallic nanoparticles from physical mixtures of Au clusters and Ag ions under dark conditions and their catalytic activity for aerobic glucose oxidation." *Journal of Alloys and Compounds* 586 (2014), 462-468. doi:10.1016/j.jallcom.2013.10.048.

[52] Sun, Baoliang, Xiaohong Jiang, Shuxi Dai, and Zuliang Du. "Single-crystal silver nanowires: Preparation and Surface-enhanced Raman Scattering (SERS) property." *Materials Letters* 63, no. 29 (2009), 2570-2573. doi:10.1016/j.matlet.2009.09.006.

[53] Biener, Jürgen, Arne Wittstock, Theodore Baumann, Jörg Weissmüller, Marcus Bäumer, and Alex Hamza. "Surface Chemistry in Nanoscale Materials." *Materials* 2, no. 4 (2009), 2404-2428. doi:10.3390/ma2042404.

[54] Kumar, Prashant, Alan Robins, Sotiris Vardoulakis, and Rex Britter. "A review of the characteristics of nanoparticles in the urban atmosphere and the prospects for developing regulatory controls." *Atmospheric Environment* 44, no. 39 (2010), 5035-5052. doi:10.1016/j.atmosenv.2010.08.016.

[55] Huang, Xiaohua, Prashant K. Jain, Ivan H. El-Sayed, and Mostafa A. El-Sayed. "Gold nanoparticles: interesting optical properties and recent applications in cancer diagnostics and therapy." *Nanomedicine* 2, no. 5 (2007), 681-693. doi:10.2217/17435889.2.5.681.

[56] Alivisatos, Paul. "The use of nanocrystals in biological detection." *Nature Biotechnology* 22, no. 1 (2003), 47-52. doi:10.1038/nbt927.

[57] Mirkin, Chad A., Robert L. Letsinger, Robert C. Mucic, and James J. Storhoff. "A DNA-based method for rationally assembling nanoparticles into macroscopic materials." *Nature* 382, no. 6592 (1996), 607-609. doi:10.1038/382607a0.

[58] Resch-Genger, Ute, Markus Grabolle, Sara Cavaliere-Jaricot, Roland Nitschke, and Thomas Nann. "Quantum dots versus organic dyes as fluorescent labels." *Nature Methods* 5, no. 9 (2008), 763-775. doi:10.1038/nmeth.1248.

[59] Grabolle, Markus, Peter Kapusta, Thomas Nann, Xu Shu, Jan Ziegler, and Ute Resch-Genger. "Fluorescence Lifetime Multiplexing with Nanocrystals and Organic Labels." *Analytical Chemistry* 81, no. 18 (2009), 7807-7813. doi:10.1021/ac900934a.

[60] Ghosh Chaudhuri, Rajib, and Santanu Paria. "Core/Shell Nanoparticles: Classes, Properties, Synthesis Mechanisms, Characterization, and Applications." Chemical Reviews 112, no. 4 (2011), 2373-2433. doi:10.1021/cr100449n.

[61] Boardman, A.D., and A.V. Zayats. "Nonlinear Plasmonics." *Modern Plasmonics*, 2014, 329-347. doi:10.1016/b978-0-444-59526-3.00011-2.

[62] Raether, Heinz. "Surface Plasmons on Smooth and Rough Surfaces and on Gratings." *Springer Tracts in Modern Physics*, 1988. doi:10.1007/bfb0048317.

[63] Myszka, David G. "Survey of the 1998 optical biosensor literature." *Journal of Molecular Recognition* 12, no. 6 (1999), 390-408. doi:10.1002/(sici)1099-1352(199911/12)12:6<390::aid-jmr482>3.0.co;2-8.

[64] Otto, Andreas. "Excitation of nonradiative surface plasma waves in silver by the method of frustrated total reflection." *Zeitschrift für Physik A Hadrons and nuclei* 216, no. 4 (1968), 398-410. doi:10.1007/bf01391532.

[65] Kretschmann, Erwin. "Die Bestimmung optischer Konstanten von Metallen durch Anregung von Oberflächenplasmaschwingungen." *Zeitschrift für Physik A Hadrons and nuclei* 241, no. 4 (1971), 313-324. doi:10.1007/bf01395428.

[66] Lee, Byoungho, Il-Min Lee, Seyoon Kim, Dong-Ho Oh, and Lambertus Hesselink. "Review on subwavelength confinement of light with plasmonics." *Journal of Modern Optics* 57, no. 16 (2010), 1479-1497. doi:10.1080/09500340.2010.506985.

[67] Li, Ming, Scott K. Cushing, and Nianqiang Wu. "Plasmon-enhanced optical sensors: a review." *The Analyst* 140, no. 2 (2015), 386-406. doi:10.1039/c4an01079e.

[68] Unser, Sarah, Ian Bruzas, Jie He, and Laura Sagle. "Localized Surface Plasmon Resonance Biosensing: Current Challenges and Approaches." *Sensors* 15, no. 7 (2015), 15684-15716. doi:10.3390/s150715684.

[69] Caucheteur, Christophe, Tuan Guo, and Jacques Albert. "Review of plasmonic fiber optic biochemical sensors: improving the limit of detection." *Analytical and Bioanalytical Chemistry* 407, no. 14 (2015), 3883-3897. doi:10.1007/s00216-014-8411-6.

[70] Jain, Prashant K., Xiaohua Huang, Ivan H. El-Sayed, and Mostafa A. El-Sayed. "Review of Some Interesting Surface Plasmon Resonance-enhanced Properties of Noble Metal Nanoparticles and Their Applications to Biosystems." *Plasmonics* 2, no. 3 (2007), 107-118. doi:10.1007/s11468-007-9031-1.

[71] Dobson, Peter J. "Introduction to Metal-nanoparticle Plasmonics, by Matthew Pelton and Garnett W. Bryant." *Contemporary Physics* 55, no. 4 (2014), 352-353. doi:10.1080/00107514.2014.948921.

[72] Maier, Stefan A. "Plasmon Waveguides." *Plasmonics: Fundamentals and Applications*, 2007, 109-139. doi:10.1007/0-387-37825-1_7.

[73] Amendola, Vincenzo, Roberto Pilot, Marco Frasconi, Onofrio M. Maragò, and Maria A. Iatì. "Surface plasmon resonance in gold nanoparticles: a review." *Journal of Physics: Condensed Matter* 29, no. 20 (2017), 203002. doi:10.1088/1361-648x/aa60f3.

[74] Homola, Jiri. "ChemInform Abstract: Surface Plasmon Resonance Sensors for Detection of Chemical and Biological Species." *ChemInform* 39, no. 18 (2008). doi:10.1002/chin.200818275.

[75] Ni, Weihai, Xiaoshan Kou, Zhi Yang, and Jianfang Wang. "Tailoring Longitudinal Surface Plasmon Wavelengths, Scattering and Absorption Cross Sections of Gold Nanorods." *ACS Nano* 2, no. 4 (2008), 677-686. doi:10.1021/nn7003603.

[76] Diaconescu, Bogdan, Karsten Pohl, Luca Vattuone, Letizia Savio, Philip Hofmann, Vyacheslav M. Silkin, Jose M. Pitarke, et al. "Low-energy acoustic plasmons at metal surfaces." *Nature* 448, no. 7149 (2007), 57-59. doi:10.1038/nature05975.

[77] Zayats, Anatoly V., Igor I. Smolyaninov, and Alexei A. Maradudin. "Nano-optics of surface plasmon polaritons." *Physics Reports* 408, no. 3-4 (2005), 131-314. doi:10.1016/j.physrep.2004.11.001.

[78] M. Cardona, G. Güntherodt. "Light Scattering in Solids IV." *Topics in Applied Physics*, 1984. doi:10.1007/3-540-11942-6.

[79] Kretschmann, Hans-Joachim, and Friedrich Wingert. "Einleitung." *Computeranwendungen bei Wachstumsproblemen in Biologie und Medizin*, 1971, 1-6. doi:10.1007/978-3-642-93006-5_1.

[80] Sanda, P. N., J. M. Warlaumont, J. E. Demuth, J. C. Tsang, K. Christmann, and J. A. Bradley. "Surface-Enchanced Raman Scattering from Pyridine on Ag(111)." *Physical Review Letters* 45, no. 18 (1980), 1519-1523. doi:10.1103/physrevlett.45.1519.

[81] Murray, C. A., D. L. Allara, and M. Rhinewine. "Silver-Molecule Separation Dependence of Surface-Enhanced Raman Scattering." *Physical Review Letters* 46, no. 1 (1981), 57-60. doi:10.1103/physrevlett.46.57.

[82] Zhu, Yifu, Daniel J. Gauthier, S. E. Morin, Qilin Wu, H. J. Carmichael, and T. W. Mossberg. "Vacuum Rabi splitting as a feature of linear-dispersion theory: Analysis and experimental observations." *Physical Review Letters* 64, no. 21 (1990), 2499-2502. doi:10.1103/physrevlett.64.2499.

[83] Gómez, D. E., K. C. Vernon, P. Mulvaney, and T. J. Davis. "Surface Plasmon Mediated Strong Exciton−Photon Coupling in Semiconductor Nanocrystals." *Nano Letters* 10, no. 1 (2009), 274-278. doi:10.1021/nl903455z.

[84] Brune, M., F. Schmidt-Kaler, A. Maali, J. Dreyer, E. Hagley, J. M. Raimond, and S. Haroche. "Quantum Rabi Oscillation: A Direct Test of Field Quantization in a Cavity." *Physical Review Letters* 76, no. 11 (1996), 1800-1803. doi:10.1103/physrevlett.76.1800.

[85] Yoshie, T., A. Scherer, J. Hendrickson, G. Khitrova, H. M. Gibbs, G. Rupper, C. Ell, O. B. Shchekin, and D. G. Deppe. "Vacuum Rabi splitting

with a single quantum dot in a photonic crystal nanocavity." *Nature* 432, no. 7014 (2004), 200-203. doi:10.1038/nature03119.

[86] Lidzey, D. G. "Photon-Mediated Hybridization of Frenkel Excitons in Organic Semiconductor Microcavities." *Science* 288, no. 5471 (2000), 1620-1623. doi:10.1126/science.288.5471.1620.

[87] Tischler, Jonathan R., M. Scott Bradley, Qiang Zhang, Tolga Atay, Arto Nurmikko, and Vladimir Bulović. "Solid state cavity QED: Strong coupling in organic thin films." *Organic Electronics* 8, no. 2-3 (2007), 94-113. doi:10.1016/j.orgel.2007.01.008.

[88] Barnes, William L., Alain Dereux, and Thomas W. Ebbesen. "Surface plasmon subwavelength optics." *Nature* 424, no. 6950 (2003), 824-830. doi:10.1038/nature01937.

[89] Fofang, Nche T., Tae-Ho Park, Oara Neumann, Nikolay A. Mirin, Peter Nordlander, and Naomi J. Halas. "Plexcitonic Nanoparticles: Plasmon−Exciton Coupling in Nanoshell−J-Aggregate Complexes." *Nano Letters* 8, no. 10 (2008), 3481-3487. doi:10.1021/nl8024278.

[90] Bonnand, C., J. Bellessa, and J. C. Plenet. "Properties of surface plasmons strongly coupled to excitons in an organic semiconductor near a metallic surface." *Physical Review B* 73, no. 24 (2006). doi:10.1103/physrevb.73.245330.

[91] Bellessa, J., C. Bonnand, J. C. Plenet, and J. Mugnier. "Strong Coupling between Surface Plasmons and Excitons in an Organic Semiconductor." *Physical Review Letters* 93, no. 3 (2004). doi:10.1103/physrevlett.93.036404.

[92] Tam, Felicia, Glenn P. Goodrich, Bruce R. Johnson, and Naomi J. Halas. "Plasmonic Enhancement of Molecular Fluorescence." *Nano Letters* 7, no. 2 (2007), 496-501. doi:10.1021/nl062901x.

[93] Schwartz, T., J. A. Hutchison, C. Genet, and T. W. Ebbesen. "Reversible Switching of Ultrastrong Light-Molecule Coupling." *Physical Review Letters* 106, no. 19 (2011). doi:10.1103/physrevlett.106.196405.

[94] Balci, Sinan, Coskun Kocabas, Simge Ates, Ertugrul Karademir, Omer Salihoglu, and Atilla Aydinli. "Tuning surface plasmon-exciton coupling via thickness dependent plasmon damping." *Physical Review B* 86, no. 23 (2012). doi:10.1103/physrevb.86.235402.

[95] Schlather, Andrea E., Nicolas Large, Alexander S. Urban, Peter Nordlander, and Naomi J. Halas. "Near-Field Mediated Plexcitonic Coupling and Giant Rabi Splitting in Individual Metallic Dimers." *Nano Letters* 13, no. 7 (2013), 3281-3286. doi:10.1021/nl4014887.

[96] Vuckovic, J., M. Loncar, and A. Scherer. "Surface plasmon enhanced light-emitting diode." *IEEE Journal of Quantum Electronics* 36, no. 10 (2000), 1131-1144. doi:10.1109/3.880653.

[97] Hakala, T. K., J. J. Toppari, A. Kuzyk, M. Pettersson, H. Tikkanen, H. Kunttu, and P. Törmä. "Vacuum Rabi Splitting and Strong-Coupling Dynamics for Surface-Plasmon Polaritons and Rhodamine 6G Molecules." *Physical Review Letters* 103, no. 5 (2009). doi:10.1103/physrevlett.103.053602.

[98] Kano, Hiroshi, and Satoshi Kawata. "Surface-plasmon sensor for absorption-sensitivity enhancement." *Applied Optics* 33, no. 22 (1994), 5166. doi:10.1364/ao.33.005166.

[99] Braun, Julia, Bruno Gompf, Georg Kobiela, and Martin Dressel. "How Holes Can Obscure the View: Suppressed Transmission through an Ultrathin Metal Film by a Subwavelength Hole Array." *Physical Review Letters* 103, no. 20 (2009). doi:10.1103/physrevlett.103.203901.

[100] Ikehata, Akifumi, Xiaoling Li, Tamitake Itoh, Yukihiro Ozaki, and Jian-Hui Jiang. "High sensitive detection of near-infrared absorption by

surface plasmon resonance." *Applied Physics Letters* 83, no. 11 (2003), 2232-2234. doi:10.1063/1.1610812.

[101] Adato, Ronen, Alp Artar, Shyamsunder Erramilli, and Hatice Altug. "Engineered Absorption Enhancement and Induced Transparency in Coupled Molecular and Plasmonic Resonator Systems." *Nano Letters* 13, no. 6 (2013), 2584-2591. doi:10.1021/nl400689q.

[102] Balci, Sinan, Askin Kocabas, Coskun Kocabas, and Atilla Aydinli. "Localization of surface plasmon polaritons in hexagonal arrays of Moiré cavities." *Applied Physics Letters* 98, no. 3 (2011), 031101. doi:10.1063/1.3529469.

[103] Wurtz, Gregory A., Paul R. Evans, William Hendren, Ronald Atkinson, Wayne Dickson, Robert J. Pollard, Anatoly V. Zayats, William Harrison, and Christopher Bower. "Molecular Plasmonics with Tunable Exciton−Plasmon Coupling Strength in J-Aggregate Hybridized Au Nanorod Assemblies." *Nano Letters* 7, no. 5 (2007), 1297-1303. doi:10.1021/nl070284m.

[104] Pendry, J. B., and A. MacKinnon. "Calculation of photon dispersion relations." *Physical Review Letters* 69, no. 19 (1992), 2772-2775. doi:10.1103/physrevlett.69.2772.

[105] Krolenko, S., S. Adamyan, T. Belyaeva, and T. Mozhenok. "Acridine orange accumulation in acid organelles of normal and vacuolated frog skeletal muscle fibres." *Cell Biology International* 30, no. 11 (2006), 933-939. doi:10.1016/j.cellbi.2006.06.017.

[106] Musso, H. "ORCEIN– UND LACKMUSFARBSTOFFE1." *Planta Medica* 8, no. 04 (1960), 432-446. doi:10.1055/s-0028-1101580.

[107] Costela, A., I. Garcia-Moreno, J. Barroso, and R. Sastre. "Laser performance of Coumarin 540A dye molecules in polymeric host media with different viscosities: From liquid solution to solid polymer

matrix." *Journal of Applied Physics* 83, no. 2 (1998), 650-660. doi:10.1063/1.366755.

[108] Nadia Hussein Sahib ," Spectroscopic Study for Some Organic Dyes " , A Thesis , Al-Mustansiriya University , College of Sciences,(2005).

[109] Raida Jbur Hamood Al-Hamadani ," Spectroscopy Study and Manfacturing of An Active Polymeric Laser Medium " , A Thesis , University of Baghdad , College of Science for Women, (2006).

[110] Zhang, Jian, Yi Fu, and Joseph R. Lakowicz. "Emission Behavior of Fluorescently Labeled Silver Nanoshell: Enhanced Self-Quenching by Metal Nanostructure." *The Journal of Physical Chemistry C* 111, no. 5 (2007), 1955-1961. doi:10.1021/jp063996u.

[111] Uwada, Takayuki, Ryo Toyota, Hiroshi Masuhara, and Tsuyoshi Asahi. "Single Particle Spectroscopic Investigation on the Interaction between Exciton Transition of Cyanine Dye J-Aggregates and Localized Surface Plasmon Polarization of Gold Nanoparticles." *The Journal of Physical Chemistry C* 111, no. 4 (2007), 1549-1552. doi:10.1021/jp067565n.

[112] Wintterlin, J. "D. A. Bonnell (Ed.): Scanning tunneling microscopy and spectroscopy, theory, techniques and applications, VCH, New York, Weinheim, 1993." *Berichte der Bunsengesellschaft für physikalische Chemie* 98, no. 7 (1994), 994-995. doi:10.1002/bbpc.19940980728.

[113] Jenkins, Robert D., and David L. Andrews. "Twin-donor systems for resonance energy transfer." *Chemical Physics Letters* 301, no. 3-4 (1999), 235-240. doi:10.1016/s0009-2614(99)00007-x.

[114] Neumann, T., M.-L. Johansson, D. Kambhampati, and W. Knoll "Surface-Plasmon Fluorescence Spectroscopy" . *Advanced Functional Materials* 12, no. 9 (2002), 575-586. doi:10.1002/1616-3028(20020916)12:9<575::aid-adfm575>3.0.co;2-4.

[115] Weber, W. H., and C. F. Eagen. "Energy transfer from an excited dye molecule to the surface plasmons of an adjacent metal." *Optics Letters* 4, no. 8 (1979), 236. doi:10.1364/ol.4.000236.

[116] Bojarski, C., R. Bujko, and P. Bojarski. "Remarks on Fluorescence Concentration Quenching of Rhodamine 6G in Methanol." *Acta Physica Polonica A* 79, no. 4 (1991), 471-478. doi:10.12693/aphyspola.79.471.

[117] Mujumdar, Sushil, Volker Türck, Renato Torre, and Diederik S. Wiersma. "Chaotic behavior of a random laser with static disorder." *Physical Review A* 76, no. 3 (2007). doi:10.1103/physreva.76.033807.

[118] Penzkofer, A., and Y. Lu. "Fluorescence quenching of rhodamine 6G in methanol at high concentration." *Chemical Physics* 103, no. 2-3 (1986), 399-405. doi:10.1016/0301-0104(86)80041-6.

[119] Williams, Alun T., Stephen A. Winfield, and James N. Miller. "Relative fluorescence quantum yields using a computer-controlled luminescence spectrometer." *The Analyst* 108, no. 1290 (1983), 1067. doi:10.1039/an9830801067.

[120] El-Dardiry, Ramy G., Sanli Faez, and Ad Lagendijk. "Classification of light sources and their interaction with active and passive environments." *Physical Review A* 83, no. 3 (2011). doi:10.1103/physreva.83.031801.

[121] Kubin, R.F., and A.N. Fletcher. "Fluorescence quantum yields of some rhodamine dyes." *Journal of Luminescence* 27, no. 4 (1982), 455-462. doi:10.1016/0022-2313(82)90045-x.

[122] Uppu, Ravitej, Anjani K. Tiwari, Sushil Mujumdar, and Dmitry N. Chigrin. "Coherent random lasing in diffusive resonant media." 2011. doi:10.1063/1.3644226.

[123] Bouvy, Claire, Evgeny Chelnokov, Wladimir Marine, Robert Sporken, and Bao-Lian Su. "Quantum Size Effect and very localized random laser in ZnO@mesoporous silica nanocomposite following a two-photon absorption process." Journal of Non-Crystalline Solids 355, no. 18-21 (2009), 1152-1156. doi:10.1016/j.jnoncrysol.2009.01.053.

[124] Burin, A. L., M. A. Ratner, H. Cao, and R. P. Chang. "Model for a Random Laser." Physical Review Letters 87, no. 21 (2001). doi:10.1103/physrevlett.87.215503.

[125] Yi, Jiayu, Guoying Feng, Liling Yang, Ke Yao, Chao Yang, Yingsong Song, and Shouhuan Zhou. "Behaviors of the Rh6G random laser comprising solvents and scatterers with different refractive indices." Optics Communications 285, no. 24 (2012), 5276-5282. doi:10.1016/j.optcom.2012.06.094.

[126] Cao, Hui. "Random Lasers with Coherent Feedback." Topics in Applied Physics (n.d.), 303-330. doi:10.1007/3-540-44948-5_14.

[127] Popov, O., A. Zilbershtein, and D. Davidov. "Random lasing from dye-gold nanoparticles in polymer films: Enhanced gain at the surface-plasmon-resonance wavelength." Applied Physics Letters 89, no. 19 (2006), 191116. doi:10.1063/1.2364857.

[128] Sakuma, Ken, Naoto Hirosaki, and Rong-Jun Xie. "Red-shift of emission wavelength caused by reabsorption mechanism of europium

activated Ca--SiAlON ceramic phosphors." Journal of Luminescence 126, no. 2 (2007), 843-852. doi:10.1016/j.jlumin.2006.12.006.